High-pressure phases of group-IV, III–V, and II–VI compounds

A. Mujica*

Departamento de Física Fundamental II, Universidad de La Laguna, La Laguna E-38205, Tenerife, Spain

Angel Rubio†

Departamento de Física de Materiales, Universidad del País Vasco, Donostia International Physics Center (DIPC) and Centro Mixto CSIC-UPV/EHU, San Sebastián/Donostia E-20018, Spain

A. Muñoz‡

Departamento de Física Fundamental II, Universidad de La Laguna, La Laguna E-38205, Tenerife, Spain

R. J. Needs§

TCM Group, Cavendish Laboratory, Cambridge CB3 0HE, United Kingdom

(Published 7 July 2003)

Advances in the accuracy and efficiency of first-principles electronic structure calculations have allowed detailed studies of the energetics of materials under high pressures. At the same time, improvements in the resolution of powder x-ray diffraction experiments and more sophisticated methods of data analysis have revealed the existence of many new and unexpected high-pressure phases. The most complete set of theoretical and experimental data obtained to date is for the group-IVA elements and the group-IIIA–VA and IIB–VIA compounds. Here the authors review the currently known structures and high-pressure behavior of these materials and the theoretical work that has been done on them. The capabilities of modern first-principles methods are illustrated by a full comparison with the experimental data.

CONTENTS

*Electronic address: amujica@ull.es
†Electronic address: arubio@sc.ehu.es
‡Electronic address: amunoz@ull.es
§Electronic address: rn11@phy.cam.ac.uk

I. INTRODUCTION

Materials at high pressures occur at the centers of planets and in stars and in both natural and man-made explosions. High pressures may also be applied to small laboratory samples in a controlled manner using devices such as the diamond anvil cell (DAC). The static pressure applied in a DAC is a continuously variable parameter which can be used for systematic studies of the properties of solids as a function of the interatomic distances.[1]

One of the interesting phenomena that may occur under applied pressure is a sudden change in the arrangement of the atoms, i.e., a structural phase transition. The Gibbs free energies of the different possible arrangements of atoms vary under compression, and at some stage it becomes favorable for the material to change the type of atomic arrangement. A phase transition is said to have occurred if the change is discontinuous or continuous but with a change in crystal symmetry. The pressures achieved in a DAC can lead to a reduction in the volume by more than a factor of 2, causing enormous changes to the inter-atomic bonding. The properties of the high-pressure phases may be very different from those under normal conditions.

This review is concerned with the high-pressure phases of group-IVA elements (C group), and IIIA–VA (B and N groups) and IIB–VIA (Zn and O groups) binary compounds. All of these $A^N B^{8-N}$ materials have an average of four valence electrons per atom and they show some similarities in the structures they adopt both under normal conditions and under applied pressure. They therefore form a group of related compounds, and it is helpful to consider them all together. The pressure-driven transitions undergone by these materials are normally associated with an abrupt change in their resistivity and indeed the earliest evidence for many of the transitions reported here was from resistivity measurements (Minomura and Drickamer, 1962; Samara and Drickamer, 1962). Systematic structural studies of the high-pressure phases of these materials were initiated in the early 1960s by Jamieson on Si and Ge (1963a) and several IIIA–VA compounds (1963b), and by Mariano and Warekois (1963), Rooymans (1963), and Owen *et al.* (1963) on IIB–VIA compounds. A broad consensus was reached by the end of the 1980s that under increasing pressure the materials adopt high-symmetry structures of increasing coordination number. However, recent experiments have shown that previously unexpected lower-symmetry phases are formed at intermediate pressures (see Nelmes and McMahon, 1998). These discoveries have been made possible by advances in the resolution of high-pressure powder x-ray diffraction studies and more sophisticated data analysis techniques (see Sec. II). The analysis of crystallographic results normally yields the simplest structure consistent (to within some tolerance) with the data. Modern higher-resolution data are now subjected to much more stringent analysis techniques, allowing the identification of previously undetected symmetry-breaking distortions. With hindsight one can perceive signatures of these distortions in the earlier experimental data, but these weaker peaks and shoulders in the data were neglected. Presumably at very high pressures simple high-symmetry structures are adopted, but the pressures at which they occur are in many cases much larger than previously thought.

The main emphasis of this review is on the first-principles (or *ab initio*) electronic structure computations that have been performed on this family of compounds and the comparison of their results with experiment. Methods for calculating the energies of solids within a quantum-mechanical framework have been under continuous development since the 1930s. Many important developments in methodology have been made (Payne *et al.*, 1992) which, combined with the relentless increase in computing power, have led to the modern field of first-principles electronic structure computations in which the only experimental input is the atomic numbers of the atoms involved. These methods allow the accurate calculation of the energies of solids (see Sec. V). The possibility of using first-principles electronic structure computations to study high-pressure phases was first demonstrated by Yin and Cohen (1980),

[1]We express pressures in GPa (gigapascal) $=10^4$ bars $=6.241$ meV/Å^3, where one bar $=10^5$ N m^{-2} (pascal) $=0.9869$ atm. The normal atmospheric pressure is about 1 atm. The following energy relations may also be helpful: 1 eV/particle $=2.306\times10^4$ cal/mol $=9.649\times10^4$ J/mol.

who calculated the energies of several structural phases of Si, obtaining good agreement with the available experimental data. This early success of the theory fostered both theoretical and experimental work in the field. More recently a large number of high-quality calculations have been performed on IVA, IIIA–VA, and IIB–VIA materials. Modern calculations allow the accurate relaxation of structures to their minimum energy configurations and the incorporation of temperature effects. The calculations may be performed with sufficient accuracy to resolve energy differences as small as a few meV per atom, which is the scale required to distinguish the relative stabilities of certain phases.

The materials discussed here exhibit a number of different kinds of structural transitions (see Sec. VI). Some of the transitions are "reconstructive," i.e., they involve large structural changes at the transition including the breaking of bonds; for example, when the fourfold-coordinated insulating phases, which are stable at normal conditions, transform under applied pressure to sixfold-coordinated metallic phases. Such strongly first-order transitions normally show a large hysteresis and in some cases they are irreversible, i.e., the original phase is not retrieved after releasing the pressure. Many "displacive" phase transitions are also observed, in which the positions of the atoms change by fairly small amounts at the transition (often accompanied by a strain). Some of these displacive transitions occur via a mechanism in which the frequency of a vibrational mode drops towards zero, as in a "soft-mode" transition, although in practice the transition is often accompanied by a small change in volume and is weakly first order. These transitions normally show only a small amount of hysteresis. A few examples of transitions from ordered to disordered phases have also been reported. There is now a large body of reliable calculations which covers high-pressure behavior in almost all of these materials. This affords a unique opportunity for a detailed comparison with the extensive experimental data (see Secs. VII and VIII).

In this review we aim to give a coherent presentation of the theoretical results, together with comparisons with experiment, leading to general conclusions about the nature of the high-pressure phase diagrams of these materials (see Sec. X). The first-principles calculations discussed here have some features that make them complementary to experimental studies. They are, of course, approximate and have a number of limitations, but they can give information that is not available from experiments. For example, one can study unstable phases in the computer, which helps in identifying trends in behavior. Because one has precise control over the physical conditions and chemical composition of the system, there is no uncertainty about the structures present and therefore the calculations can play a role in verifying experimental results. It is also easy to perform calculations at very high pressures, although performing the corresponding experiments may be very difficult. The calculations can therefore be used to predict new high-pressure phases. Experimental information about the actual path by which a transition takes place is very hard to obtain, but first-principles calculations also allow investigations of transition paths and activation barriers.

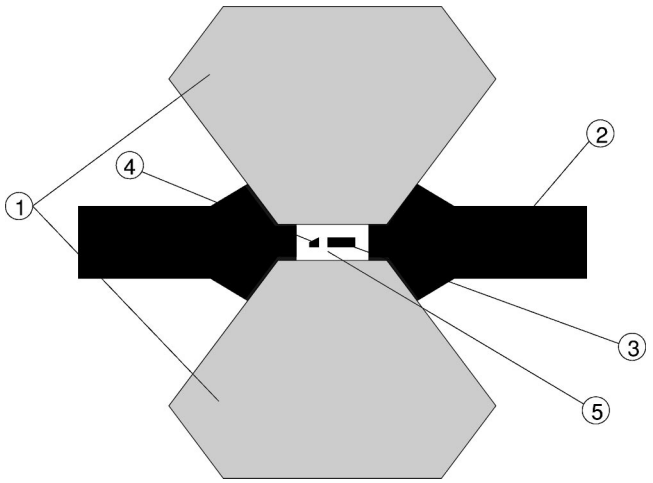

FIG. 1. Schematic depiction of a diamond anvil cell (DAC): 1, diamonds; 2, gasket; 3, sample; 4, reference material such as ruby; 5, pressurizing medium.

A number of excellent reviews of different aspects of high-pressure physics can be found in the literature. Of particular relevance to the present article are the reviews of the experimental structural data for most IVA elements and IIIA–VA and IIB–VIA compounds under pressure by Nelmes and McMahon (1998) and of both theoretical and experimental work on IVA elements and IIIA–VA compounds by Ackland (2001a).

II. HIGH-PRESSURE EXPERIMENTAL TECHNIQUES

The technology of high-pressure experiments is a highly developed but steadily evolving field, which we can only briefly survey here. The interested reader may wish to consult the book by Eremets (1996) and the collection of review articles edited by Holzapfel and Isaacs (1997) for recent and more detailed expositions.

A. High-pressure devices: the diamond anvil cell

Research into materials under high pressures has been largely dependent on the evolution of high-pressure cells. Diamond anvil cells (DAC's) are currently the most widely used of all high-pressure devices. The DAC gives laboratory access to very high static pressures in a relatively easy and safe manner, allowing experimental measurements at pressures above 100 GPa.

The DAC was first developed by Jamieson, Lawson, and Nachtrieb (1959) and Weir *et al.* (1959). A schematic diagram of a DAC is shown in Fig. 1. The operating principle of a DAC, and indeed of all high-pressure cells, is similar; a force F is applied to a small surface of area S, creating a pressure $p=F/S$, which can be made large by reducing the size of the area of contact. The generation of very high pressures is limited by the deformation and eventual fracture of the material forming the pressure device. The DAC can generate very high pres-

sures because of the exceptional hardness of diamond, but even high-quality diamonds will shatter under sufficiently high loads.

In a DAC the sample is placed between the flat faces (*culets*) of two brilliant-cut diamonds. The culets are separated by a thin metallic foil (*gasket*) which has previously been indented by the diamonds. In the middle of the indented zone there is a small hole constituting the pressure chamber into which the sample is placed. Typical dimensions are 0.1–1 mm for the diameter of the culet, 0.3–0.2 mm for the thickness of the gasket (reduced to $\sim 50\,\mu$m at the indented zone), and ~ 50–$200\,\mu$m for the diameter of the circular hole. The sample is normally immersed in a fluid, which fills the chamber and acts as a pressurizing medium ensuring hydrostatic (or quasihydrostatic) and homogeneous conditions. The transparency of diamond over a wide range of frequencies from the near ultraviolet (~ 5.5 eV) to the infrared, and more importantly for these applications, to hard x rays (>10 keV), allows the use of radiation in studying the sample.

B. Powder x-ray diffraction studies

The structures formed in high-pressure experiments are studied using powder-diffraction techniques because single crystals do not usually survive the abrupt volume changes that occur at discontinuous phase transitions. X-ray diffraction (Nelmes and McMahon, 1994) is by far the most widely used technique, but neutron diffraction is also used, although it is normally limited to much lower pressures (see Klotz *et al.*, 1996). Other techniques are also useful to detect the occurrence of structural changes (Raman scattering, optical transmittance, resistivity measurements, etc.). See, for example, Besson *et al.* (1991) for a discussion of the merits of different methods for locating the thresholds of reconstructive phase transitions.

Due to the very small size of the samples (of order 100 μm) the diffracted x-ray beam is very weak. From the early 1980s synchrotron facilities became widely available for performing energy-dispersive x-ray-diffraction (EDX) studies in which the full synchrotron beam, containing a large range of wavelengths, falls on the sample and the diffraction pattern is recorded as a function of the x-ray energy at a single scattering angle. The introduction of the image plate detector by Shimomura *et al.* (1992) was an important advance in high-pressure powder-diffraction techniques. Nelmes and McMahon (1994) further developed these techniques so that a large part of the two-dimensional diffraction pattern could be recorded, which heralded the switch to angle-dispersive powder diffraction (ADX) in the 1990s. In this method a monochromatic beam of x rays is used, so that the intensity of the beam is much weaker. However, in compensation one records all of the diffraction lines at once. Integration around the diffraction rings then provides accurate values for the peak intensities and improves the signal/noise ratio. The structural determination normally involves full-profile Rietveld refinement (Rietveld, 1969; Langford and Louër, 1996), in which a structural model is proposed whose parameters are refined by minimizing the deviation of the calculated diffraction pattern from the observed one. The use of DAC's, ADX, and advanced methods for data acquisition and analysis has revealed many new and surprising results on high-pressure phases.

C. Experimental challenges

1. The pressurizing medium

The pressure-transmitting medium has a significant effect on conditions within the sample chamber. Ideally the medium should remain fluid at high pressures, and therefore materials such as a 4:1 methanol-ethanol mixture or silicon oil are used. However, at high enough pressures these materials become solid, and the stress in the pressure chamber then develops strong nonhydrostatic components and some inhomogeneity. This can affect the diffraction pattern and cause difficulties in determining the (average) pressure inside the chamber (see Sec. II.D). The use of N_2, Ar, or He increases the pressure range over which the stress remains nearly isotropic and homogeneous, but requires the use of cryogenic techniques or high-pressure gas loading which complicate the experimental setup.

The occurrence of nonhydrostatic stresses is both a difficulty and an opportunity. Experiments under nonhydrostatic conditions could be of significant value in exploring the elastic properties of solids. Moreover, the effects of nonhydrostatic stress on the structural stability of high-pressure phases is as yet a relatively unexplored field.

2. Coexistence of phases

The coexistence of different phases has often been reported over a range of pressures (see Sec. VI). The diffraction pattern then contains peaks arising from each phase, and the model of the diffraction pattern used in the Rietveld refinement procedure should consist of a weighted mean of the diffraction patterns of the constituent phases.

3. The effects of microstructure (texture)

The diffraction patterns of powder samples are complicated by the effects of microstructure or texture. The force in the DAC is applied uniaxially, and nonspherical microcrystallites will tend to align with their long axes perpendicular to the cell axis. This preferred orientation effect is relatively common in high-pressure samples and can alter diffraction peak intensities substantially. The effects of other microstructural features such as planar defects can also be significant. In these cases the availability of the two-dimensional diffraction pattern can be useful in detecting the effects of microstructure (Wright *et al.*, 1996) and offers the possibility of correcting for it by, for example, simply averaging over the diffraction rings.

4. Site order in binary compounds

The similarity in x-ray scattering powers of the chemical species in a binary compound often makes it difficult to distinguish between different occupations of the atomic sites which are compatible with a proposed structure. There are many examples of this among the IIB–VIA and IIIA–VA families (see Sec. VIII.E). In these cases extended x-ray-absorption fine-structure (EXAFS) spectroscopy can provide information on the degree of local ordering (see, for example, Hayes and Boyce, 1982). Total energy calculations can also be of significant value in determining the energies of different site occupations.

D. The measurement of high pressures

1. Direct calibration of the pressure

The static pressure p exerted on a body can be simply calculated as the ratio of the applied force to the surface area, $p=F/S$. However, when considering the transmission of the applied force to the sample contained within a high-pressure device, one must take into account the friction and deformation of the materials that constitute the pressure cell. In some simple cases where the behavior of the pressure device can be reliably modeled, it is indeed possible to evaluate accurately the pressure in the interior of the cell by measuring the externally applied macroscopic load. This is the case for hydrostatic pressure cells operating in the interval $\sim 0-10$ GPa, in which a piston compresses the liquid contained in a cylinder (piston-cylinder devices).

However, in a DAC or any other high-pressure cell operating above 10 GPa, the macroscopic force externally applied on the device is transmitted to the interior of the pressure chamber and to the sample in a complicated manner. This process is difficult to model because it depends on the mechanical properties of the materials from which the cell is composed and the design of the device. Although sophisticated calculations of the distributions of stress within a DAC under external loads have been performed (see Eremets, 1996, and references therein), this "direct" approach to calculating the pressure in DAC experiments is impractical.

2. Equations of state and primary scales

The key to measuring high pressures is to establish transferable *pressure scales*. Returning to the hydrostatic pressure cell, suppose we introduce a small sample of some material such as NaCl into the cylinder, which contains a much larger volume of liquid. By measuring the lattice parameter of NaCl using x-ray-diffraction techniques, we can establish a correspondence between the lattice parameter and the pressure. This scale can then be used to measure the pressure in the sample chamber of other cells (in the interval $\sim 0-10$ GPa), provided we place a sample of NaCl in the chamber and measure its lattice parameter.

Beyond ~ 10 GPa, pressure measurements are based on the equations of state or $p(V)$ isotherms of certain reference materials (e.g., Cu, Ag, Au, Pt, or NaCl). These equations of state, known as *primary scales* or *pressure standards*, are normally established from a combination of ultrasonic data and results from shock-wave experiments. Comparisons between different primary scales show a good degree of consistency (Holzapfel *et al.*, 2001). The equation of state of a material can also be calculated and used as a pressure scale. Among these scales, the equation of state of NaCl calculated by Decker (1971) is widely used. The Decker equation yields pressures that are consistent with other experimentally established practical pressure scales.

These scales can be directly applied to the measurement of pressure inside a DAC or other high-pressure devices. This is done by introducing a small chip of the reference material into the cell, along with the sample to be studied. Under compression, the lattice parameter of the reference material can be accurately measured using x-ray diffraction, and the pressure can be obtained through the reference equation of state.

3. The ruby technique

The practical pressure scales are commonly used in the calibration of other "secondary" scales, which can be more easily used in high-pressure experiments. At very high pressures it becomes harder to measure the lattice parameters of reference materials, but fluorescence studies are straightforward. By far the most widely used of these secondary scales is the *ruby scale*, in which a small grain of ruby ($Al_2O_3:Cr^{3+}$) is introduced into the cell and fluorescent emission is stimulated by a laser or other means. The shift in wavelength $\Delta\lambda$ of the so-called R_1 ruby fluorescence line is then measured. This line has an intense red color ($\lambda_0=6942$ Å under normal conditions), and under moderately high compression ($\lesssim 10$ GPa) its shift is almost linear with applied pressure, with $dp/d\lambda=0.2746$ GPa Å^{-1} (Piermarini *et al.*, 1975). At higher pressures the small deviation from linear behavior is satisfactorily accounted for by the empirical expression

$$p(\mathrm{GPa})=\frac{1904}{B}\left[\left(1+\frac{\Delta\lambda}{\lambda_0}\right)^{B}-1\right], \tag{1}$$

where $B=7.665$ for quasihydrostatic conditions (Mao, 1989). This is a simple and convenient way of measuring the pressure in a DAC. The R_1 line is also sensitive to temperature, with a temperature coefficient $d\lambda/dT=0.068$ Å K^{-1}. A variation in temperature of 10 K therefore has the same effect as a variation in pressure of 0.2 GPa. Other materials can also be used to establish similar luminescence scales (e.g., SrFCl:Sm^{2+}).

4. Accuracy in the measurement of pressure

The pressures of interest in this review cover a very large range of several hundreds of GPa. The first pressure-induced phase transition occurs at pressures as "low" as ~ 1 GPa, in the zb→cinn transition of HgSe, or as high as ~ 50 GPa in the wur→NaCl transition of GaN. Pressures above 400 GPa have been achieved in-

side a DAC. "Acceptable accuracy" in this context might be ~0.1 GPa in the range up to ~10 GPa, and 0.5–1 GPa at pressures of a few tens of GPa. It is not always easy to assess the absolute accuracy achieved in the measurement of pressure within a DAC, particularly in the range of several tens or hundreds of GPa. This certainly cannot be better than the accuracy of the primary scale used in the calibration of the pressure sensor, but several other factors may add to the uncertainty. In the ruby technique, for example, the spectral resolution of the R_1 line, the control of the temperature, whether the pressure is isotropic or not, and the applicability of Eq. (1) all affect the measured pressure. At pressures at which the R_1 lines are very well resolved, a *variation* in pressure can be measured with a precision of 0.03 GPa or even 0.01 GPa, under optimal conditions and at very low temperatures. At pressures of around 100 GPa, the intensity of the R_1 line is reduced and fluorescence from the diamond anvils occurs, which results in rather poor resolution. The sensitivity of the ruby scale is also poor at very low pressures (<1 GPa). Holzapfel *et al.* (2001) estimate that, taking into account all the factors, the accuracy of the measurement of the pressure with the ruby technique is typically ~1% up to about 10 GPa and possibly ~3% around 100 GPa. These figures should be kept in mind when comparing the different theoretical and experimental data.

III. THERMODYNAMIC STABILITY

A. Global thermodynamic stability

The *globally stable phase* at some pressure and temperature is the one with the lowest Gibbs free energy G, where

$$G = U + pV - TS, \tag{2}$$

and U is the internal energy, p is the pressure, V is the volume, T is the temperature, and S is the entropy. Very often the observed phase corresponds to the globally stable one, although there are examples of long-lived metastable phases. We shall also have occasion to refer to the Helmholtz free energy F, defined as

$$F = U - TS. \tag{3}$$

The very large pressures that can be obtained in high-pressure experiments may result in volume reductions in the materials considered here of greater than a factor of 2. The variations in temperature that will normally concern us produce much smaller changes in the relative stabilities of different phases. We shall therefore be mostly concerned with the Gibbs free energy at zero temperature, which is the enthalpy H and is given by

$$H = U + pV. \tag{4}$$

At zero temperature the globally thermodynamically stable phase at pressure p is the one with the lowest enthalpy.

Although the zero-temperature theory often results in excellent agreement with experiment, the effects of finite temperature may be significant. One effect is that on increase of temperature it becomes easier to pass over energetic barriers to other structures, so that hysteresis is reduced. Another important effect is that the vibrational contribution to the Gibbs free energy may alter the equilibrium coexistence pressures and volumes (see Sec. V.F).

B. Local stability

We use the term *local stability* to describe the stability of a crystal under pressure to infinitesimal changes in structure. A crystal is locally stable if the change in the enthalpy is positive for all possible infinitesimal changes in structure, i.e., the first-order change in the enthalpy must be zero and the second-order change must be positive. Local stability is a necessary condition for global stability, but of course it is not a sufficient condition. However, it is not straightforward to locate the globally stable phase via calculations because of the effectively infinite number of structures which must be investigated.

The sample in a DAC consists normally of a powder, each grain of which contains a very large number of atoms. A grain may be modeled by a perfect crystal, i.e., an infinite periodic array of atoms. In the standard theory of lattice dynamics (see Born and Huang, 1956), continuous changes in the structure are described in terms of a homogeneous strain (in which the atoms move with the strain) and additional "phonon" displacements of the atoms, which may vary from one unit cell of the reference state to the next. A phonon displacement does not change the volume of the sample, and therefore the pV term in the enthalpy is unchanged, and for local stability we require that the second-order change in the internal energy be positive for any phonon displacement. This condition reduces to the familiar criterion that all the phonon frequencies must be real. The important difference for homogeneous strains is that they change the shape and/or volume of the sample, and therefore the second-order changes in both the U and pV terms contribute, which results in a modification to the stability relations for the elastic energy. The conditions for stability against homogeneous strains have been discussed by Wang *et al.* (1993, 1995).

IV. SIMPLE CONCEPTS AND MODEL CALCULATIONS

In this section we deal with simple concepts of interatomic bonding and model calculations of structural phase transitions. In today's world there is no need to rely on these to obtain theoretical transition pressures and structures—that is what first-principles methods are for. The point of discussing them here is that their simplicity yields insights into the underlying physics and provides a proper context for considering the first-principles calculations.

Some of the behavior of structures under pressure can be understood in terms of very simple concepts. As the pressure is increased there is a tendency to adopt structures with higher coordination numbers and larger pack-

ing fractions so as to reduce the nuclear repulsion energy. At high enough pressures it is expected that close-packed structures will be formed, but, among the compounds considered here, only Si and Ge have so far been observed to transform into close-packed structures, adopting the hcp structure at 41 GPa and 160–180 GPa, respectively.

The $A^N B^{8-N}$ materials studied here are primarily s-p bonded. In the low-pressure tetrahedral phases the bonding is covalent in the group-IVA elements, while in the group IIIA–VA and IIB–VIA compounds some fraction of the electronic charge is transferred from the cation to the anion because of the electronegativity difference between the atoms. In this case the bonding is partially ionic and the electrostatic attraction between nearest-neighbor ions tends to lower the energy. One of the simple consequences of this is that IIIA–VA or IIB–VIA structures with "wrong bonds," i.e., adjacent atoms of the same type, are generally not energetically favored.

A historical model within a billiard-ball view of crystal structure was formulated in terms of the ratio of the cation and anion radii, r_c and r_a (Born and Meyer, 1932). One can argue that when, for example, the anion is much larger than the cation, highly unfavorable anion-anion contacts may occur. In the NaCl structure this happens when $r_c/r_a < \sqrt{2}-1$, at which point a transition might be predicted to a tetrahedral structure in which the anions are further apart. The ratio r_c/r_a then defines a critical value which distinguishes between fourfold- and sixfold-coordinated structures. This argument is of course very crude, and the empirical rule is often violated, but it does illustrate the idea of phenomenological scales, which will be discussed in more detail in Sec. IX and used to identify trends in behavior in Sec. X.

To make further progress we must consider the electronic structure of the constituent atoms and use simple concepts from molecular-orbital or tight-binding theory. The occurrence of fourfold-coordinated structures at low pressures is explained by the formation of strong sp^3 hybridized orbitals on each atom which are directed from the center of a cube along the opposite body diagonals. In the IIIA–VA and IIB–VIA compounds the difference in electronegativities leads to partially ionic bonding, which lowers the energy, but at the cost of reducing the sp hybridization. In the IA–VIIA compounds, such as NaCl, the bonding is very strongly ionic, and even at zero pressure sixfold-coordinated structures are adopted. The first phase transition in the group-IVA, IIIA–VA and IIB–VIA compounds is to a sixfold-coordinated phase, and in these structures the bonding has more p^3 character because the degree of sp hybridization is reduced, and the occupation of the d orbitals becomes significant.

There are also significant changes in the electronic properties of atoms as one goes down a column of the Periodic Table; for example, the sp hybridization generally decreases. Taking the group-IVA atoms as an example, the sp hybridization in C is very strong, while it is significantly weaker in Si, Ge, and Sn and is essentially absent in Pb. In C the absence of a p core means that the potential felt by the $2p$ electrons is very strong, so that the $2p$ orbitals are of similar size and energy to the $2s$ orbital, which results in very strong sp hybridization. In Pb relativistic effects lower the energy of the $6s$ orbital substantially, and the cost of promoting an electron from the $6s$ to $6p$ orbitals is so large than neither sp^2 or sp^3 bonding arrangements are favorable (Christensen *et al.*, 1986).

One of the surprising conclusions from early studies of the electronic structure of solids was that nearly free-electron theory is applicable even to the valence bands of diamond (Mott and Jones, 1936). In pseudopotential theory this fact is exploited by introducing an effective potential felt by the valence electrons which includes the electrostatic and Pauli repulsion from the core electrons. For sp bonded materials these pseudopotentials are often weak enough to be treated within nearly-free-electron theory. The development of pseudopotential theory for electronic structure calculations started in the late 1950s (Phillips and Kleinman, 1959) and is still underway today. The pseudopotential theory of cohesion and structure, based on calculating the total energy to second order in the pseudopotential, has been reviewed by Heine and Weaire (1970), including a discussion of high-pressure phases.

Quite accurate results for coexistence pressures and volumes in some IIIA–VA and IIB–VIA compounds were obtained by Soma (1978) using pseudopotential perturbation theory. The expression for the total energy within second-order perturbation theory can be written in terms of a pairwise interatomic interaction potential. The potential obtained in this way is in fact a rearrangement potential for the atoms at constant total volume, i.e., it describes the differences in energy between structures at constant volume. Hafner and Heine (1983) described the trends in the crystal structures of the sp bonded elements in terms of rearrangement potentials, including a p-T phase diagram for the group-IVA elements.

V. FIRST-PRINCIPLES ELECTRONIC STRUCTURE CALCULATIONS

First-principles electronic structure calculations allow an accurate evaluation of the total energy of a system as a function of the atomic positions (see Payne *et al.*, 1992, and Pickett, 1989).

A. Density-functional theory

The complicated many-body problem for the electrons is simplified using density-functional theory (DFT). DFT is a rigorous formulation of the many-body problem in which the fundamental variable is the (electronic) charge density. Hohenberg and Kohn (1964) proved that the total energy of the ground state is a unique functional of the charge density and that this functional is minimal for the correct density. The variational principle of DFT provides the theoretical basis for

studying interacting electronic systems entirely in terms of the electronic density. However, in a direct application of the Hohenberg-Kohn theorems, approximations to both the kinetic and exchange-correlation energy functionals are required, which leads to Thomas-Fermi-like theories giving rather poor agreement with experimental data (Dreizler and Gross, 1990). The Hohenberg-Kohn theorems are in themselves a considerable conceptual advance, but they do not immediately lead to a practical advance in the calculations. A second breakthrough was made by Kohn and Sham (1965), who avoided the necessity for approximating the large and important contribution from the kinetic energy, which has proved very difficult to approximate accurately as an explicit functional of the density. Kohn and Sham (1965) introduced the idea of an auxiliary noninteracting system which exactly reproduces the charge density of the interacting system. The ground state of the noninteracting system is described by a set of noninteracting Schrödinger-like equations, known as Kohn-Sham equations, which must be solved self-consistently. In atomic units (Hartree) the Kohn-Sham equations are

$$\left[-\frac{1}{2}\nabla^2 + V_{\mathrm{H}}(\mathbf{r}) + V_{\mathrm{XC}}(\mathbf{r}) + V_{\mathrm{ext}}(\mathbf{r})\right]\psi_i(\mathbf{r}) = \varepsilon_i \psi_i(\mathbf{r}), \tag{5}$$

where V_{H} is the electrostatic potential from the electronic charge density, which is known as the Hartree potential, V_{XC} is the exchange-correlation potential, and V_{ext} is the external potential from the ions. The electronic density is given by $\rho(\mathbf{r}) = \Sigma_{i=1}^{N} |\psi_i(\mathbf{r})|^2$, where the sum is over the N levels of lowest energy (N is the number of electrons in the system).

There is still a need for approximation, but only for the contribution to the energy from the effects of the exchange-correlation interactions between the electrons. Many approximate exchange-correlation functionals are available, but almost all the results reviewed here were obtained with the local-density approximation (LDA), in which the contribution to the exchange-correlation energy from a point in space is taken as that from a uniform electron gas at the density appropriate for that point. The domain of applicability of the LDA has been found to extend far beyond the uniform electron gas, and accurate results may be obtained for strongly inhomogeneous systems. However, in some situations the LDA is inadequate (see Jones and Gunnarsson, 1989), and it is desirable to improve upon it. Ideas on how to improve on the LDA include the generalized gradient approximation (GGA), which involves the density and its gradient at each point (Perdew *et al.*, 1996), and orbital-dependent functionals, e.g., exact exchange potentials (Gross *et al.*, 1994; 1996). One of the motivations for carrying out theoretical studies of materials under pressure is to investigate how well approximate functionals such as the LDA and GGA perform in describing the wide range of chemical bonding that occurs in high-pressure phases.

B. Band-structure methods

One of the important advantages of Kohn-Sham DFT is that the interacting problem is mapped onto a set of single-particle equations familiar from band-structure theory. The well-developed machinery of band-structure theory can therefore be used to solve them, and the field of "band-structure calculations" has evolved into the modern field of "total-energy calculations." The computational method chosen to solve the Kohn-Sham equations is of great importance. One would like to obtain equal accuracy for high- and low-symmetry phases, and it is enormously advantageous to be able to calculate the derivatives of the total energy with respect to the positions of the atoms and the shape of the unit cell, i.e., the forces on the atoms and the stress tensor. Preeminent in these regards is the plane-wave method, in which the periodic parts of the Kohn-Sham wave functions are represented by Fourier series. Many plane waves are required to represent the wave functions, but the simplicity of the plane-wave representation allows for very efficient algorithms to be used in the solution of the equations. Plane waves are therefore used almost exclusively with pseudopotentials, which replace the core electrons and make smooth pseudovalence wave functions. Care must be taken when dealing with systems in which polarizable semi-core electrons (the outermost occupied d electrons in the core for the IIB and IIIA families) play a role in the chemical bonding, as is the case, for example, in GaN (see Sec. VII.B.3). A proper account of such semi-core effects requires the explicit treatment of these orbitals in the valence (Fiorentini *et al.*, 1993; Serrano *et al.*, 2000) although for many purposes it is perfectly acceptable to consider these orbitals to be frozen.

The vast majority of the calculations reviewed here were performed using the plane-wave pseudopotential (PWPP) method, although today there are worthy rivals capable of yielding the very high numerical accuracy required for such studies. Two other widely used schemes are the full-potential linearized muffin-tin orbital method (FP-LMTO; see Dreysse, 2000) and the full-potential linearized augmented plane-wave method (FP-LAPW; see Singh, 1994). Other DFT implementations of the all-electron and pseudopotential methods use basis sets consisting of linear combinations of Gaussian orbitals or linear combinations of atomic orbitals (LCAO), in particular for Hartree-Fock (HF) -type calculations. If the calculations are performed carefully enough, the PWPP, FP-LMTO, and FP-LAPW methods normally give results in very good agreement with one another. As an example, consider Si-VI, the elusive high-pressure phase of Si intermediate between the simple hexagonal (sh) Si-V phase and the hexagonal-close-packed (hcp) Si-VII phase (see Sec. VII.A.2.c). Si-VI was first observed in 1984 (Olijnyk *et al.*) but its structure (Cmca) has only recently been resolved (Hanfland *et al.*, 1999). Both LMTO calculations (Ahuja *et al.*, 1999; Christensen, Novikov, and Methfessel, 1999) and PWPP calculations (Mujica *et al.*, 2001a, 2001b) confirm the exis-

tence of an interval of stability for the Cmca phase with sh/Cmca and Cmca/hcp coexistence pressures that agree very well both among the different calculations [(33(2),41(5)) GPa (Christensen, Novikov, and Methfessel 1999); (34.0,41.5) GPa (Ahuja *et al.*, 1999); (36.0,43.5) GPa (Mujica *et al.*, 2001a, 2001b)] and with the experimental values for the onset of the sh→Cmca transition (~38 GPa) and Cmca→hcp transition (~42 GPa; Hanfland *et al.*, 1999). This agreement is all the more outstanding if one realizes that an error of ~20 meV per atom in the calculation of the difference in the energies of the phases would result in the total disappearance of the calculated interval of stability of the Cmca phase (see Fig. 2 of Christensen, Novikov, and Methfessel, 1999)! A similar level of agreement exists for the structural parameters of the Cmca phase.

C. First-principles molecular dynamics

One of the most important milestones in practical DFT calculations was achieved by Car and Parrinello (1985), who invented the first-principles molecular-dynamics method. This work led to much more efficient algorithms and opened the way for applications to many new problems. In first-principles molecular dynamics the motions of the atoms are taken to be classical and are followed using Newton's laws of motion, just as in a classical molecular-dynamics simulation, but the forces on the atoms are calculated using first-principles DFT methods. The greater accuracy of first-principles methods gives a realistic description of the bond breaking which often occurs in phase transitions. The important point about molecular dynamics is that it allows dynamical simulations in which one can watch what happens without imposing one's preconceived notions of events. First-principles molecular-dynamics simulations can be used to follow the evolution of a phase transition and, for example, determine the transition path and the relative orientation of the two phases, or one can gradually cool down a solid from high temperatures in the computer and try to find new stable phases. One can also study the melting of solids using first-principles molecular-dynamics methods (Sugino and Car, 1995), so that the entire p-T phase diagrams of materials could be investigated. Focher *et al.* (1994) have used first-principles molecular-dynamics methods to study phase transitions in Si, while Scandolo *et al.* (1995) studied the gra→cd transition in C, as will be described in Sec. VII.A.1. Such calculations are computationally expensive, and currently simulations can only be run for periods of tens of picoseconds, which is not long enough for some of the processes of interest. However, first-principles molecular dynamics is expected to play an important role in future theoretical studies of phase transitions.

D. Accuracy of DFT calculations

The energy differences between many of the competing phases are very small, and a resolution of a few meV per atom is sometimes required to distinguish their relative stabilities (see Sec. V.E). The accuracy of the LDA or GGA is orders of magnitude worse than this, so how is it possible for such calculations to give reasonable results? The answer is that one relies on a cancellation of errors between the energies of the competing phases, which appears to work extremely well as long as the nature of the bonding is similar. One also requires cancellation of the inevitable numerical approximations in the calculated energies of the competing phases, which are mostly due to the finite basis sets used to describe the wave functions and the approximations used in the Brillouin-zone integrations. The control of numerical approximations is particularly simple within the PWPP method, but we emphasize that excellent results can also be obtained with other techniques.

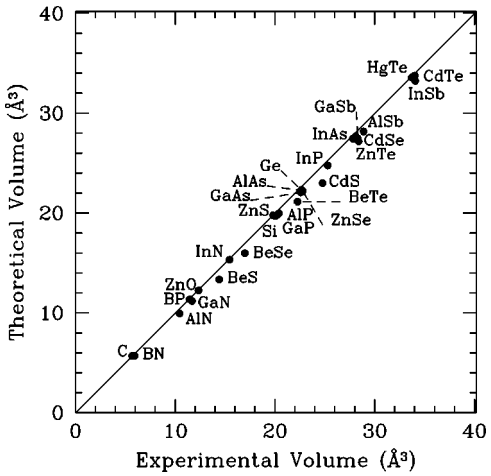

FIG. 2. Comparison between calculated (using the LDA) and experimental equilibrium volumes per atom for the low-pressure phase of several $A^N B^{8-N}$ materials.

To illustrate the accuracy of DFT calculations we show in Fig. 2 the experimental equilibrium volumes at zero pressure for different materials and those calculated using the LDA. It is well known that the LDA-DFT scheme normally yields equilibrium volumes that are smaller than experimental values (within ~1–3% for the materials reviewed here). Nevertheless, Fig. 2 shows very good agreement with experiment, which can also be expected for the high-pressure phases of interest in the present review (see also Fig. 6).

E. Theoretical studies of phase stability; fixed-symmetry calculations

Two different computational strategies are commonly used for identifying the lowest-enthalpy structure as a function of pressure. One can either minimize the internal energy with respect to the structural parameters at constant volume and construct the enthalpy using Eq. (4), or one can directly minimize the enthalpy at constant pressure. The minimization of the energy or enthalpy is performed by driving the system towards lower

energy or enthalpy states using the calculated values of the forces on the atoms and the components of the stress tensor (see, for example, Pfrommer *et al.*, 1997b).

Whether one minimizes the energy at constant volume or the enthalpy at constant pressure, one faces the problem of the likely existence of many local minima. As one can never investigate all possible starting points for the minimization, one can never be sure that the global minimum has been obtained. This is a difficult problem common to many branches of science, and one to which there is no wholly satisfactory solution. It should be remembered, of course, that Nature itself sometimes finds this problem difficult—hence the occurrence of metastable phases—but Nature generally explores far more possible structures than can be investigated in calculations. This fact has limited the predictive power of the calculations, although we will describe instances where successful predictions of new phases have been made, and where predictions are still waiting to be tested.

Typically the search of configuration space is restricted to certain *classes of configurations* defined by the number of atoms in the unit cell and particular space-group symmetries. In this case one cannot immediately decide whether the structures obtained would even be local minima if the imposed restrictions were to be relaxed. There is, however, a solution to this problem, which is becoming very important in first-principles studies of high-pressure phases. As described in Sec. III.B, a crystal is locally stable if all of its phonon frequencies are real and its elastic constants satisfy certain inequalities. These quantities can, however, be obtained directly from first-principles calculations using density-functional perturbation theory (DFPT) (see Baroni *et al.*, 2001). These developments have not so far been used very widely in theoretical studies of phase stability, but it is clear that they offer considerable advantages and will prove very important in the future. It is unlikely that one can predict many phase transitions by analyzing local stability because the vast majority of transitions are first order, i.e., the transition is from one locally stable phase to another one. However, starting from an equilibrium structure one can use the stability analysis to determine whether the structure is stable or unstable with respect to infinitesimal changes. If it is unstable the analysis also reveals which small changes in the structure lower the enthalpy, which can be used to predict more stable configurations. Such calculations have been performed for several group-IVA, IIIA–VA, and IIB–VIA materials by Ozoliņš and Zunger (1999) and Kim *et al.* (1999).

In Fig. 3 we show schematic energy-volume $[E(V)]$ and enthalpy-pressure $[H(p)]$ curves for four phases of some material. This figure illustrates typical output data from a series of total-energy calculations with fixed symmetry and how it can be analyzed to obtain the transition pressures. Phases I and II have equal enthalpies at the two points $E_{\mathrm{I}}(V_{\mathrm{I}})$ and $E_{\mathrm{II}}(V_{\mathrm{II}})$, respectively, where the common tangent touches the energy-volume curves shown in Fig. 3(a). The negative of the slope of the common tangent gives the coexistence or equilibrium pressure, $p_e(\mathrm{I/II})=-(E_{\mathrm{II}}-E_{\mathrm{I}})/(V_{\mathrm{II}}-V_{\mathrm{I}})$. In Fig. 3(b) the corresponding enthalpy-pressure relations are illustrated. The two $H(p)$ curves for phases I and II cross at the pressure $p_e(\mathrm{I/II})$. The large variation of the enthalpy with pressure, which obscures the relative stability of the phases (for which only the difference in enthalpies is relevant) has been subtracted in Fig. 3(c) by plotting the enthalpy with respect to that of phase I, which is taken as a reference. Phases iii and iv are not stable in any pressure range. However, the enthalpy of phase iii is rather close to those of phases I and II near $p_e(\mathrm{I/II})$ and it is conceivable that the effects of temperature or an improvement in the calculations could result in the emergence of a narrow field of stability for phase iii.

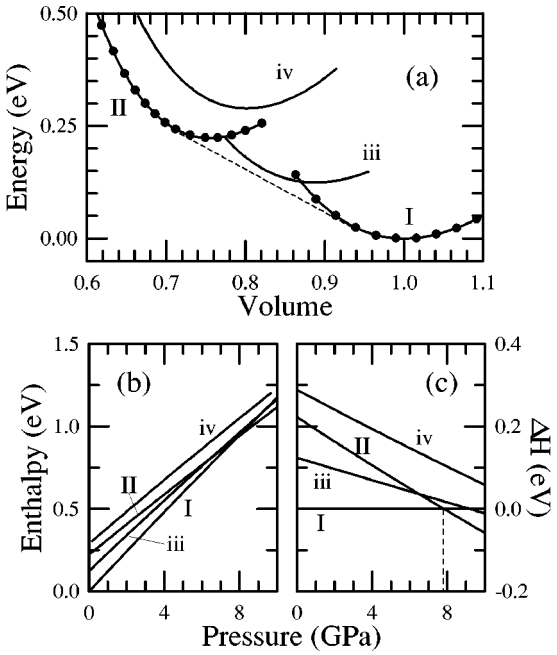

FIG. 3. Typical output data from a series of total-energy calculations: (a) Schematic diagram of the energy-volume curves for four phases of a material. For phases I and II we have indicated by filled circles the discrete set of calculated $E(V)$ points. The curves correspond to fitting of the calculated points [in the present case, using a Murnaghan-type expression (Murnaghan, 1944)]. (b) Schematic diagram of the enthalpy-pressure curves for the same four phases. (c) The difference in enthalpy, ΔH, from phase I.

Even if phase iii is unstable it is possible that the I $\rightarrow$iii transition could be observed at a slightly larger pressure if the I$\rightarrow$II transition were suppressed by a large activation barrier. Conversely, a iii$\leftarrow$II transition could be favorable on *decrease* of pressure from phase II if the I$\leftarrow$II transition were impeded. In both cases, phase iii would exist only as a metastable phase. Of course, a proper theoretical study of these possibilities would require the investigation of the actual mechanisms of the transitions. We shall have an opportunity to mention several instances of metastable phases obtained upon decrease of pressure from high-pressure phases.

F. Effects of finite temperature on phase stability

Density-functional perturbation theory can be very useful in calculating the contribution to the Gibbs free energy from vibrational effects. The differences in Gibbs free energy between two phases can be calculated using a number of methods, such as thermodynamic integration or biased Monte Carlo methods, but these are very expensive. A simple alternative is to use the harmonic phonon frequencies which can be obtained within DFPT calculations (Baroni *et al.*, 2001). In the quasiharmonic approximation the vibrational contribution to the Gibbs free energy is written as a sum over the harmonic modes $(\nu,\mathbf{q})$, and the frequencies of the modes are allowed to depend on the volume, $\omega_\nu(\mathbf{q},V)$. The vibrational contribution to the Helmholtz free energy is then

$$F_{\mathrm{vib}}=k_B T\sum_{\nu,\mathbf{q}} \log\left[2\sinh\left(\frac{\hbar\omega_\nu(\mathbf{q},V)}{2k_B T}\right)\right], \tag{6}$$

which includes both finite temperature and zero-point motion effects. The total Gibbs free energy is then

$$G=U+pV+F_{\mathrm{vib}}, \tag{7}$$

where U is the internal energy at $T=0$. One scheme for obtaining the equilibrium structure at pressure p is as follows. First, minimize the Helmholtz free energy $F=U+F_{\mathrm{vib}}$ with respect to the structural degrees of freedom x_i, while holding the temperature and volume fixed. This gives the values of the structural degrees of freedom as a function of volume and temperature, $x_i(V,T)$, and the Helmholtz free energy $F(V,T)$. The most stable structure at temperature T and pressure p is the one with the lowest value of $G(T,p)$. Gaál-Nagy *et al.* (1999) used DFPT methods to study the temperature dependence of the diamond-to-β-Sn transition in Si (see Sec. VII.A.2.a). Neglect of the anharmonic effects at fixed volume is often a very good approximation at room temperature, but at higher temperatures or when there are soft phonon modes present, anharmonic effects can be important.

VI. SOLID-SOLID PHASE TRANSITIONS

At low pressures, group-IVA, IIIA–VA, and IIB–VIA materials tend to adopt open crystal structures and are mostly covalently bonded semiconductors, with some degree of ionic bonding in the IIIA–VA and IIB–VIA materials. At higher pressures more compact metallic structures are formed. The observed structures vary in coordination number from 3 to 12. The wide variety of bonding and structures adopted naturally leads to a wide range of types of structural phase transition.

Solid-solid phase transitions driven by changes in pressure can be divided into *reconstructive transitions*, which involve large changes at the transition including the breaking and forming of bonds, and *displacive transitions*, in which the positions of the atoms change by fairly small amounts at the transition (often accompanied by a small strain). Phase transitions can also be classified according to their thermodynamic "order," which is the order of the derivative of the Gibbs free energy that first shows a discontinuity. In most text books the case of temperature-induced phase transitions is discussed and the derivative is with respect to temperature, but here we are mainly interested in pressure-induced phase transitions, so that we have

$$\left.\frac{\partial G}{\partial p}\right|_T = V, \tag{8}$$

i.e., a first-order phase transition involves a discontinuous change in volume at the transition. In a second-order phase transition the second derivative of the Gibbs free energy with respect to volume, which is proportional to the compressibility, is discontinuous. Experimentally it can be very difficult to distinguish between a second-order phase transition and a weakly first-order one. Group-theoretical methods based in the Landau theory of phase transitions (Landau, 1937; Landau and Lifshitz, 1980) have proved very useful in the analysis of the symmetry changes consistent with second-order phase transitions. A brief review of the symmetry rules used in the Landau theory can be found, for example, in the book by Evarestov and Smirnov (1993). Group theoretical analysis can also be used to propose possible transition paths for reconstructive phase transition (Stokes and Hatch, 2002).

Many of the phase transitions discussed here are of the displacive type, and most are certainly first order, although the discontinuity in the volume can be small. Second-order displacive phase transitions occur via the "soft-mode" mechanism, in which the energy associated with a vibrational mode or a volume-preserving shear strain goes to zero. In practice the energy of the mode often does not go precisely to zero, but instead the transition is accompanied by a small change in volume and is weakly first order. These transitions normally show only a small amount of hysteresis. Such transitions are quite common in the materials discussed here, for example, the β-Sn$\rightarrow$Imma$\rightarrow$sh transitions in Si might best be described as due to a soft optic phonon at the zone center which couples to cell strain (see Fig. 4 and Sec. VII.A.2.b).

All reconstructive phase transitions are first order, sometimes strongly so. In this case there may be large kinetic barriers which impede the transition at the equilibrium pressure of the two phases. The transition may then not be observed at all, and when it is observed it is "sluggish." This leads to hysteresis in which the transition pressure observed on increasing the pressure is larger than that observed on decreasing the pressure. The true equilibrium thermodynamic pressure should lie somewhere in between. The middle of the hysteresis interval is conventionally taken as a crude approximation to the equilibrium pressure, and the half width of the interval as a measure of its uncertainty, although there is no firm theoretical basis for these assumptions. Early practitioners tended to compare the onset or threshold of the forward transition with calculated equilibrium pressures, but in fact the actual equilibrium pressure may be significantly lower.

High-temperature experiments can be of significant

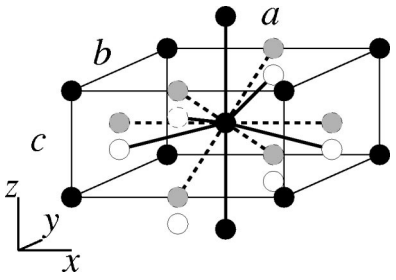

FIG. 4. The β-Sn, Imma, and sh structures in the common Imma representation. The black circles form sublattice 1, which is common to all three structures. In the β-Sn$\rightarrow$Imma $\rightarrow$sh transitions the atoms of sublattice 2 move from the positions of the unfilled circles (β-Sn structure) to the positions of the gray circles (sh structure), with some accompanying lattice strains. Imma structures are formed at the intermediate positions. Note that the c (or hexagonal) axis of sh is along the x axis in this representation.

value here. At higher temperatures the amount of hysteresis decreases, and therefore the equilibrium pressure can be identified more accurately (see Fig. 9). Moreover, with enough experimental information about the p-T behavior of the material, one can attempt to give a better experimental estimate of the equilibrium pressure using thermodynamic relations and the location of the triple point. This pressure could be compared more properly with theoretical values, as long as the effects of temperature are included in the calculations (see Sec. V.F). In many first-order pressure-driven transitions the equilibrium pressure is not very sensitive to temperature.

In some cases the transition is absolutely irreversible, i.e., the original structure is not retrieved after releasing the pressure. In this case a metastable phase is obtained, which may be very long lived. Metastable phases are most commonly encountered in covalently bonded materials. If a transformation involves a covalently bonded network structure, then the intermediate states must contain broken bonds and therefore be high in energy, which results in a large kinetic barrier. In transitions between metallic phases the atoms can often slide over one another without major disruption to the bonding, and therefore the kinetic barriers tend to be smaller.

For most of the materials considered here the first transition encountered on increasing the pressure from atmospheric conditions is from a low-pressure fourfold-coordinated covalently bonded semiconducting phase to a sixfold-coordinated metallic phase. For example, in germanium the low-pressure diamond phase transforms to the metallic β-Sn phase. This transition is reconstructive because it involves a complete reorganization of the interatomic bonding. On rapid release of pressure at room temperature from the β-Sn phase, the diamond structure is not recovered, but the metastable fourfold-coordinated bc8 phase appears, which over a period of about a day transforms into a phase that is believed to have the same structure as Si-IV (Nelmes, McMahon, Wright, Allan, and Loveday, 1993; see Sec. VII.A.2.e). On slow decrease of pressure from β-Sn-Ge a different metastable phase occurs, the fourfold-coordinated st12 form, which appears to last indefinitely under ambient conditions. The st12$\leftarrow\beta$-Sn transition is reversible (Qadri *et al.*, 1983). Presumably the rate constant for β-Sn to transform into the diamond phase at room temperature is very small in germanium, but that for st12 is considerably larger, and that for bc8 is larger still. However, at high temperatures (400–500 K) Brazhkin *et al.* (1995) report the transformation of the β-Sn phase into the diamond phase on decrease of pressure, whereas at low temperatures ($\sim$100 K) the recovered phase is amorphous. This example shows the considerable complexity in behavior that can be introduced by kinetic factors and the occurrence of metastable phases.

Most of the high-pressure phases of the IIIA–VA and IIB–VIA compounds appear to be well ordered, but some show strong evidence of being site disordered. Equilibrium order-disorder transitions can only occur at finite temperatures. Such transitions can be induced by a change in temperature or sometimes by a change in pressure. Site disorder is not generally energetically favored in IIIA–VA and IIB–VIA compounds because "wrong bonds" (see Sec. IV) between like atoms are high in energy, but disordered phases can be stabilized at elevated temperatures by their larger configurational entropy. Site-disordered phases have been reported in several IIIA–VA compounds such as the site-disordered Cmcm phase observed in GaP and the site-disordered Imma phases of GaSb and InSb. Whether these disordered structures are true equilibrium phases or whether they arise from kinetic effects is uncertain at the moment.

The concept of "wrong bonds" is very important in understanding the behavior of these materials. The fact that wrong bonds are high in energy makes the analog of some phases which are highly competitive in group-IVA elements not favored in the IIIA–VA and IIB–VIA binary compounds. This also means that phase separation in the binary compounds is unlikely, and they can be considered to be one-component systems. The coexistence of different phases has been often reported in high-pressure experiments over a range of pressures, but according to the Gibbs phase rule (see Callen, 1985) no two solid phases in a one-component system can exist in thermodynamic equilibrium over a finite range of applied pressures. This behavior must therefore result from an inhomogeneous distribution of stress in the sample or kinetic effects.

VII. RESULTS FOR EACH MATERIAL

In this section we review the present experimental and theoretical knowledge of the pressure-induced phase transitions and phase diagrams of the group-IVA elements and IIIA–VA and IIB–VIA compounds. A brief description of the structures of the phases is given in the Appendix. The abbreviations used for the structures are given in Tables IV and V in the Appendix. We also provide the label of each phase (I, II, . . .) which is commonly used in the literature, although this nomen-

clature requires some rationalization in order to accommodate the new discoveries. Not all the phases have been labeled.

A summary of the information concerning the observed sequence of transitions at room temperature is given in Tables I–III, where we have collected representative experimental and theoretical results for each transition. The transition pressure reported in experiments, p_t, corresponds normally to the pressure at the onset of the transition, that is, when the first indication of the new phase is observed. Some transitions are irreversible and in several other instances the reverse transition (decreasing pressure) has not been studied, and therefore most values listed in the tables pertain to the direct transition (increasing pressure) only. The theoretical value p_e is the calculated equilibrium pressure of the two phases, at zero temperature unless otherwise stated (see Sec. V.E). ΔV is a measure of the fractional change in volume at the direct transition (in percent). Two practices coexist in the literature: (a) giving $\Delta V_t = (V^t_{\rm LP} - V^t_{\rm HP})/V^t_{\rm LP}$, with $V^t_{\rm HP}$ and $V^t_{\rm LP}$ being the volumes of the high- and low-pressure phases at the transition, respectively, and (b) giving $\Delta V_0 = (V^t_{\rm LP} - V^t_{\rm HP})/V_0$, with V_0 the volume of the equilibrium phase at zero pressure. Rather than adhering to one of these definitions we have preferred to quote the experimental and theoretical results as originally published, signifying the second case (ΔV_0) by the use of italics.

A. Group-IVA elements

1. C

The stable form of C under normal conditions is hexagonal (or Bernal) graphite (gra). The denser diamond phase (cd), which lends its name to that of the structure, is estimated to be thermodynamically stable above 1.7 GPa at 0 K. The gra→cd transition does not occur at low temperatures, due to its very large activation energy, and it requires the concurrence of high pressures and temperatures (~5–9 GPa and 1200–2800 K using transition-metal catalysts). Along with the cd and the gra phases, C occurs naturally in the metastable rhombohedral-graphite (r-gra) modification. A metastable hexagonal-diamond (hd) form can also be synthesized in the laboratory (Bundy and Kasper, 1967). More exotic forms, such as crystalline C_{60} and other fullerites, have also been reported (see Sundqvist, 1999). Other metastable phases may be generated and remain untransformed due to large activation energies and kinetic effects (see Bundy *et al.*, 1996, and references therein for the p-T phase and transformation diagrams of C).

The diamond phase is insulating with a wide indirect band gap, while the layered graphite phase is a zero-gap semimetal. The very strong sp^3 bonding of diamond leads to its extreme hardness. Other outstanding properties are its chemical inertness and very large thermal conductivity. It is also transparent in a large range of wavelengths, which allows its use as a window for the radiation in the DAC (see Sec. II). In graphite, there is stiff sp^2 covalent bonding between nearest neighbors within a layer, but the weak van der Waals bonding between layers leads to a considerably larger compressibility than in the diamond form. The weak interlayer bonding makes graphite a very good solid lubricant.

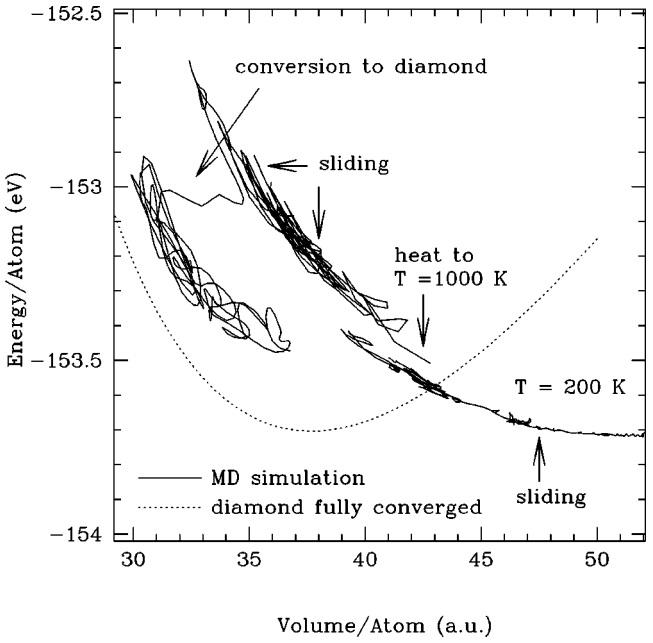

FIG. 5. Evolution of the gra→cd transition in C on the E-V plane as obtained from constant-pressure molecular-dynamics simulation for a 48-atom cell (from Scandolo *et al.*, 1995). The process simulated, from right to left, consists of the compression of graphite up to 30 GPa at $T=200$ K, then heating to 1000 K, and compression at a rate of ~300 GPa/ps up to 90 GPa, when the formation of diamond was observed. Pressure was then released. The dotted curve represents the fully converged $E(V)$ curve of the diamond phase.

At ambient conditions "diamonds are forever," persisting indefinitely as a metastable form, although they may revert to the stable graphite phase if exposed to intense heat or radiation. The zero-pressure stability of the diamond and graphite phases has been addressed theoretically in several first-principles studies (Mailhiot and McMahan, 1991; Furthmüller *et al.*, 1994). These studies yield a very small energy difference between the gra and cd phases. The gra→cd/hd transition has also been the subject of first-principles theoretical research aimed at gaining an understanding of its microscopic mechanism. Fahy *et al.* (1986) considered the activation barriers at zero temperature for the r-gra→cd transition, assuming a highly symmetric transition path in which atoms move collectively along the c axis of graphite. The gra→cd/hd transition has been studied *without* symmetry constraints by Scandolo *et al.* (1995), using first-principles molecular-dynamics methods. They find that the transition path proceeds via an intermediate orthorhombic stacking resulting from the sliding of graphite planes, which then collapses into either the hd or cd forms (see Fig. 5). Tateyama *et al.* (1996) have also studied the activation barriers and transition states of gra →cd/hd using molecular-dynamics and find that the formation of cd is favored over that of hd.

Once in the diamond phase no further transitions at low temperature have been observed up to the highest pressures reached. However, various first-principles studies indicate that at pressures above 1.1–1.2 TPa, diamond becomes unstable to a so-called bc8 phase (Yin, 1984; Biswas *et al.*, 1987; Fahy and Louie, 1987; Furthmüller *et al.*, 1994). At even higher pressures (~2.7 TPa) the simple cubic (sc) structure has been predicted to be favored over bc8 (Yin, 1984). Clark *et al.* (1995) have found a much lower coexistence pressure of 0.5 TPa between diamond and a r8 phase (precursor of the bc8 phase obtained in Si; see Sec. VII.A.2.e). First-principles calculations by Scandolo *et al.* (1996) suggest that a metallic sixfold-coordinated structure is formed at TPa pressures. Grumbach and Martin (1996) have also made a systematic study of solid and liquid phases of C using first-principles molecular-dynamics methods.

It may seem that the ultrahigh pressures involved in the predicted transitions undergone by diamond are beyond any "useful" range, but the issue of its stability is nonetheless important. First, it marks an absolute limit to the use of DAC-type high-pressure devices. Second, extreme pressures in this range can be found within planets (in conjunction with high temperatures), and therefore this kind of research is relevant to planetary science. In fact, C is a material in which the power of first-principles theoretical methods may lead to the prediction of many interesting properties currently not accessible experimentally.

2. Si and Ge

Si and Ge crystallize in the diamond structure and are indirect band-gap semiconductors. Their properties at high pressures show remarkable similarities, and they will be considered jointly here. There are, however, some significant differences because Ge has a larger and more polarizable core containing the $3d$ electrons, which gives an additional interatomic repulsion and leads to higher transition pressures between metallic phases (Chang and Cohen, 1986; Lewis and Cohen, 1993).

Several theoretical studies support the experimental sequence of transitions cd→β-Sn→Imma→sh→Cmca →hcp in Si and Ge, and a further hcp→fcc transition in Si. The calculated coexistence pressures and transition volumes are in rather good agreement with experiment (see Table I). This sequence indicates a monotonic increase in the coordination number of the structures adopted as pressure increases (see Table IV in the Appendix). Due to the greater uniformity of the environment of each atom the energy bands and density of states of the highest-pressure phases have a nearly-free-electron character, although remnants of the σ-type bonds can be found even at very high pressures (Schwarz *et al.*, 2000). The experimental and calculated variation of volume with pressure for the observed phases of Si is shown in Fig. 6.

We comment below separately on the different transitions because of the importance of these materials and the very large number of experimental and theoretical studies they have been subjected to.

a. cd→β-Sn

Under pressures of about 10–11 GPa, the diamond phases of both Si and Ge undergo a transition to the metallic β-Sn phase (Jamieson, 1963a; Baublitz and Ruoff, 1982a; Werner *et al.*, 1982; Qadri *et al.*, 1983; Hu and Spain, 1984; Olijnyk *et al.*, 1984; Hu *et al.*, 1986; Menoni *et al.*, 1986). One of the earliest successes of first-principles pseudopotential theory was the determination by Yin and Cohen (1980, 1982) that, from among the several candidates studied, the β-Sn structure was indeed favored in Si and Ge at high pressures, with a cd/β-Sn coexistence pressure in quite good agreement with experiment. Since this seminal paper the relative stability of the cd and β-Sn phases of Si (and to a lesser extent also of Ge) has been the subject of numerous theoretical studies[2] and it has become a benchmark for new theoretical methods (Moll *et al.*, 1995; Dal Corso *et al.*, 1996).

Values of the cd/β-Sn coexistence pressure calculated within the LDA tend to be lower than the experimental values for the onset of the cd→β-Sn transition, which is a general trend in the A^NB^{8-N} compounds reviewed here (see Sec. VIII.F). For example, accurate LDA-PWPP calculations give $p_e \approx 7.5$ GPa for Si (Needs and Martin, 1984; Boyer *et al.*, 1991; Needs and Mujica, 1995); cf. the experimental value of $p_t = 11.7$ GPa (McMahon *et al.*, 1994a). Calculations using the GGA give somewhat higher values of the coexistence pressures (10.2 GPa, according to Lee and Martin, 1997; see also Moll *et al.*, 1995, and Dal Corso *et al.*, 1996). The comparison between theory and experiment is complicated by the fact that significant kinetic barriers occur between the covalently bonded diamond phases and the metallic β-Sn phases. These transitions are irreversible, i.e., releasing pressure from the β-Sn phases does not result in recovery of the diamond phases (see Sec. VII.A.2.e), which makes determination of the coexistence pressure more difficult. Another issue is that the experimental values reported here are for room temperature, while the calculations correspond to zero temperature. Gaál-Nagy *et al.* (1999) have performed density-functional perturbation theory calculations of the Gibbs free energy within the quasiharmonic approximation (see Sec. V). They have found that including dynamical effects *reduces* the calculated coexistence pressures in Si and Ge by about 1.3 GPa at a temperature of 300 K. This increases the discrepancy between the calculated LDA values for the coexistence pressure and the experimental onset of the transition.

The pressure-driven transformation of cd-Si was simulated using molecular dynamics by Focher *et al.* (1994).

[2]See, for example, Biswas *et al.*, 1984, 1987; Chang and Cohen, 1984, 1985; Needs and Martin, 1984; Methfessel *et al.*, 1989; Boyer *et al.*, 1991; Needs and Mujica, 1995; Piltz *et al.*, 1995; Mujica *et al.*, 2001a, 2001b.

TABLE I. Observed sequence of transitions (at room temperature unless otherwise stated) and summary of experimental (left) and theoretical (right) data pertinent to each transition for Si, Ge, Sn, Pb, and SiC; p_t, experimental onset of the transition; p_e, theoretical coexistence pressure; ΔV, percentage change in volume; see the introduction to Sec. VII for details. When two values of p_t are provided separated by a vertical bar, the right one refers to the upwards transition (increase of pressure) and the left one to the downwards transition (decrease of pressure). The maximum pressure reached in experiments is given at the end of the sequence. The experimental technique used is indicated in parentheses beside each experimental reference. The theoretical results correspond to first-principles LDA-DFT calculations at zero temperature in a PWPP, LAPW, or LMTO scheme, unless otherwise stated. The term "n.d." (not determined) stands for a phase whose structure has not been resolved. Metastable phases and the intermediate phases observed in very small pressure ranges are signified by bracketing their names.

Reference (experiment)	p_t (GPa)	ΔV	Transition	p_e (GPa)	ΔV	Reference (theory)
Si Compression: cd(I)→β-Sn(II)→[Imma(XI)]→sh(V)→Cmca(VI)→hcp(VII)→fcc(X)<250 GPa Decompression: [bc8(III)]←[r8(XII)]←β-Sn(II)						
McMahon *et al.*, 1994a (ADX)	11.7	*21.0(1)*	cd→β-Sn	7.8	23.7	Needs and Mujica, 1995
McMahon *et al.*, 1994a (ADX)	13.2(3)	*0.2(1)*	β-Sn→[Imma]	See text		Lewis and Cohen, 1993
McMahon *et al.*, 1994a (ADX)	15.4	*0.5(1)*	[Imma]→sh	See text		Lewis and Cohen, 1993
Hanfland *et al.*, 1999 (ADX)	~38	5.1	sh→Cmca	33(2)	~6.0	Christensen, Novikov, and Methfessel, 1999
Hanfland *et al.*, 1999 (ADX)	~42	1.9	Cmca→hcp	41(5)	~2.2	Christensen, Novikov, and Methfessel, 1999
Duclos *et al.*, 1990 (EDX)	79(2)|80(3)	*0.3(6)*	hcp→fcc	84.3	1.5	Needs and Mujica, 1995
Nelmes and McMahon, 1998 (ADX)	9.4	*10.7(2)*	[r8]←β-Sn	7.4	-	Pfrommer *et al.*, 1997a
Piltz *et al.*, 1995 (ADX)	2	*2.1(2)*	[bc8]←[r8]	−1.9	1.2	Pfrommer *et al.*, 1997a
Observations: A cd←β-Sn transition has been reported in decompression above 400 K (Brazhkin *et al.*, 1995). Si-IV is obtained upon moderate heating of the bc8 phase (Besson *et al.*, 1987). Two other unresolved low-pressure metastable phases (labeled VIII and IX) have been reported after decompression from β-Sn-Si (Zhao *et al.*, 1986).						
Ge Compression: cd(I)→β-Sn(II)→[Imma]→sh→Cmca→hcp<190 GPa Decompression: [st12(III)]←β-Sn(II) (slow) [bc8(IV)]←β-Sn(II) (rapid)						
Menoni *et al.*, 1986 (EDX)	10.6(5)	18.9(7)	cd→β-Sn	7.4	18.4	Mujica *et al.*, 2001a, 2001b
Nelmes, Liu, *et al.*, 1996 (ADX)	~75	-	β-Sn→[Imma]	70(3)	*0.2*	Ribeiro and Cohen, 2000
Nelmes, Liu, *et al.*, 1996 (ADX)	~85†	-	[Imma]→sh	89(5)	*0.1*	Ribeiro and Cohen, 2000
Takemura *et al.*, 2000 (ADX)	~100	-	sh→Cmca	90(2)	*0.7*	Ribeiro and Cohen, 2000
Takemura *et al.*, 2000 (ADX)	~170	-	Cmca→hcp	137(10)	*0.2*	Ribeiro and Cohen, 2000
Menoni *et al.*, 1986 (EDX)	7.6(5)	9.2(10)‡	[st12]←β-Sn	5.7	*6.7*	Mujica *et al.*, 2001a, 2001b
Nelmes, McMahon, Wright, Allan, and Loveday, 1993 (ADX)	~7|~14	-	[bc8]←β-Sn	4.3	*9.4*	Mujica *et al.*, 2001a, 2001b
Observations: (†) Extrapolated value; (‡) Calculated as $(V^t_{III}-V^t_{II})/V^t_{III}$. The [bc8]←$\beta$-Sn transition is observed upon rapid decompression at room temperature. It has also been reported at low temperatures (100–200 K), whereas the cd←β-Sn transition has been reported above 400 K (Brazhkin *et al.*, 1995).						
Sn β-Sn(I)→bct(II)→bcc<120 GPa						
Olijnyk and Holzapfel, 1984 (EDX)	~9.5	-	β-Sn→bct	19	3.6	Cheong and Chang, 1991
Liu and Liu, 1986 (EDX)	40–50	-	bct→bcc	~46	~0	Cheong and Chang, 1991

TABLE I. (*Continued*).

Observations: α-Sn (cd) is the stable phase at zero temperature and pressure. At normal conditions the stable phase is β-Sn.						
Pb fcc(I)→hcp(II)→bcc(III)≲270 GPa						
Mao *et al.*, 1990 (EDX)	14	~1	fcc→hcp	13(1)	~0.5	Liu *et al.*, 1991
Vanderborgh *et al.*, 1990 (EDX)	109	~0.3	hcp→bcc	87(10)	~0.2	Liu *et al.*, 1991
Observations: Very sluggish transitions.						
SiC zb(3C)→NaCl<100 GPa and 6H→n.d.<100 GPa						
Yoshida *et al.*, 1993 (ADX)	>35|100	20.3	zb→NaCl	67	17.9	Karch *et al.*, 1996
Sekine and Kobayashi, 1997 (Shock)	105(4)	15(3)	6H→n.d.			

Due to the small interval of stability of the β-Sn phase in Si, they found a direct transition to the simple hexagonal structure (see below).

b. β-Sn→Imma→sh

On further increase of pressure the β-Sn phase transforms into a phase with the simple hexagonal structure (sh) via the intermediate orthorhombic Imma phase. The interval of stability of the β-Sn phase of Si is now known to be very small, from 13.2 to 15.6 GPa according to McMahon and Nelmes (1993). However, in Ge the β-Sn phase remains stable over a very large pressure interval from ~10 GPa to ~75 GPa (Nelmes, Liu, *et al.*, 1996; Nelmes and McMahon, 1998). The possibility of the intermediate Imma phase had first been postulated on the basis of first-principles calculations (Needs and Martin, 1984) though conclusive experimental evidence for its existence was precluded at the time by the limited resolution of EDX diffraction studies. The existence of the Imma phase passed unnoticed until the very accurate experiments of McMahon and Nelmes (1993), who, taking full advantage of image-plate ADX techniques, unmasked it from what had previously appeared to be an admixture of the β-Sn and sh phases (Hu and Spain, 1984).

Experimentally, the β-Sn→Imma and Imma→sh transitions are first order, although the volume discontinuity is in both cases very small (McMahon *et al.*, 1994a). The internal parameter u also changes discontinuously at the transition, from 0.25 (β-Sn) to 0.3–0.4 (Imma) and then to 0.5 (sh). Several first-principles calculations support the picture of a stable Imma phase intermediate between β-Sn and sh [Needs and Martin, 1984 (Si); Lewis and Cohen, 1993 (Si), 1994 (Ge)]. Due to the very small differences in energies between the β-Sn, Imma, and sh phases, the character of the transition, its onset, and the precise evolution of the structural parameters are difficult to ascertain. The mechanism of the transition is, however, clear; this is related to the softness of the LO(Γ) mode of the β-Sn structure, whose pattern of distortion corresponds to the displacement of atoms leading to Imma. The coupling of this mode to the strain parameters results in the instability of the β-Sn structure towards the orthorhombic Imma structure. It is interesting to note that the frequency of the LO(Γ) mode does not go to zero at the transition, although in Si it decreases slightly (Olijnyk, 1992a), and that the concourse of the strain parameters is required in the destabilization of the structure. The transition can then be regarded as displacive, although it may be weakly first order.

c. Cmca

The application of pressure to the sh phase induces a change to an orthorhombic phase with 16 atoms in the conventional unit cell and space group *Cmca* [Hanfland *et al.*, 1999 (Si); Takemura *et al.*, 2000 (Ge)]. The first evidence for the existence of the Cmca phase of Si (Olijnyk *et al.*, 1984) was in fact gathered much before

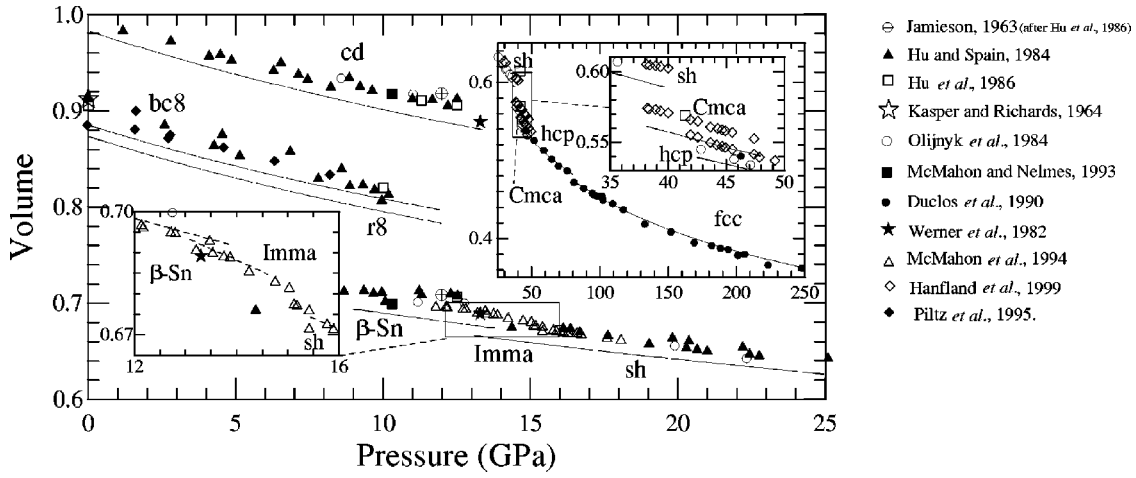

FIG. 6. Variation of the volume (in units of the experimental zero-pressure volume of the cd phase) with applied pressure for the observed phases of Si (various symbols). The solid lines are the results of first-principles plane-wave pseudopotential (PWPP) LDA calculations (Needs and Mujica, 1995; Mujica *et al.*, 2001b). The differences between experimental and theoretical results are related to the theoretical underestimation of the zero-pressure volume. These differences may be "corrected" in plots such as this by shifting the theoretical $V(p)$ curves in either pressure or volume, or by expressing them in units of the theoretical zero-pressure volume.

the correct structural characterization of the phase by Hanfland and co-workers, but the identification of the structure was precluded at that time by the limited resolution of early high-pressure EDX diffraction studies when applied to a relatively complex phase such as Cmca. In Ge the transition from the sh phase was initially reported to be to a double hexagonal-close-packed structure (Vohra *et al.*, 1986), but very recent first-principles calculations (Ribeiro and Cohen, 2000; Mujica *et al.*, 2001a) have predicted it to be towards the same Cmca structure as reported in Si, and concurrently and independently Takemura *et al.* (2000) reported its existence on the basis of ADX diffraction experiments. A similar Cmca structure had earlier been found in Cs (Cs-V, Schwarz *et al.*, 1998) and in Rb (Rb-VI, Schwarz *et al.*, 1999).

d. Close-packed phases

On further increase of pressure the Cmca structure undergoes a transition to the hexagonal-close-packed (hcp) structure, which in Si starts experimentally at about 41 GPa (Olijnyk *et al.*, 1984; Hu *et al.*, 1986; Duclos *et al.*, 1990; Hanfland *et al.*, 1999) and in Ge at the much higher pressure of 160–180 GPa (Takemura *et al.*, 2000). The hcp phase of Si undergoes a further transition to the face-centered-cubic (fcc) structure at a pressure of about 87 GPa, which remains stable up to the highest pressure reached so far, of 248 GPa (Duclos *et al.*, 1990). In Ge, the hcp phase does not undergo any further transitions up to the highest pressure yet reached of about ~190 GPa (Takemura *et al.*, 2000). Theoretical calculations rule out the possibility of the hcp→fcc transition in Ge (Ribeiro and Cohen, 2000; Mujica *et al.*, 2001a), so that a clear difference in the very-high-pressure phases of Si and Ge is predicted, which awaits the test of experiment.

e. Phases obtained on decrease of pressure

Release of pressure from the high-pressure phases of Si and Ge at room temperature does not result in the recovery of the cd phase, but several other denser tetrahedral metastable phases are formed instead. Slow decompression from the β-Sn phase of Si leads first to the rhombohedral r8 phase at about 10 GPa, which in turn transforms to the cubic bc8 phase at about 2 GPa (Crain, Ackland, *et al.*, 1994; Piltz *et al.*, 1995). This transition is perfectly reversible. The bc8 phase (Kasper and Richards, 1964) remains as a metastable phase under normal conditions. However, moderate heating of the bc8 phase results in a transformation to a phase Si-IV which has been identified as having the hexagonal-diamond structure (Wentorf and Kasper, 1963; Besson *et al.*, 1987), though this assignment has been challenged (Nelmes, McMahon, Wright, Allan, and Loveday, 1993). In a single experimental study in which the β-Sn-Si phase was brought rapidly to ambient pressure under different conditions, two other different phases, believed to consist of large tetragonal unit cells, were reported (Zhao *et al.*, 1986). The formation of the r8 and bc8 phases has also been reported in silicon indentations (see Domnich and Gogotsi, 2001, for this and other aspects of structural transitions after indentation).

In Ge, slow decompression of the β-Sn phase leads to the tetragonal st12 phase, which persists metastably at zero pressure (Bundy and Kasper, 1963; Qadri *et al.*, 1983; Menoni *et al.*, 1986; Nelmes, McMahon, Wright, Allan, and Loveday, 1993). Rapid release of pressure leads, however, to the formation of a bc8 phase similar to that observed in Si, although in Ge it does not persist for long periods of time (Nelmes, McMahon, Wright, Allan, and Loveday, 1993). The phase to which bc8-Ge transforms appears to be similar in structure to the reported hd phase of Si, with the same caveats about this assignment.

To add to the complexity of the behavior of Si and Ge

upon decompression, the formation of the cd-Si and cd-Ge phases has been reported at *high* temperatures ($\sim$400–500 K), whereas at low temperatures ($\sim$100 K) the amorphous phases *a*-Si and *a*-Ge were recovered (Brazhkin *et al.*, 1995).

There have been a number of theoretical studies of the bc8, r8, and st12 phases, and their calculated structures are in excellent agreement with experiments.[3] Their internal energies at zero pressure are very similar and are larger than those of the corresponding cd phases, indicating the metastable character of these forms. The st12 phase is slightly favored over bc8 and r8 at positive or zero pressure in Ge (Mujica and Needs, 1993; Mujica *et al.*, 2001b), while the reverse situation is observed in Si (Needs and Mujica, 1995; Piltz *et al.*, 1995; Mujica *et al.*, 2001b). First-principles calculations also indicate that in both materials the bc8 phase becomes unstable with respect to the r8 phase when a small pressure is applied [(Si) Pfrommer *et al.*, 1997a; (Ge and Si) Mujica *et al.*, 2001b]. All of these theoretical results are consistent with the experimental observations, although only the r8 phase of Si has been reported experimentally.

3. Sn

The zero-gap α phase of Sn (diamond structure), also known as "gray tin," is stable at zero pressure and temperature. An increase in either of these variables induces a transition to the metallic tetragonal β phase or "white tin" (see Jayaraman *et al.*, 1963, and references therein). Under normal conditions the observed phase is the common β form, but the α form is very close to stability. There is a large collapse in volume ($\sim$20%) accompanying the $\alpha \rightarrow \beta$ transition.

First-principles theoretical studies agree on the closeness of the energies of the α and β phases (Ihm and Cohen, 1981; Cheong and Chang, 1991; Corkill *et al.*, 1991; Christensen and Methfessel, 1993). The effect of zero-point motion and finite temperatures on the relative stability of the two forms has also been studied using first-principles DFPT methods by Pavone *et al.* (1998). At $T=0$ K the free energy of the diamond phase is only about 15 meV per atom below that of the β phase. This confirms the marginal stability of the diamond structure and is also in good agreement with experimental estimates of this magnitude (see Ihm and Cohen, 1981). The $\alpha \leftrightarrow \beta$ transition is calculated to occur at 311(20) K (Pavone *et al.*, 1998), in excellent agreement with the experimental observation ($\sim$285 K; see Jayaraman *et al.*, 1963).

On application of pressure to the β phase, an abrupt transition to a body-centered-tetragonal (bct) phase is observed experimentally at about 9.5 GPa (Barnett *et al.*, 1966), and from this to a body-centered-cubic (bcc) phase at pressures between 40 and 50 GPa (Olijnyk and Holzapfel, 1984; Liu and Liu, 1986). No further transitions have been reported up to the highest pressures achieved, of $\sim$120 GPa (Desgreniers *et al.*, 1989). First-principles studies (including arguably important relativistic effects) support the sequence of transitions β-Sn$\rightarrow$bct$\rightarrow$bcc, although the very small energy difference between the bct and bcc phases leads to a rather large uncertainty in the bcc/bct coexistence pressure (Corkill *et al.*, 1991) and suggests a large temperature dependence for this magnitude. In the pressure range in which bct-Sn has been observed, the calculated energy as a function of the c/a ratio exhibits two local minima separated by a very small energy barrier [$\sim$3 meV at $\sim$10 GPa (Christensen and Methfessel, 1993)]. The lower minimum corresponds to the value $c/a \approx 0.91$ observed in experiments while the other one is located at $c/a=1$ (bcc structure). As pressure is increased the bcc minimum decreases in energy, while the bct minimum becomes very shallow and ultimately disappears at about 40 GPa, indicating an instability of the bct phase towards the bcc phase. At higher pressures, Cheong and Chang (1991) find that an hcp phase becomes lower in enthalpy than bcc with both phases separated by a small energy barrier. However, Christensen and Methfessel (1993) find hcp slightly higher in enthalpy than bcc using the LMTO method.

It is interesting to note that the low-frequency LO(Γ) mode of the β phase, which in Si and Ge is related to the β-Sn$\rightarrow$Imma$\rightarrow$sh transitions, becomes stiffer with pressure in Sn (Olijnyk, 1992b; Christensen and Methfessel, 1993), for which such a sequence of transitions has indeed not been observed.

4. Pb

Pb crystallizes in the fcc structure under normal conditions and is a metal. A transition to the hcp structure is observed at 14 GPa (Takahashi *et al.*, 1969). At about 110 GPa a further transition to the bcc structure is observed (Mao *et al.*, 1990; Vanderborgh *et al.*, 1990). In both cases the volume reduction is very small and there is a large region of phase coexistence, consistent with a very small enthalpy difference between the phases over a large pressure interval.

Liu *et al.* (1991) studied the stability of Pb at high pressures using PWPP methods, including scalar-relativistic and spin-orbit effects. The three structural phases fcc, hcp, and bcc were found to be very close in energy, but nonetheless the sequence of transitions was correctly described, as well as the structural properties of the phases. However, the hcp$\rightarrow$bcc coexistence pressure came out too low in the calculation, which could at least partially be attributed to the very small energy differences between the phases. No other structural phases were considered in the calculations.

5. SiC

SiC has unique mechanical, chemical, electrical, and thermal properties, which have led to various techno-

[3]See, for example, Biswas *et al.*, 1984, 1987; Yin, 1984; Mujica and Needs, 1993; Crain, Ackland, *et al.* 1994; Crain, Clark, *et al.*, 1994; Needs and Mujica, 1995; Piltz *et al.*, 1995; Pfrommer *et al.*, 1997a; Mujica *et al.*, 2001b.

logical applications.[4] Under normal conditions, SiC may adopt a large variety of semiconducting polytypic forms, which are all very close in energy (Cheng *et al.*, 1987, 1988; Käckell *et al.*, 1994). They consist of different stackings of hexagonal Si-C bilayers, the most common of which are 3C (zb structure, the stable form), 6H, 4H, and 2H (wurtzite structure); see the Appendix. All known polytypes have indirect band gaps.

First-principles LDA calculations indicate that, among the phases examined (NaCl, b-β-Sn, NiAs, anti-NiAs, and CsCl), the NaCl form becomes favored over the low-pressure polytypes at pressures of about 66 GPa (Chang and Cohen, 1987; Karch *et al.*, 1996). The pressure dependence of lattice-dynamical and dielectric properties of the most common polytypes have also been considered by Karch *et al.* (1996), who find remarkable differences among them. Experiments do indeed find a zb→NaCl transition (Yoshida *et al.*, 1993), though its onset is located at much higher pressures (~100 GPa) and the transition displays a very large hysteresis. A phase transition to an undetermined phase has also been reported in 6H-SiC subject to shock compression (Sekine and Kobayashi, 1997).

Shimojo *et al.* (2000) have reproduced the zb→NaCl transition in a molecular-dynamics study using an interatomic potential model. Using a LCAO-DFT scheme, Catti (2001) has found a low activation-enthalpy pathway between the zb and NaCl phases, involving an intermediate orthorhombic state of *Imm2* symmetry. Transition pathways for the zb→NaCl transition in SiC have been also investigated by Miao *et al.* (2002) using the FP-LMTO method.

B. IIIA–VA compounds

1. BN

Since B and N lie on either side of C in the Periodic Table it is not surprising that many of the properties of the binary compound BN resemble those of C. As in C, BN can exist under normal conditions in four different polymorphic states, two graphitelike and two diamondlike, with a very large difference in densities between the layered and the dense forms. The two graphitelike modifications are commonly referred to as the "hexagonal" and "rhombohedral" forms (h-BN and r-BN, respectively). The two dense phases have zinc-blende (zb) and wurtzite (wur) structures and they are normally referred to as the "cubic" and "wurtzitic" forms (c-BN and w-BN, respectively). These are the binary analogs of the cubic- and hexagonal-diamond forms of C (see Appendix).

The cubic phase of BN shares a number of extraordinary properties with the diamond phase of C: extreme hardness (second only to diamond), chemical inertness, high melting temperature, and high thermal conductivity. In contrast to diamond, c-BN does not dissolve in iron or steel and is therefore an excellent material for the protective coating of heavy-duty tools. Its electronic properties, dominated by a wide band gap and a relatively small dielectric constant, may have applications in ultraviolet optics and high-temperature microelectronics. Because of these fascinating properties c-BN has received a great deal of attention from experimentalists and theoreticians alike.

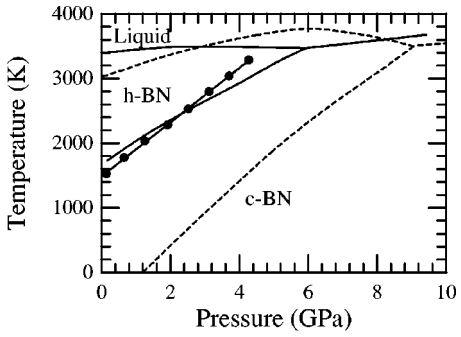

FIG. 7. Phase diagram of BN: dashed lines, Corrigan and Bundy (1975); solid lines, Solozhenko (1995; refined in Solozhenko *et al.*, 1999); ●, theoretical calculation of the c-BN/h-BN phase boundary by Albe (1997).

There has been some dispute as to which of the two forms, hexagonal or cubic, corresponds to the thermodynamically stable phase of BN under normal conditions. Until recently, the accepted picture was essentially similar to that for C, with the most common h-BN modification being stable (Corrigan and Bundy, 1975). An alternative phase diagram in which (unlike C) c-BN is the stable phase at normal conditions, was later proposed (see Solozhenko, 1995 and Fig. 7). Independently, the results of several DFT-LDA first-principles calculations indicated that c-BN had the lowest equilibrium static energy of all the BN polymorphs (Wentzcovitch *et al.*, 1988; Furthmüller *et al.*, 1994). The r-BN and w-BN forms are metastable and lie very close in energy to, respectively, the h-BN and c-BN forms. The calculated difference in equilibrium energies between the layered and dense phases is significantly larger than that found between the diamond and graphite phases in C, which is an effect of the heteropolarity of BN. The effects of zero-point motion and of finite temperature have also been investigated theoretically by Albe (1997) and by Kern *et al.* (1999) within the quasiharmonic approximation, but they do not alter the conclusions about the stability of c-BN. At zero pressure, the calculated coexistence temperature is ~1400–1500 K (Albe, 1997; Kern *et al.*, 1999), in good agreement with Solozhenko's (1995) proposal (~1600 K).

It is not obvious that c-BN should be the stable form at normal conditions, since the dense phases are not the usual forms in Nature. The most common form in Nature is h-BN. The r-BN phase is normally found in small regions within natural BN, although it can also be chemically synthesized as an almost pure phase (Solozhenko, 1995). The two dense c-BN and w-BN phases

[4]In spite of not being homonuclear, SiC is included in this review along with the group-IVA family to which both of its constituents belong.

can be formed from the layered ones by static or dynamical compression and, eventually, heating in order to overcome the large activation barriers between phases. The observed sequence of direct and reverse transitions between the phases is determined not only by the equilibrium phase diagram but also by kinetic factors and the starting material. This is similar to the synthesis of hexagonal and cubic diamond from graphite and, as in that case, the use of catalysts significantly reduces the very large hysteresis of the transitions. It is also possible to grow thin films of the technologically important c-BN phase by chemical or physical vapor deposition (Mirkarimi *et al.*, 1997). Solozhenko (1995) has reviewed the experimental thermodynamic properties of the phases of BN, analyzing the formation of the different polymorphs after structural transformation at high pressures and/or high temperatures, and by crystallization in systems including catalysts.

Although the synthesis of the dense phases from the layered ones is experimentally well established, the mechanism of the transitions and the role played by the different factors involved is not yet completely understood. Wentzcovitch *et al.* (1988) have considered the transformation of r-BN into c-BN, and of h-BN into w-BN. In both cases there exists a simple structural relation between the "parent" and "daughter" phases (see the Appendix), and one can be transformed into the other by following a path involving the collective motion of layers of atoms. The experimental results suggest that, at room temperature, a displacive mechanism based on these distortions is a plausible model for the h-BN→w-BN and r-BN→c-BN transitions (see Ueno, Hasegawa, *et al.*, 1992, and references therein). Compared with the gra→cd transition in C, the transition between the layered and dense structures in BN involves smaller activation energies, which is consistent with its larger heteropolarity (Wentzcovitch *et al.*, 1988).

A PWPP study of the zb, NaCl, b-β-Sn, and CsCl structures by Wentzcovitch *et al.* (1987) suggests that c-BN would become unstable against a NaCl phase at the very large pressure of 1.11 TPa, which agrees with a later study using ultrasoft pseudopotentials (Furthmüller *et al.*, 1994). Christensen and Gorczyca (1994) find 0.85 TPa using the LMTO method. Such high pressures cannot be reached experimentally.

2. BP, BAs, and BSb

Under normal conditions, BP and BAs crystallize in the zinc-blende structure. They are, however, difficult to synthesize, and experimental and theoretical studies of their properties are very scarce. The synthesis of BSb has still not been reported, and its hypothetical properties have attracted even less theoretical attention than those of BP and BAs. The zb phases of BP and BAs are known to be semiconductors with an indirect band gap; first-principles calculations (Ferhat *et al.*, 1998) indicate that the same is likely to be true for BSb.

The properties of these compounds are, however, rather interesting from a theoretical point of view. In fact, their behavior is truly unique among the IIIA–VA and IIB–VIA families. This originates from the absence of p electrons in the core of the B atom and its small size. The resulting deeply attractive pseudopotential of B competes with that of the VA element for the valence electrons. According to the scale of Phillips (1973), B is more electronegative than P, As, or Sb. In fact, first-principles calculations show that the B atoms play the role of the anion in BP, BAs, and BSb (Wentzcovitch *et al.*, 1987; Bouhafs *et al.*, 1999). The result is a situation of both small heteropolarity and ionicity, with BP, BAs, and BSb being the least ionic (or most "covalent") of the IIIA–VA and IIB–VIA compounds (Phillips, 1973; García and Cohen, 1993a; Bouhafs *et al.*, 1999).

Theoretical work on the high-pressure phases of BP and BAs has so far been limited to the study of the energetics of the NaCl, b-β-Sn, and CsCl phases (Wentzcovitch *et al.*, 1987). The NaCl phase was found to be marginally lower in enthalpy than the b-β-Sn phase. The zb/NaCl coexistence pressure was calculated to be 160 GPa in BP and 110 GPa in BAs. This is much larger than the pressures of the transitions observed in most IIIA–VA and IIB–VIA binary compounds (see Table II). Experimentally, zb-BP does not undergo any transition up to at least 110 GPa (Xia *et al.*, 1993b), while zb-BAs has been reported to transform into an amorphous state at a pressure of 125 GPa (Greene, Luo, Ruoff, Trail, and DiSalvo, 1994). This amorphous state does not undergo any further transition up to the maximum pressure reached in the experiment of 165 GPa and persists as a metastable phase upon release of pressure. The fact that the onset of the pressure-induced amorphization of BAs is just above the calculated zb/NaCl coexistence pressure was interpreted by Greene, Luo, Ruoff, Trail, and DiSalvo (1994) as an indication of amorphization being the result of a kinetically frustrated zb→NaCl transition.

3. AlN, GaN, and InN

Under normal conditions AlN, GaN, and InN crystallize in the wurtzite structure, although it has also proved possible to grow a zinc-blende modification using epitaxial techniques (Lei *et al.*, 1991). First-principles calculations confirm that the zb phases are indeed metastable, although they lie close in enthalpy (<50 meV) to the stable wur forms (Serrano *et al.*, 2000). Technological applications arising from the direct wide band gap exhibited by the wur phases have stimulated intensive research into these materials. They are, however, difficult to grow and manipulate and only recently have their properties at high pressures been studied. Nonetheless, the literature on the high-pressure properties of these compounds has grown at a very fast pace. Concerning the structural properties of the low-pressure wur phases, Stampfl and Van de Walle (1999) have performed a detailed theoretical study, to which the interested reader is referred, including careful comparisons with a large body of experimental and theoretical work.

TABLE II. Same as Table I but for the IIIA–VA materials considered in this review. No transitions in BN, BP, and BSb have been reported, whereas BAs transforms to an amorphous phase at 125 GPa (Greene, Luo, Ruoff, Trail, and DiSalvo, 1994). A question mark accompanying the name of a structure indicates that there are doubts about its characterization.

Reference (experiment)	p_t (GPa)	ΔV	Transition	p_e (GPa)	ΔV	Reference (theory)
AlN wur(I)→NaCl(II)<132 GPa						
Ueno, Onodera, *et al.*, 1992 (ADX)	22.9	17.9	wur→NaCl	12.5	19	Christensen and Gorczyca, 1993
Xia *et al.*, 1993c (EDX)	14	18.6	wur→NaCl	9.2	20.1	Serrano *et al.*, 2000
Observations: The NaCl phase does not transform back into wur after depressurization (Xia *et al.*, 1993c).						
AlP zb(I)→NiAs(II)<43 GPa						
Greene, Luo, and Ruoff, 1994 (EDX)	4.8–8.4|14.2	~17	zb→NiAs	7.7	20.8	Mujica, Rodríguez-Hernández, *et al.*, 1999
AlAs zb(I)→NiAs(II)<46 GPa						
Greene, Luo, Li, and Ruoff, 1994 (EDX)	4.5–2|12	~17	zb→NiAs	6.1	20.1	Liu *et al.*, 1995
AlSb zb(I)→Cmcm(II)→n.d.(III)<97 GPa						
Nelmes *et al.*, 1997 (ADX)	8.1	*19.5(2)*	zb→Cmcm	4.7	20.8	Mujica, Rodríguez-Hernández, *et al.*, 1999
Hirano *et al.*, 2001 (ADX)	57(2)	-	Cmcm→n.d.			
GaN wur(I)→NaCl(II)<91 GPa						
Xia *et al.*, 1993a (EDX)	~25|37	17.0	wur→NaCl	51.8	14.8	Christensen and Gorczyca, 1994
Ueno *et al.*, 1994 (ADX)	52.2	17.9	wur→NaCl	42.9	15.0	Serrano *et al.*, 2000
Observations: Note the discrepancies in transition pressures.						
GaP zb(I)→Cmcm(II)<52 GPa.						
Nelmes *et al.*, 1997 (ADX)	26(1)	*14.0(2)*†	zb→Cmcm	17.7	18.4	Mujica and Needs, 1997
Observations: (†) At 29.4 GPa. The Cmcm phase is believed to be site disordered.						
GaAs: Compression: zb(I)→Cmcm(II)<108 GPa Heating at high pressure: sc16←Cmcm(II) Decompression: zb(I)←[*cinn*]←Cmcm(II) or zb(I)←Cmcm(II)						
McMahon and Nelmes, 1997 (ADX)	11.2(3)|17.3(2)	*14.3*†	zb→Cmcm	12.1	17.8	Mujica *et al.*, 1995
McMahon and Nelmes, 1997 (ADX)	11.9(1)|15.1(2)	*6.9*†	[*cinn*]←Cmcm	10.0	*7.8*	Mujica *et al.*, 1998
McMahon and Nelmes, 1997 (ADX)	8.1(2)	*7.4*†	zb←[*cinn*]	14.5	*7.6*	Mujica *et al.*, 1998
McMahon *et al.*, 1998 (ADX)	−|22.0(7)	*7.4*‡	sc16←Cmcm	12.7	*8.0*	Mujica and Needs, 1996

TABLE II. (*Continued*).

Observations: (†) From data at 8.3 GPa; (‡) From data at 18.9 GPa. The sc16←Cmcm transition requires heating to 450 K in the range 13–14.5 GPa. It is presently unclear whether the Cmcm phase undergoes a further structural change at pressures of the order of ~50 GPa (McMahon and Nelmes, 1996).						
GaSb zb(I)→β-Sn/Imma(II)→bcc?<110 GPa Heating at high pressure: Imma→β-Sn/Ammm						
Mezouar *et al.*, 1999 (ADX)	~7	-	zb→β-Sn	6.3	18.6	Zhang and Cohen, 1987
McMahon *et al.*, 1994b (ADX)	7	18.3(1)	zb→Imma			
Nelmes and McMahon, 1998 (ADX)	63–71	-	Imma→bcc?			
Observations: Experiments show that GaSb-II is disordered and that the formation of either β-Sn or Imma depends on the stress conditions of the pressurizing medium. The reported bcc phase is disordered CsCl. The Imma→Ammm transition requires heating to ~473 K at pressures above ~13 GPa while heating Imma at pressures below ~13 GPa results in the disordered β-Sn phase.						
InN wur(I)→NaCl(II)<72 GPa						
Xia *et al.*, 1994 (EDX)	10	20(2)	wur→NaCl	21.6	15.3	Christensen and Gorczyca, 1994
Ueno *et al.*, 1994 (ADX)	12.1	17.6	wur→NaCl	11.1	17.4	Serrano *et al.*, 2000
InP zb(I)→NaCl(II)→Cmcm<46 GPa						
McMahon *et al.*, 1993b (ADX)	9.8(5)	*16.0(2)*	zb→NaCl	5.6	18.4	Mujica and Needs, 1997
Nelmes *et al.*, 1997 (ADX)	28(1)	-	NaCl→Cmcm	11–12	~0	Mujica and Needs, 1997
InAs zb(I)→NaCl(II)→Cmcm<46 GPa.						
Nelmes, McMahon, Wright, Allan, Liu, and Loveday, 1995 (ADX)	7	-	zb→NaCl	3.9	18.7	Mujica and Needs, 1997
Nelmes and McMahon, 1998 (ADX)	9	-	NaCl→Cmcm	3–4.5	~0	Mujica and Needs, 1997
Observations: There is some evidence of an intermediate phase between NaCl and Cmcm (Nelmes and McMahon, 1998).						
InSb zb(I)→[β-Sn+Immm]→s-Cmmm(IV)→[Imma]→Immm(III)→[n.d.]→bcc?<66 GPa.						
Nelmes, McMahon, Hatton, *et al.*, 1993 (ADX)	~2.1	*~21*	zb→[β-Sn+Immm]			
Nelmes and McMahon, 1995 (ADX)	~3.0	*19.5(1)*	zb→s-Cmcm	2.4	-	Kelsey and Ackland, 2000
Nelmes and McMahon, 1996 (ADX)	~4|~10	*~1.5*	s-Cmcm→Immm†	26	-	Kelsey and Ackland, 2000
Nelmes and McMahon, 1996 (ADX)	21(1)	*3.0(2)*	Immm→bcc?‡			
Observations: Sequence of transitions according to Nelmes and McMahon (1998). The transition from zb to s-Cmcm can occur directly or via the intermediate mixture [β-Sn+Immm]. (†) This transition proceeds via an intermediate disordered Imma phase. The phase boundary shows a strong T dependence. (‡) This transition proceeds via an intermediate undetermined phase. The reported bcc phase is disordered CsCl.						

For each of the three compounds, the low-pressure wur phase undergoes a transition to a NaCl phase as pressure is increased (Vollstädt *et al.*, 1990; Perlin *et al.*, 1992, 1993; Ueno, Onodera, *et al.*, 1992; Xia *et al.*, 1993a, 1993c, 1994; Uena *et al.*, 1994; Uehara *et al.*, 1997). First-principles calculations indicate that the high-pressure NaCl phases are semiconducting with an indirect energy gap (Serrano *et al.*, 2000). There is some spread in the values of the reported experimental data concerning the wur→NaCl transitions (see Table II), and the interested reader should consult the critical compilation of results by Nelmes and McMahon (1998) as well as the original experimental articles for specific details on experimental values. In AlN and GaN the transition displays a rather large hysteresis, with persistence of the NaCl phase down to ambient pressure in the case of AlN (Xia *et al.*, 1993c), which makes it very difficult to locate the coexistence pressure for the two phases. Taking these uncertainties into account, the calculated values for the coexistence pressure are plausibly close to the middle of the experimental hysteresis cycles and within the error bars of the experimental data. The theoretical calculations (Muñoz and Kunc, 1991, 1993; Van Camp *et al.*, 1991, 1992; Christensen and Gorczyca, 1994; Serrano *et al.*, 2000) and the experiments agree in that the wur →NaCl coexistence pressure of GaN is much larger than for AlN and InN.

Experiments by Ueno *et al.* (1994) indicate a nonlinear variation in the c/a ratio near the onset of the wur →NaCl transition in InN, and on the basis of first-principles calculations Bellaiche *et al.* (1996) have postulated that such pretransitional behavior is indicative of a second-order isostructural transition which in fact induces the reconstructive first-order wur→NaCl transition. Based on LMTO calculations for AlN, Christensen and Gorczyca (1993) have predicted a transition from the NaCl structure to the NiAs structure at pressures of about 30–35 GPa, which, however, has not been confirmed experimentally (Ueno, Onodera, *et al.*, 1992) and is in disagreement with other theoretical studies (Serrano *et al.*, 2000). From first-principles calculations, the formation of such structural phases as Cmcm, cinnabar, sc16, b-β-Sn, or CsCl is not to be expected in these materials (Serrano *et al.*, 2000).

In fact, the main feature of the high-pressure behavior of AlN, GaN, and InN appears to be the enhanced stability, over the other compounds considered in this review, of their respective NaCl phases. The absence of p electrons in the core of the N atoms favors the transfer of charge towards them, which results in a larger ionicity than in the rest of IIIA–VA and IIB–VIA compounds (García and Cohen, 1993a, 1993b). This is responsible for the local stability of the NaCl phase against a Cmcm-like distortion (Ozoliņš and Zunger, 1999; Serrano *et al.*, 2000), whereas such a distortion is observed in other IIIA–VA and IIB–VIA compounds which also exhibit the NaCl structure (see Sec. VIII.B).

A further point of interest is the role played by the semi-core d electrons of the Ga and In ions in the structural properties of the solid phases of GaN and InN (particularly GaN, where any effect is expected to be larger due to the near degeneracy of the Ga $3d$ and N $2s$ levels). The main effect of freezing these orbitals in pseudopotential calculations is that the closed-shell repulsion arising from overlap between core states (or core and valence states) on neighboring sites is missed (Fiorentini *et al.*, 1993). This approximation yields smaller equilibrium volumes (Fiorentini *et al.*, 1993; Wright and Nelson, 1994, 1995) and smaller wur →NaCl coexistence pressures (Serrano *et al.*, 2000) than if the d electrons are explicitly relaxed in the calculations.

4. AlP, AlAs, and AlSb

At normal conditions, AlP, AlAs, and AlSb crystallize in the zinc-blende structure. High-pressure experiments on these compounds are difficult because of sample-handling problems; AlP is unstable in air, AlAs is toxic, and AlSb is highly hygroscopic. These issues may well explain the experimental difficulties encountered in characterizing their high-pressure phases.

A high-pressure NiAs phase was first postulated for AlAs after the PWPP calculations of Froyen and Cohen (1983). The experimental confirmation of such a phase in AlAs as well as AlP came much later (Greene, Luo, Li, and Ruoff, 1994; Greene, Luo, and Ruoff, 1994). The calculated and experimental c/a ratios are in perfect agreement, with values slightly below the ideal ratio. (Calculated c/a ratios for other IIIA–VA compounds, for which the NiAs phase is higher in enthalpy than the NaCl phase, tend to give values larger than the ideal; see Fig. 13 below.) However, after critical revision of the available experimental data for AlP and AlAs, Nelmes and McMahon (1998) consider the NiAs assignment of the phase as being likely to be correct but not yet certain. This invites further theoretical and experimental studies of these phases. Previous to the characterization of the high-pressure phase as NiAs, Wanagel *et al.* (1976) and Yu *et al.* (1978b) in AlP, and Weinstein *et al.* (1987) and Venkateswaran *et al.* (1992) in AlAs, had observed the existence of transitions, though the structure of the high-pressure phases was not identified at the time.

Experimental reports of a transition in AlSb date from 1962 (Minomura and Drickamer), but the structure of the high-pressure phase has been the subject of controversy. It has been assigned at various times as b-β-Sn (Jamieson, 1963b), NaCl (Yu *et al.*, 1978b), orthorhombic with tentative space group $Fmmm$ (Baublitz and Ruoff, 1983), and b-β-Sn again (Greene, Luo, Ghandehari, and Ruoff, 1995). However, the more recent experimental study of Nelmes *et al.* (1997) indicates that the high-pressure phase of AlSb is in fact Cmcm, and the theoretical study of Mujica, Rodríguez-Hernández, *et al.* (1999) supports this.

No further transitions have been observed up to the highest pressures investigated in AlP and AlAs; there is, however, experimental evidence for a transition to an unidentified phase in AlSb, beginning at about 41(3)

GPa (Greene, Luo, Ghandehari, and Ruoff, 1995; Nelmes *et al.*, 1997; Hirano *et al.*, 2001).

We can view the qualitative high-pressure behavior of AlP, AlAs, and AlSb described by first-principles calculations as being essentially the same, with the three compounds having a NiAs phase that is low in enthalpy (Liu *et al.*, 1995; Mujica *et al.*, 1995; Mujica, Rodríguez-Hernández, *et al.*, 1999). In this, these compounds are remarkably unlike the rest of the compounds considered here. In AlSb, the zb/NiAs coexistence pressure is slightly higher than that for zb/Cmcm and the Cmcm phase becomes strongly favored as pressure increases, with the result that in AlSb the interval of stability of the NiAs phase is obliterated by that of Cmcm (Mujica, Rodríguez-Hernández, *et al.*, 1999). The reported transitions show a very large hysteresis, and a precise location of the experimental coexistence pressure between the low- and high-pressure phases of these compounds is therefore not possible. Taking this uncertainty into account, the calculated values of the coexistence pressure are in reasonable agreement with experiments (Table II).

Prompted by the observation of the Cmcm phase in AlSb, Mujica, Rodríguez-Hernández, *et al.* (1999) have considered theoretically the existence of this phase in AlP and AlAs and have indeed found it to be favored over the NiAs phase at higher pressures. This prediction requires further experimental investigation. The number of structures considered in the theoretical work in these compounds is rather limited, and the existence of phases with even lower enthalpy cannot be ruled out. As in other compounds of the family, the CsCl phase is a possible candidate for AlP, AlAs, and AlSb at very high pressures (Mujica, Rodríguez-Hernández, *et al.*, 1999, but see Sec. VIII.D about the stability of CsCl phases).

5. GaP

At pressures a little above 20 GPa, the low-pressure zinc-blende phase of GaP undergoes a structural transition to a metallic phase II (Onodera *et al.*, 1974), which was initially thought to have a β-Sn-type structure (Baublitz and Ruoff, 1982b; Hu *et al.*, 1984) though several features of its diffraction pattern were not accounted for by this assignment (Yu *et al.*, 1978b). More recent ADX studies by Nelmes *et al.* (1997) indicate that a site-disordered Cmcm structure can in fact account for all of the features of the diffraction pattern of GaP-II. No further changes have been observed up to a pressure of 52 GPa. Rapid depressurization results in a mainly amorphous sample (Itié *et al.*, 1989).

First-principles calculations by Mujica and co-workers (Mujica and Needs, 1997; Mujica, Muñoz, and Needs, 1998) show that the (ordered) Cmcm and Imm2-type phases are very close in enthalpy at high pressures, with Immm (Imm2 with internal parameter $v=0.5$) being favored as the compression proceeds. The Immm phase has not, however, been reported in experiments. Interestingly, other results from these calculations, such as the existence of a field of stability for a sc16 phase and the near stability of a fourfold cinnabar phase, are very similar to findings for the more thoroughly researched material GaAs. As in that case, the combination of high pressure and high temperature as well as a detailed study of the reverse transition from Cmcm might lead to the observation of the sc16 and/or cinnabar phases.

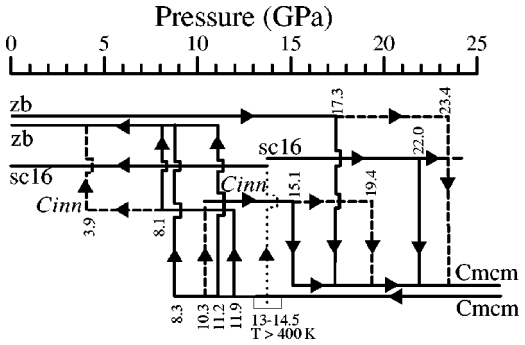

FIG. 8. Sequence of transitions followed by GaAs up to 25 GPa, after McMahon and Nelmes (1997) and McMahon *et al.* (1998): solid vertical lines, onset of the transition; dashed vertical lines, completion of the transitions; dotted line, the high-pressure temperature-driven transition to a sc16 phase.

6. GaAs

GaAs crystallizes in the zinc-blende structure. The first report of a pressure-driven transition in GaAs was due to Minomura and Drickamer (1962). Since then, there has been much interest in the structural response to compression of this technologically important material. A scheme of the pressure-driven structural transitions of GaAs, indicating their onset and completion, is shown in Fig. 8.

The structure of the high-pressure phase II was the matter of much debate and some confusion. Yu *et al.* (1978b) reported it to be orthorhombic, with an onset at about 17 GPa, and although it could not be conclusively solved at the time using EDX methods, all later experimental studies agreed on its orthorhombic symmetry (Baublitz and Ruoff, 1982b). Weir *et al.* (1989) considered it as having space group *Pmm2*, with atomic positions at 1(a) $(0,0,z_1=0)$ and 1(b) $(0,1/2,z_2\approx 0.35)$. However, their written description of the structure corresponds to a different ordering of the two atomic species among the lattice of sites of a true Pmm2 structure. Such a structure had been independently proposed in the theoretical study of Zhang and Cohen (1989) as the simplest ordering that maximizes the number of unlike nearest neighbors. Although it was not realized at the time, this ordered crystal corresponds in fact to the Cmcm structure later described in ZnTe-III (Nelmes, McMahon, Wright, and Allan, 1994), though using a different setting and further constraining Δy to be 0.5 (incorrectly, as this is not dictated by the symmetry), see the Appendix. It seems as though these two facts misled research in this field.

The Cmcm structure was later confirmed by Nelmes and McMahon (1998; see also McMahon and Nelmes, 1996). Although the ordering of the atoms in the pres-

surized sample at room temperature is difficult to ascertain due to the similar scattering powers of the two species and the broadening of the diffraction peaks, the diffraction pattern obtained after heating corresponds unequivocally to site-ordered Cmcm. The direct and reverse I↔II transitions were comprehensively studied by Besson *et al.* (1991) using different experimental methods.

A second transition was reported by Weir *et al.* (1989) at about 24 GPa, to another orthorhombic structure, Imm2 (with internal parameter $v=0.425$), which then gradually approaches an "sh-type" structure ($v=0.5$); see the Appendix. This, however, is not supported by the later ADX studies of McMahon and Nelmes (1996). First-principles calculations by Mujica, Needs, and Muñoz (1995) and Mujica and Needs (1996) show that the Cmcm and β-Sn-type (or Imm2-like) phases are close in enthalpy at high pressures and are clearly favored over other structures. The differences in their enthalpies border are, however, similar to the precision of the calculations, with Cmcm being favored at the pressures at which this phase is observed.

Release of pressure from GaAs-II results in a reversible transition to a fourfold-coordinated *cinnabar*-type (*cinn*) phase, which on further reduction of pressure reverts to the zb phase (McMahon and Nelmes, 1997). However no direct zb→*cinn* transition has been observed, which might indicate that the *cinn* phase is metastable, though low in enthalpy, as found in first-principles calculations (Kelsey *et al.*, 1998; Mujica *et al.*, 1998, 1999). The calculated internal coordinates are $u=v=0.5$, for which the symmetry becomes $P6_422$ (see the Appendix). The experimental values of the internal parameters are indeed close to 0.5. This is the first (and only) observation of a *cinnabar*-type phase in the IIIA–VA family.

First-principles studies had predicted the existence of a field of stability for an sc16 phase (binary analog of the bc8 phase observed in Si and Ge), which was, however, close to the numerical precision of the calculations (Crain, Piltz, *et al.*, 1994; Mujica *et al.*, 1995). Heating GaAs-II to ~450 K at about 14 GPa does indeed result in the sc16 phase, which persists at room temperature and also when pressure is released (McMahon *et al.*, 1998). Under compression, sc16 transforms into the Cmcm phase at 22 GPa. However, it is believed that only in the range 13–14.5 GPa (where the temperature-induced Cmcm→sc16 transition is observed) is the sc16 phase stable, which is in excellent agreement with the theoretical prediction.

7. GaSb

GaSb undergoes a transition at ~7–8 GPa (Minomura and Drickamer, 1962), from the zinc-blende phase to a phase II whose structure was initially reported as β-Sn-like (Jamieson, 1963b; Yu *et al.*, 1978b; Weir *et al.*, 1987). The actual ordering of the atomic species could not, however, be ascertained and the assignment was challenged by McMahon *et al.* (1994b), who found several features in the ADX diffraction profile of GaSb-II that do not accord with the β-Sn structure but that are in agreement with a closely related *disordered* orthorhombic Imma structure. However, Mezouar *et al.* (1999) did find a disordered β-Sn phase after taking great care to ensure that the pressure is hydrostatic, and concluded that the occurrence of the Imma phase was due to nonhydrostatic conditions in the pressure cell. Further experimental work by Vanpeteghem *et al.* (2002) has shown that heating the Imma phase at pressures up to ~13 GPa results in a transformation to the β-Sn structure, which suggests that β-Sn is indeed the stable phase in this pressure range. When the Imma phase is heated at pressures above ~13 GPa a new Ammm phase appears (mixed with the β-Sn phase below ~20 GPa). This is also a disordered (quasimonatomic) orthorhombic structure, closely related to the Imma structure. The Ammm and β-Sn phases remain stable at room temperature. The discovery of a β-Sn-like phase fulfills the expectation that the behavior of GaSb should be close to that of Si and Ge (for which similar phases are also observed), as GaSb has the lowest ionicity among the IIIA–VA family.

Weir *et al.* (1987) have reported a transition from GaSb-II to a "sh"-type phase at 27.8(6) GPa though the ordering (or lack thereof) of the atomic species in the crystal sites could not be determined. Application of pressure to the Imma phase by McMahon *et al.* (1994b) produced a slow increase of the v parameter towards 0.5, thus bringing the structure closer to Ammm (or sh-type, as the value of the axial ratio b/c is not far from the sh value $\sqrt{3}$, see the Appendix). However McMahon *et al.* (1994b) could not find evidence for a proper transition. Further changes in the diffraction profile of GaSb occur above 60 GPa (Weir *et al.*, 1987), indicating the onset of a new and as yet undetermined phase which appears to be site-disordered bcc (Nelmes and McMahon, 1998).

Martínez-García, Le Godec, Syfosse, and Itié (1999) have studied the phase diagram of GaSb for $p<8$ GPa and $250\ \mathrm{K}<T<1000\ \mathrm{K}$ (see Fig. 9).

8. InP and InAs

The behavior of InP and InAs appears to be similar in the range of pressures investigated. There is experimental evidence for a transition from the low-pressure zinc-blende phase to a site-ordered NaCl phase (Vohra *et al.*, 1985; Menoni and Spain, 1987; Nelmes, McMahon, Wright, Allan, Liu, and Loveday, 1995), which as pressure is further increased undergoes a Cmcm-type distortion (Nelmes, McMahon, Wright, Allan, Liu, and Loveday, 1995; Nelmes, McMahon, and Belmonte, 1997; Pascarelli *et al.*, 2002). As in other cases, previous experimental work reported the existence of a high-pressure β-Sn-type structure (Vohra *et al.*, 1985; Menoni and Spain, 1987), which was later ruled out. There is some evidence for the existence of an intermediate phase between NaCl and Cmcm in InAs (Nelmes, McMahon, Wright, Allan, Liu, and Loveday, 1995; see,

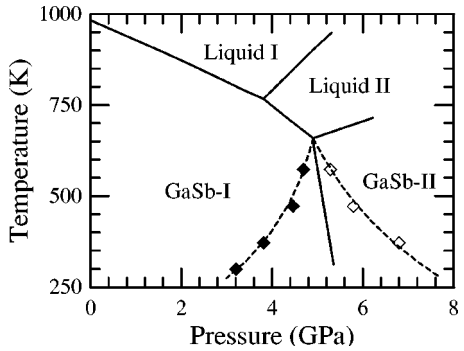

FIG. 9. Phase diagram of GaSb for $p<8$ GPa and 250 K$<T<$1000 K, adapted from Martínez-García, Le Godec, Syfosse, and Itié (1999): ◇, observed onsets of the I→II transitions at each constant temperature; ◆, observed onsets of I←II transitions; solid line, the phase boundary crudely evaluated as the midpoint between the two onsets. Note the much smaller T dependence of this estimated equilibrium pressure in comparison to that of the nonequilibrium boundaries (dashed lines), as well as the very large hysteresis at ambient T and its decrease as T increases.

however, Pascarelli *et al.*, 2002), and several features of the diffraction pattern of this material obtained on both pressure increase and decrease are not yet explained (Nelmes and McMahon, 1998). A slight *Pmma* distortion of the Cmcm structure has been observed in InAs (Pascarelli *et al.*, 2003). No further transitions in InP and InAs have been reported up to the maximum pressure reached of ~80 GPa.

Theoretical calculations support the NaCl structure as that of the first high-pressure phase (Christensen, 1986; Zhang and Cohen, 1987; Gorczyca *et al.*, 1989), and a continuous NaCl→Cmcm transition [although in the case of InP the calculated coexistence pressure is much lower than the transition pressure reported in the experiments (Mujica and Needs, 1997)]. The theoretical region of stability of NaCl-InAs appears to be rather small (Mujica and Needs, 1997; Christensen, Novikov, Alonso, and Rodriguez, 1999). At even higher pressures, the Immm structure becomes lower in enthalpy than Cmcm (Mujica and Needs, 1997).

9. InSb

It would not be an exaggeration to affirm that, to date, the high-pressure behavior of InSb is the most thoroughly studied experimentally of all the IIIA–VA semiconductors. However, the full phase diagram of InSb is not yet completely understood, and only recently has a coherent picture for pressures below 8 GPa and $T<800$ K emerged (Mezouar *et al.*, 1996; Nelmes and McMahon, 1998). In common with other recent advances in the field, this picture is radically different from the previously accepted one. New phenomena or reinterpretations of the fascinatingly complex phase diagram of InSb may well appear in the future.

InSb is isoelectronic to Sn and, as in that case, a moderate compression and/or increase of temperature already produces changes in the low-pressure zinc-blende structure. The full story of InSb, however, is too complicated to be told here in its entirety, particularly with regard to early research, and we shall be content with giving an overview of the current experimental observations, emphasizing only the most recent chapter. See Nelmes, McMahon, Hatton, *et al.* (1993) and Nelmes and McMahon (1998), and references therein for a fuller account of the earlier experimental studies.

The first indication of a pressure-driven phase transition was reported by Gebbie *et al.* (1960). Soon afterwards Jayaraman *et al.* (1961) located the transition pressure near 2 GPa and estimated the volume decrease as ~20%. Jayaraman *et al.* (1961) suggested that the structure of the new phase (II) was the binary analog of β-Sn, which much later proved not to be correct. The next few years saw the discovery of phases III and IV at moderately high pressures and temperatures, which were suspected to be hexagonal and orthorhombic, respectively. Darnell and Libby (1963) found that releasing pressure from ~2.5 GPa at low temperature resulted in a phase with the β-Sn structure, which was long believed to be the same as InSb-II. Following the rapid accumulation of experimental results, a phase diagram was first proposed by Banus and Lavine (1967, 1969). Yu *et al.* (1978a) confirmed the orthorhombic symmetry of InSb-IV, with space group *Pmm2* (the same structure that was later proposed for GaAs-II; see Sec. VII.B.6), and also suggested an orthorhombic structure for InSb-III. Later work by Vanderborgh *et al.* (1989) reported a new transition to a phase V at 6 GPa, described as an orthorhombic distortion of the hexagonal structure of phase III, which then gradually transformed to phase III (hexagonal). They also observed a new structure, reported as bcc, at pressures above 27.5(25) GPa. However, no definitive conclusion about the ordering of the atoms in any of these structures could be reached.

Since the beginning, the task of putting together a phase diagram for InSb from the different experimental observations was severely hampered by the presence of metastable intermediate phases, the difficulty in characterizing the structure of the phases, and the observation of different and yet reproducible sequences of transitions which the pressurized InSb samples may follow under different conditions. The comprehensive series of studies performed by Nelmes and co-workers (Nelmes, McMahon, Hatton, *et al.* 1993; Nelmes and McMahon, 1995, 1996, 1998) represents a significant advance in clarifying the high-pressure behavior of this material. According to these studies, at room temperature the zb phase may either transform at ~2.1 GPa to a mixture of a site-disordered β-Sn phase and an orthorhombic Immm phase, which in time recrystallizes to an s-Cmcm phase (super-Cmcm), or alternatively it may transform directly to s-Cmcm at the higher pressure of ~3 GPa. The s-Cmcm phase (see the Appendix) has a large orthorhombic unit cell and can be regarded as a site-ordered superstructure of the Cmcm phase observed in several other materials, corresponding to a certain decoration of its sites. At 9 GPa it transforms to the Immm phase via a site-disordered intermediate Imma phase [that is, disordered Imm2, with $v=0.392$ (Nelmes and McMahon, 1996)]. The appearance of Immm as a meta-

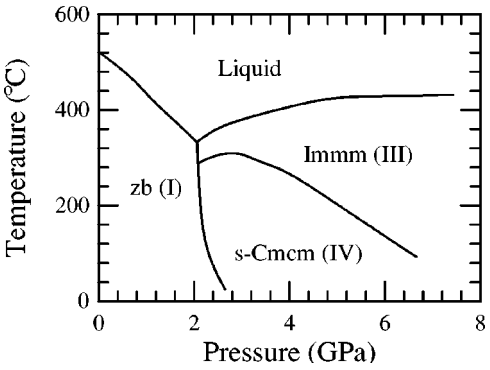

FIG. 10. Phase diagram of InSb for $p<8$ GPa and $T<600\,^{\circ}$C, after Mezouar *et al.* (1996).

stable intermediate phase at low pressures (and room temperature) as well as a truly stable phase at higher pressures is most curious. On further increase of pressure Immm transforms to another intermediate phase at ~17 GPa, of unknown structure, and then to a site-disordered bcc structure starting at 21(1) GPa (Nelmes and McMahon, 1996). This transition had been previously reported by Vanderborgh *et al.* (1989), who found the bcc phase to be stable up to at least 66 GPa. Further work by Mezouar *et al.* (1996) at high temperatures and (moderately) high pressures has led to the currently accepted phase diagram of InSb below 9 GPa and 800 K shown in Fig. 10.

Theoretical work by Guo *et al.* (1993) indicates that in the relaxed Imm2 phase the internal parameter v is very close to 0.5, which corresponds to the observed Immm phase. However, the s-Cmcm phase was not considered by these authors. More recently, Kelsey and Ackland (2000) have reported a study of the s-Cmcm, Cmcm, and Imm2 structures (including Immm and b-β-Sn). The enthalpies of these structures were found to be close at each pressure, with s-Cmcm slightly favored at lower pressures and Immm slightly favored at higher pressures. Their results are therefore in agreement with the present understanding of the phase diagram of this material, although the calculated s-Cmcm→Immm equilibrium pressure is too large (see Table V in the Appendix). Given that the $E(V)$ curves of these two phases are very close, this could be partly the result of small inaccuracies in the calculations. These results suggest that the equilibrium pressure might show a strong T dependence, which is evident in the phase diagram of Fig. 10. The calculated zb→s-Cmcm equilibrium pressure of 2.3 GPa (Kelsey and Ackland, 2000) is in excellent agreement with the experimental value of ~3 GPa (Nelmes and McMahon, 1995).

C. IIB–VIA compounds

1. ZnO

The first indication of a transition from the low-pressure wurtzite phase of ZnO (zincite) to a high-pressure NaCl phase at ~10 GPa was reported by Bates *et al.* (1962) and later confirmed by Jamieson (1970), and by Yu *et al.* (1978b) at 8.0(3) GPa. Recent EDX studies by Decremps *et al.* (2000, 2001) indicate that the transition occurs at ~9.8 GPa at room temperature. Although it shows a rather large hysteresis it was found to be fully reversible. Other studies, however, report the persistence of a large fraction of the NaCl phase after complete pressure release (Bates *et al.*, 1962; Recio *et al.*, 1998; Jiang *et al.*, 2000). Further experimental studies of the wur→NaCl transition in ZnO have been reported by Gerward and Olsen (1995), Karzel *et al.* (1996), Desgreniers (1998), and Kusaba *et al.* (1999).

Due to its technological importance in various fields (photovoltaics, optical coating, catalysis, ceramics, etc.) the properties of ZnO have been the subject of several theoretical studies in recent years (see Ahuja *et al.*, 1998, and references therein). The high-pressure behavior of ZnO has also attracted theoretical interest (Jaffe and Hess, 1993; Karzel *et al.*, 1996; Recio *et al.*, 1998; Jaffe *et al.*, 2000). The calculations confirm the stability of a NaCl phase at high pressure. Self-interaction-corrected PWPP calculations by Qteish (2000) indicate that it is an indirect-gap semiconductor with a wide band gap. However, the equilibrium pressure calculated using this approach (13.3 GPa) is significantly larger than both the LDA and GGA values (6.6 GPa and 9.3 GPa, respectively; see Jaffe *et al.*, 2000) and the experimental transition pressure.

2. ZnS

The stable low-pressure form of ZnS is zinc-blende. The metastable wurtzite phase is common at ambient conditions, and many intermediate polytypes have also been observed. As pressure is applied to zb-ZnS it transforms into the NaCl phase. Smith and Martin (1965) reported a transition pressure of 11.7 GPa, although later studies have placed it at a somewhat higher pressure [14.5(5) GPa according to Nelmes and McMahon, 1998; 15.5 GPa according to Uchino *et al.*, 1999]. The NaCl phase is found to be an indirect-gap semiconductor (Ves *et al.*, 1990; Zhou *et al.*, 1991), which has been confirmed by first-principles calculations (Jaffe *et al.*, 1993). The wur-ZnS phase has been reported to transform to the zb structure prior to a transition at higher pressures to NaCl (Desgreniers *et al.*, 2000). The effect of the decrease of grain size on the increase of the onset of the transition has been studied by Jiang *et al.* (1999) and Qadri *et al.* (2001). At pressures of about ~65 GPa the NaCl phase has been reported to undergo a Cmcm-like distortion with no significant change in volume (Nelmes and McMahon, 1998; Desgreniers *et al.*, 2000).

The high-pressure behavior of ZnS has been the subject of several recent theoretical studies which support the stability of the NaCl phase, with zb/NaCl equilibrium pressures in good agreement with the experimental observations (Qteish *et al.*, 1998; López-Solano *et al.*, 2003). However, self-interaction-corrected-PWPP calculations by Qteish (2000) yield a much larger value (21.1 GPa) for the equilibrium pressure, a situation already found in ZnO. López-Solano *et al.* (2003) have found

that, at pressures of about 65 GPa, the NaCl phase distorts into the Cmcm phase. Nazzal and Qteish (1996) have calculated the existence of a field of stability for a cinnabar phase, intermediate between the zb and NaCl phases, but this is not supported by experiments (Desgreniers *et al.*, 2000) or by later calculations (Qteish *et al.*, 1998). A hypothetical sc16 phase has been studied by Qteish and Parrinello (2000), who find it lower in enthalpy than the zb and NaCl phases between 12.8 and 16.2 GPa. By analogy with the behavior observed in GaAs, the validation of this possibility would require a combination of high pressures and temperatures, which so far has not been attempted in this material.

3. ZnSe

Similarly to ZnS, ZnSe transforms from the low-pressure zinc-blende phase into a site-ordered NaCl phase around 13 GPa (Smith and Martin, 1965; Karzel *et al.*, 1996). Recent Raman experiments have reported the existence of anomalies below that pressure (Greene, Luo, and Ruoff, 1995; Lin *et al.*, 1997), but other Raman (Arora *et al.*, 1988; Arora and Sakuntala, 1995) and ADX studies (McMahon and Nelmes, 1996) have not been able to locate any apparent structural discontinuity in this region. A continuous though very slow NaCl $\rightarrow$Cmcm transition has been observed at 30.0(5) GPa by McMahon and Nelmes (1996), who also report the possibility of a further distortion above 48 GPa.

The theoretical calculations indicate a situation similar to that in ZnS, with values for the zb$\rightarrow$NaCl transition in good agreement with the experimental observations [about 15 GPa from LAPW calculations by Smelyansky and Tse (1995); $\sim$11 GPa from PWPP calculations by Côté *et al.* (1997)]. The NaCl phase is calculated to be stable up to $\sim$36 GPa, where according to Côté *et al.* (1997) it becomes unstable against a Cmcm distortion. These authors also report the existence of a narrow field of stability (10.2–13.4 GPa) for a fourfold-coordinated *cinnabar*-type phase, intermediate between the zb and NaCl phases, which is, however, close to the resolution of the calculations. Qteish and Muñoz (2000) also find the *cinnabar* phase to be close in enthalpy at the zb/NaCl coexistence pressure and further predict an interval of stability for an sc16 phase (9.2–16.4 GPa). Motivated by these theoretical results, a very recent EDX experiment by Pellicer-Porres *et al.* (2002) has been able to obtain a *cinnabar* phase in ZnSe similar to that found in ZnTe. The *cinnabar* phase was observed within the very small pressure interval 10.1–10.9 GPa while slowly releasing the pressure from the NaCl phase.

4. ZnTe

The application of pressure to the zinc-blende phase of ZnTe induces a transition at about 9 GPa into a semiconducting phase II and a second transition at about 12 GPa into a metallic phase III (Smith and Martin, 1965; Ohtani *et al.*, 1980; Strössner *et al.*, 1987). The structural characterization of these high-pressure phases eluded the best experimental efforts for several years. ZnTe-II was finally solved as having the "*cinnabar*" structure with internal parameters u and v close to 0.5, which results in the fourfold-coordinated crystal described in the Appendix (McMahon *et al.*, 1993c; San Miguel *et al.*, 1993; Nelmes *et al.*, 1995b). Using the high resolution permitted by modern ADX techniques, Nelmes, McMahon, Wright, and Allan (1994) later characterized the structure of ZnTe-III as being Cmcm. This was the first time that such a structure was properly described in the literature (although in fact it had been lying unrecognized among the theoretical and experimental evidence gathered for GaAs and other IIIa–Va compounds; see Sec. VII.B.6). At $\sim$85 GPa there are indications of a transition to a new phase which remains unchanged up to the highest pressure reached in this material of 93 GPa (Nelmes and McMahon, 1998). A very recent Raman study has found some further evidence for an intermediate phase between *cinnabar* and Cmcm (Camacho *et al.*, 2002). Although the NaCl structure is not stable in ZnTe at room temperature at any pressure, it has been reported to be stable at high temperature (Shimomura *et al.*, 1997) [as cited by Nelmes and McMahon (1998)].

First-principles calculations confirm the sequence of transitions zb$\rightarrow cinn\rightarrow$Cmcm, with equilibrium pressures in good agreement with the experimental observations (Lee and Ihm, 1996; Côté *et al.*, 1997). They also show that, for both transitions, rotation of bonds towards lower-symmetry positions occurs near the equilibrium pressure to relieve excessive strain (Lee *et al.*, 1997). However, the limited number of structures considered so far has not yielded predictions of stable phases of ZnTe beyond Cmcm. The fact that ZnTe is the only member of the IIB–VIA family for which the NaCl phase has not been observed at room temperature is related to its having the lowest ionicity of that family (see Sec. VIII.B).

5. CdO

CdO crystallizes in the NaCl structure at normal conditions and does not undergo any transitions up to the highest pressure so far investigated of $\sim$30 GPa (Liu and Basset, 1986). The high-pressure behavior of CdO has not been the subject of any first-principles calculation, though a model calculation by Majewski and Vogl (1987) suggests that the CsCl structure is favored at large compressions.

6. CdS and CdSe

CdS and CdSe occur at normal conditions both in the semiconducting wurtzite and (metastable) zinc-blende structures. In both materials the low-pressure wur phases are known to transform at about 2 GPa (Edwards and Drickamer, 1961) to an (indirect band-gap) semiconducting NaCl phase (Mariano and Warekois, 1963; Rooymans, 1963). There are two reports of an additional transition in CdS at about 50 GPa to an orthorhombic phase (CdS-III), which appears to be a site-ordered distortion of the NaCl phase and for which the low-temperature KCN-type structure with space group

Pmmn (according to Suzuki *et al.*, 1983) and the Cmcm structure (according to Nelmes and McMahon, 1998) have both been proposed. For CdSe, Nelmes and McMahon (1998) find a continuous transition to a site-ordered Cmcm structure at about 27 GPa and some evidence of a further (unresolved) distortion at about 36 GPa. No further changes have been observed in these materials.

The NaCl→Cmcm transition in CdSe had been anticipated by the first-principles calculations of Côté *et al.* (1997), who also found a cinn-type structure very close in enthalpy at the calculated zb→NaCl equilibrium pressure. Calculated equilibrium pressures are in excellent agreement with the experimental observations. However, the existing theoretical studies do not shed any light on the post-Cmcm behavior of CdS or CdSe.

7. CdTe

The low-pressure phase of CdTe has the zinc-blende structure. Although a direct zb→NaCl transition was initially reported at about 3.5 GPa (Mariano and Warekois, 1963), it was later found that the transition occurs via an intermediate semiconducting cinnabarlike phase which has a very small field of stability (McMahon *et al.*, 1993a; Nelmes, McMahon, Wright, and Allan, 1993). In fact this cinn-like structure has $4+2$ coordination, instead of the twofold coordination of α-HgS (true cinnabar), and upon compression it approaches the sixfold coordination of NaCl. A further transition is observed at about 10 GPa (Samara and Drickamer, 1962) to a phase that Nelmes *et al.* (1995a) have conclusively identified as site-ordered Cmcm. As in several other cases, this Cmcm phase had previously been reported to have a β-Sn-type structure (Owen *et al.*, 1963; Hu, 1987). A new and as yet unidentified phase has been observed at 42(2) GPa (Nelmes and McMahon, 1998), which does not undergo any further transitions up to the maximum pressure reached of 55 GPa.

Martínez-García, Le Godec, Mezouar, *et al.* (1999) have studied the p-T phase diagram of CdTe in the region up to 5 GPa and ~1200 K. As temperature is increased, the field of stability of the cinnabar phase decreases until it disappears at the triple point of the coexistence of phases I (zb), II (cinn), and III (NaCl), which is located at 2.6(1) GPa and 735(20) K.

The zb→cinn→NaCl→Cmcm sequence is correctly reproduced in the PWPP theoretical study of Côté *et al.* (1997), as is the small field of stability of the cinnabar phase, although the calculated NaCl→Cmcm equilibrium pressure slightly overshoots the experimental onset. Ahuja *et al.* (1997) have further found that the CsCl structure is favored over the Cmcm structure at pressures above 28 GPa, but such a phase has not been observed in the range of pressures covered by the experiments. As for other IIB–VIA compounds, the limited search of local minima over a reduced set of structures has so far not given more information about the phases of CdTe beyond Cmcm.

8. HgO, HgS, HgSe, and HgTe

Very few theoretical studies of the mercury chalcogenides under pressure have been reported so far. Lu *et al.* (1989) considered only the NaCl and b-β-Sn structures in their LAPW study of the high-pressure stability of HgTe and HgSe.

There have been, however, a number of experimental studies that indicate that the mercury chalcogenides show rather similar sequences of structures under pressure. The common form of HgO at normal conditions is orthorhombic, with space group *Pnma* and eight atoms in the unit cell. This twofold-coordinated structure can be seen as being built up of zigzag chains in which the Hg and O atoms alternate (Aurivillius, 1956). A cinnabarlike phase, similar to that of HgS, as well as other more complex forms have also been observed (Aurivillius and Carlsson, 1958). The structure of the high-pressure phases of HgO has yet to be conclusively settled. The first transition, at 14(1) GPa, is to a phase that has been tentatively characterized as a (slight) tetragonal distortion of the NaCl structure with space group $I4/mmm$ or a very close variant (Nelmes and McMahon, 1998; Zhou *et al.*, 1998). A second transition towards an undistorted NaCl phase, beginning at 26(3) GPa, has been reported by Nelmes and McMahon (1998). A previous Raman study indicated a transition to a metallic state near 28 GPa (although the authors did not consider that it was related to any structural change) and suggested the possibility of a new structural transition above 34 GPa (Zhou *et al.*, 1998; see therein for references to previous work).

HgS is observed under normal conditions in both the cinnabar phase (α or "red" form) and the (metastable) zb phase ("black" form). The cinnabar phase transforms into a NaCl phase at a pressure that has recently been located at about 20 GPa using high-resolution ADX techniques (Nelmes and McMahon, 1998). In earlier work, Huang and Ruoff (1985) had reported the existence of the NaCl phase at 30 GPa, although the onset of the cinn→NaCl transition was located at the much lower pressure of ~13 GPa. Nelmes and McMahon (1998) found evidence for a continuous transition to a phase III that appears to be a distortion of NaCl. The Cmcm assignment would be in line with observations for HgSe and HgTe.

HgSe and HgTe appear to have similar behavior under compression. Their ambient-pressure (semimetallic) zinc-blende phases transform first into a semiconducting cinnabar-type structure at the very low "high pressure" of ~1 GPa (Kafalas *et al.*, 1962; Mariano and Warekois, 1963) which on further compression transforms into a NaCl phase (Ohtani *et al.*, 1982; Onodera *et al.*, 1982; Werner *et al.*, 1983; Huang and Ruoff, 1985). A second, very close transition from zb to an orthorhombic phase with space group $C222_1$, which is a distortion of zb, has been reported at pressures slightly above the onset of the zb→cinn transition, in the region of coexistence of the zb and cinn phases (McMahon, Nelmes, Liu, and Belmonte, 1996). This "hidden" $C222_1$ transition is

therefore formed when the zb phase is already thermodynamically unstable with respect to the cinn phase, though it has not yet completely transformed to cinn as a result of the sluggish kinetics of the transition. The $C222_1$ phase further transforms into the cinn phase upon slight pressure increase. A precise *in situ* characterization of the cinn-HgTe phase and its pressure evolution has been reported by Wright *et al.* (1993) and San Miguel *et al.* (1995).

There is a further transition at 25–30 GPa in HgSe and at $\sim$10 GPa in HgTe to a phase which has been identified as site-ordered Cmcm by McMahon, Wright, *et al.* (1996) and Nelmes *et al.* (1997), and which, as in most other cases of reported Cmcm phases, had been previously characterized as β-Sn-type or bct-type (Werner *et al.*, 1983; Huang and Ruoff, 1985). This is a first-order transition, although the change in volume is very small. For HgTe, there is a further transition into a structure reported as distorted CsCl by Huang and Ruoff (1985) or disordered CsCl (bcc) by Nelmes *et al.* (1995b), who also find a much lower onset. There are no further transitions up to the highest pressures reached of about 50 GPa.

VIII. HIGHLIGHTS OF THE RESULTS: THE NEW SYSTEMATICS

During the last decade our understanding of the high-pressure phase diagrams of these families of compounds has changed beyond all recognition. The "old systematics" was essentially that Si and Ge transformed from cd$\rightarrow\beta$-Sn$\rightarrow$sh and then into close-packed phases, while the IIIA–VA and IIB–VIA compounds transformed from the low-pressure zb or wur phases into the b-β-Sn or NaCl structures. The old systematics involved only high-symmetry phases after the first transition. The new systematics is much richer than this and yet it shows some well-defined trends (see also Sec. X).

In the new systematics most of the materials transform into structures with quite low symmetries, so there is much more complexity at intermediate pressures. Si and Ge have been studied more intensively and to higher pressures than the other semiconductors reviewed here. So far only they have been persuaded to adopt high-symmetry close-packed structures and this occurs at rather large pressures. There might be a greater reluctance of the IIIA–VA and IIB–VIA compounds to adopt close-packed structures because they involve a large number of "wrong bonds," which are not energetically favored.

A. Nonexistence of the binary analog of the β-Sn structure

A striking result of recent research is the nonexistence of b-β-Sn (Imm2 with $v=0.25$ and $b/a=1$, see the Appendix), the *ordered* binary analog of the β-Sn structure, in the phase diagrams of the IIIA–VA and IIB–VIA binary compounds (Nelmes *et al.*, 1997). Several phases that were initially believed to have a b-β-Sn-type structure have been reassessed as Cmcm (see below) after careful examination of higher-resolution experimental data. However, the *disordered* β-Sn structure as well as the closely related Imma structure (disordered Imm2) have been observed in GaSb and InSb; and the *ordered* Immm structure (Imm2 with $v=0.5$) is stable at high pressures in InSb, which is also supported by calculations (Kelsey and Ackland, 2000). In fact, restricted-symmetry first-principles studies of the energetics of the Imm2-type structure, of which b-β-Sn and Immm are particular cases, have found that they have rather low enthalpies at high pressures in several other IIIA–VA binary compounds [see, for example, Mujica and Needs (1997) for InP and InAs], so that they are at least competitive in some range of pressures. In some cases, however, these β-Sn-type phases are dynamically unstable (Ozoliņš and Zunger, 1999), so that one can find structures with even lower enthalpy if the symmetry restrictions are relaxed.

B. The ubiquitous Cmcm phase

A most conspicuous result is the discovery of an orthorhombic Cmcm phase at high pressures in many members of the IIIA–VA and IIB–VIA families (or of related superstructures with the same *Cmcm* symmetry, as in the case of InSb). The quasi-eightfold-coordinated Cmcm form can be understood as a binary analog of the homonuclear simple hexagonal structure observed in Si and Ge at high pressures (Kelsey and Ackland, 2000; see also the Appendix). Cmcm can be obtained as a deformation of the NaCl structure, whose primary distortion is a shearing of alternate (001) planes in the [010] direction. Such a pattern of atomic displacements corresponds to a transverse-acoustic phonon at an X point on the zone boundary, which effectively doubles the dimension of the primitive unit cell with respect to that of NaCl. The NaCl$\rightarrow$Cmcm transition observed in InP, InAs, ZnTe, CdSe, CdTe, HgSe, and HgTe, and possibly also in ZnS, CdS, and HgS (see Tables II and III) is related to the softening of the TA(X) phonon of the NaCl phase under increasing pressure [negative Grüneisen parameter $\gamma_{TA}(X)=\partial \ln \omega_{TA}(X)/\partial \ln V$]. This is a general trend in these families of compounds (Mujica and Needs, 1996, 1997; Mujica *et al.*, 1996; Côté *et al.*, 1997; Ozoliņš and Zunger, 1999).

Ozoliņš and Zunger (1999) have, moreover, shown that the compression required to produce the instability increases as the ionicity of the material increases, on account of the positive contribution of the Madelung energy to $\gamma_{TA}(X)$. This explains why the high-pressure NaCl phases of AlN, GaN, and InN (which are the members of the IIIA–VA family with largest ionicity) do not undergo a Cmcm-type distortion in the range of pressures so far investigated experimentally. PWPP calculations by Serrano *et al.* (2000) indicate that extremely large pressures of several hundreds of GPa would be required to reach the onset of the instability in these cases. Conversely, this also explains why ZnTe (the least ionic of the IIB–VIA compounds) is the only compound

of the family that does not have a NaCl phase at high pressure and room temperature; the NaCl structure is already unstable when the transition from *cinn* to Cmcm takes place. A similar statement holds for AlSb, InSb, GaAs, and GaP, which transform directly from the low-pressure zb structure into high-pressure Cmcm-type structures.

C. Other recent findings

Other interesting results have emerged from recent research: the singular observation of NiAs-type phases in AlP and AlAs (Greene Luo, Li, and Ruoff, 1994; Greene, Luo, and Ruoff, 1994), which previous first-principles calculations had found as promising candidates in these compounds (Froyen and Cohen, 1983); the observation of a sc16 phase in GaAs, after heating of Cmcm-GaAs at high pressure (McMahon *et al.*, 1998) [also anticipated by theoretical calculations (Crain, Piltz, *et al.*, 1994; Mujica *et al.*, 1995) and still a prediction for other members of these families]; the identification of Si-VI as Cmca (Hanfland *et al.*, 1999), a structure which was afterwards discovered in Ge (Takemura *et al.*, 2000) and which further emphasizes the similarity in the behavior of these two elements; the experimental discovery of several intermediate phases (e.g., Imma in Si and Ge); and, in particular, the observation of several cases of cinnabar-type phases in IIIA–VA and IIB–VIA compounds, a structure that plays an important role in the new systematics of these compounds (Nelmes and McMahon, 1998).

Until recently it was thought that the existence of a low-enthalpy cinn-type phase at low or moderately high pressures was a characteristic exclusively of the mercury chalcogenides. However, the last decade has seen the discovery of cinn-type phases in ZnTe (San Miguel *et al.*, 1993), CdTe (Nelmes, McMahon, Wright, and Allan, 1993), and GaAs (McMahon and Nelmes, 1997), and very recently also in ZnSe (Pellicer-Porres *et al.*, 2002). In these compounds, first-principles calculations unequivocally show that the relative positioning of the $E(V)$ curves of the cinn-type phases is "intermediate" (in the volume and energy scales) between those of the low-pressure zb phases and the NaCl or Cmcm high-pressure phases (similar to phase iii with respect to phases I and II in Fig. 3; see, for example, the case of GaAs in Mujica *et al.*, 1998). [In *all* the mercury chalcogenides, the well-known cinn phases are characteristically much lower in enthalpy (in the case of HgS it is in fact the stable phase under normal conditions).] For this reason, a small shift in energy may result in the disappearance of the field of stability of the cinn-type phase (see Sec. V.E), which is in agreement with (a) the small range of pressures in which these phases are observed, (b) its disappearance as T increases in the case of CdTe, and (c) the possible metastable character of *cinn*-GaAs and *cinn*-ZnSe (which are only observed on decrease of pressure). Possibly, the role of the cinn-type structure in these materials, as an "intermediate" between low-pressure fourfold structures and high-pressure sixfold NaCl-like configurations, is related to its ability to accommodate both tetrahedral and sixfold coordination by variation of its free structural parameters.

D. IIIA–VA and IIB–VIA binary compounds at very high pressures: further transitions

More research is still needed to arrive at a clear picture of the behavior of the IIIA–VA and IIB–VIA families under very high pressures. The CsCl structure has long been considered as a candidate at very large compressions on account of its low Madelung energy, which becomes dominant in determining structures at small volumes (Froyen and Cohen, 1983; Zhang and Cohen, 1987). Indeed, a CsCl phase should be favored at high pressures by most compounds on the basis of first-principles calculations with fixed symmetry (Mujica *et al.*, 1995; Mujica and Needs, 1997). From x-ray studies, a pseudo-bcc structure (the disordered analog of CsCl) has in fact been proposed for the very-high-pressure phases observed in GaSb, InSb, and HgTe.

DFPT calculations by Kim *et al.* (1999) indicate, however, that whereas the CsCl phase is stable in InSb, it is dynamically unstable within some range of high pressures with respect to transverse-acoustic [$\xi\xi 0$] phonons in the cases of GaP, GaAs, InP, and InAs, a result that could well carry over to other members of the family. From symmetry analysis of the soft phonon modes, Kim *et al.* proposed two structures with lower *Pmma* and $P4/nmm$ symmetry as likely candidates to replace the CsCl phase in InP at such pressures. These are the AuCd-type structure (oP4 or B19; see the caption to Table IV) and the InBi-type structure (tp4 or B10), respectively. Similar structures might be low in enthalpy in other cases as well.

E. Site-disordered phases

The ordering of the two atomic species of a binary compound on the sites of a crystal lattice is difficult to determine from x-ray-diffraction experiments. It hinges on the detection of "difference reflections" in which the two sublattices of atoms scatter in antiphase, with the result that their intensity depends on the difference in scattering powers of the two chemical species (see Sec. II.C.4). Nonetheless, the higher resolution of modern ADX techniques permits the detection of such reflections in many cases where they had passed unnoticed in earlier studies. The absence of difference reflections indicates that the crystal lacks long-range site ordering, although this does not necessarily mean that the two atomic species are randomly distributed over the lattice sites. The length scale of the ordering cannot in fact be precisely established solely from diffraction experiments, though they may give an upper bound for its range.

ADX studies performed during the last decade have revealed that most of the high-pressure phases of the IIIA–VA and IIB–VIA binary compounds are site ordered (Nelmes and McMahon, 1998). Some of the

TABLE III. Same as Table I, for the IIB–VIA materials considered in this review. No transitions in CdO have been reported. A question mark accompanying the name of a structure indicates that there are doubts about its characterization.

Reference (experiment)	p_t (GPa)	ΔV	Transition	p_e (GPa)	ΔV	Reference (theory)
ZnO wur(I)→NaCl(II)<56 GPa						
Desgreniers, 1998 (EDX)	1.9(2)|9.1(2)	16.7	wur→NaCl	6.6	16.7	Jaffe *et al.*, 2000
ZnS zb(I)→NaCl(II)→Cmcm?<96 GPa						
Ves *et al.*, 1990 (EDX)	14.7(10)	15.7	zb→NaCl	14.35	16.0	Qteish *et al.*, 1998
Nelmes and McMahon, 1998 (ADX)	69(3)	-	NaCl→Cmcm	~65	~0	López-Solano *et al.*, 2003
ZnSe Compression: zb(I)→NaCl(II)→Cmcm(III)<120 GPa Decompression: zb(I)←[*cinn*]←NaCl(II)						
Karzel *et al.*, 1996 (ADX)	9.5(5)|13.0(5)	15.3(6)	zb→NaCl	~11	-	Côté *et al.*, 1997
McMahon and Nelmes, 1996 (ADX)	~30	~0	NaCl→Cmcm	36.5	1	Côté *et al.*, 1997
Pellicer-Porres *et al.*, 2002 (EDX)	10.9	6.3	[*cinn*]←NaCl	13.4	7.7	Côté *et al.*, 1997
Pellicer-Porres *et al.*, 2002 (EDX)	10.1	9.8	zb←[*cinn*]	10.2	9.2	Côté *et al.*, 1997
Observations: The Cmcm phase might undergo a distortion at ~50 GPa (Nelmes and McMahon, 1998).						
ZnTe zb(I)→*cinn*(II)→Cmcm(III)→n.d.<93 GPa						
San Miguel *et al.*, 1993 (EDX/XAS)	~8|9.5(5)	*~13*	zb→*cinn*	8.1	*9.0*	Lee and Ihm, 1996
Nelmes, McMahon, Wright, and Allan, 1994 (ADX)	11	*5.7(2)*	*cinn*→Cmcm	10.2	*6.0*	Lee and Ihm, 1996
Observations: An unidentified phase has been observed in experiments above ~85 GPa (Nelmes and McMahon, 1998).						
CdS wur(I)→NaCl(II)→n.d.(III)†<68 GPa						
Nelmes and McMahon, 1998 (ADX)	2.3(3)	-	wur→NaCl	3.1	19.8	‡Knudson *et al.*, 1999
Nelmes and McMahon, 1998 (ADX)	51(9)	-	NaCl→n.d.†			
Observations: (†) Believed to consist of a distortion of the NaCl structure for which both the *Pmmn* space group (Suzuki *et al.*, 1983) and the Cmcm structure (Nelmes and McMahon, 1998) have been proposed; (‡) HF-DFT calculation.						
CdSe wur(I)→NaCl(II)→Cmcm→~Cmcm<85 GPa.						
Cline and Stephens, 1965 (EDX)	1.72(7)|2.52(1)	*16.4*	wur→NaCl	2.5†	19.8†	Côté *et al.*, 1997
Nelmes and McMahon, 1998 (ADX)	27.0(5)	-	NaCl→Cmcm	29	1.7	Côté *et al.*, 1997
Nelmes and McMahon, 1998 (ADX)	36(1)	-	Cmcm→~Cmcm			

TABLE III. (*Continued*).

Observations: ~Cmcm stands for an unresolved distortion of the Cmcm phase. (†) Values for the zb→NaCl transition.						
CdTe zb(I)→[cinn(II)]→NaCl(III)→Cmcm(IV)→n.d.<55 GPa.						
McMahon *et al.*, 1993a (ADX)	2.67|3.53	*13.4(1)*	zb→[cinn]	2.5	13.1	Côté *et al.*, 1997
McMahon *et al.*, 1993a (ADX)	3.70|3.8	*2.6(2)*	[cinn]→NaCl	2.8	7.5	Côté *et al.*, 1997
Nelmes, McMahon, Wright, and Allan, 1995a (ADX)	10.1	~0	NaCl→Cmcm	12	1.8	Côté *et al.*, 1997
Observations: A transition from Cmcm to an unresolved phase has been reported at 42 GPa (Nelmes and McMahon, 1998).						
HgO Pnma(I)→I4/mmm?(II)→NaCl<34 GPa.						
Zhou *et al.*, 1998 (ADX/Raman)	14(1)	~0	Pnma→I4/mmm?			
Nelmes and McMahon, 1998 (ADX)	26(3)	-	I4/mmm?→NaCl			
HgS cinn(I)→NaCl(II)→n.d.(III)†<55 GPa.						
Nelmes and McMahon, 1998 (ADX)	20.5(7)	-	cinn→NaCl			
Nelmes and McMahon, 1998 (ADX)	52(3)	-	NaCl→n.d.†			
Observations: (†) Presumed to be a distortion of NaCl, possibly Cmcm.						
HgSe zb(I)→cinn(II)→NaCl(III)→Cmcm(IV)<50 GPa and zb(I)→[$C222_1$]→cinn(II) (see Sec. VII.C.8).						
McMahon, Nelmes, Liu, and Belmonte, 1996 (ADX)	~0.4|1.15(5)	*9.9(1)*†	zb→cinn			
McMahon, Nelmes, Liu, and Belmonte, 1996 (ADX)	14.6(6)	*0.2(4)*‡	cinn→NaCl			
Nelmes *et al.*, 1997 (ADX)	~25	*0.9(5)*	NaCl→Cmcm			
McMahon, Nelmes, Liu, and Belmonte, 1996 (ADX)	2.1	*1.2(1)*	zb→[$C222_1$]			
McMahon, Nelmes, Liu, and Belmonte, 1996 (ADX)	2.25	*8.6(1)*	[$C222_1$]→cinn			
Observations: (†) From data at 1.80 GPa. (‡) From data at 15.7 GPa.						
HgTe zb(I)→cinn(II)→NaCl(III)→Cmcm(IV)→bcc(V)<51 GPa and zb(I)→[$C222_1$]→cinn(II) (see Sec. VII.C.8).						
San Miguel *et al.*, 1995 (ADX)	1.5	*11(2)*	zb→cinn			
San Miguel *et al.*, 1995 (ADX)	8	*3(1)*	cinn→NaCl			
McMahon, Wright, *et al.*, 1996 (ADX)	10.2(3)	*1.2(1)*	NaCl→Cmcm			
Nelmes *et al.*, 1995b (ADX)	28	*3.0(3)*	Cmcm→bcc			
McMahon, Nelmes, Liu, and Belmonte, 1996 (ADX)	2.25	*1.2(1)*	zb→[$C222_1$]			
McMahon, Nelmes, Liu, and Belmonte, 1996 (ADX)	2.6	*8.7(1)*	[$C222_1$]→cinn			

phases observed are, however, reported to be site disordered because of the absence of difference reflections. Site disorder is more commonly found in IIIA–VA compounds than in the IIB–VIA family. This may be associated with the occurrence of wrong bonds in disordered compounds, which are very unfavorable in the IIB–VIA compounds. Interestingly, the compound in which the strongest evidence for the presence of only very short-ranged order (of the length of two unit cells at most) has been found is GaSb, which has a very low ionicity so that the energy penalty for wrong bonds is expected to be small. In some cases it may be that the true equilibrium phases are ordered but that the kinetics of the phase transition prevents the ordered structure from being formed, although this requires further investigation.

Disordered structures are challenging to treat from first principles. Ackland (2001b) has recently studied disordered β-Sn phases (which have been observed in GaSb and InSb) using a next-nearest-neighbor antiferromagnetic Ising model with coupling constants determined from PWPP-LDA calculations. Three different decorations of the β-Sn lattice of sites were proposed and it was concluded that some IIIA–VA compounds (e.g., GaSb) could adopt one or another as a function of T.

F. Lessons about the calculations

The most important lesson about the application of first-principles density-functional calculations to the high-pressure phases of these materials is that the agreement with experiment is outstandingly good. There are rather few differences between the theoretical and experimental sequences of stable phases under pressure. The energy differences between candidate structures are often very small, and the calculations must be done with the highest possible numerical precision. The majority of the most accurate density-functional calculations reviewed here were performed using the PWPP method, although we must emphasize that some excellent results have been obtained with other techniques. The impressive results indicate that the standard pseudopotential approximation works well even at highly compressed volumes. The pseudopotential approximation must eventually break down, but with modern techniques such as the projector augmented wave method (Blöchl, 1994) and the ultrasoft pseudopotential method (Vanderbilt, 1990) it is not too costly to allow some of the core electrons to relax.

There are, however, some significant and systematic differences between the theoretical equilibrium pressures and the experimental transition pressures. In Fig. 11 we have plotted calculated LDA equilibrium pressures at $T=0$ (p_e) for the first observed transitions against the corresponding experimental values at room temperature of the transition pressure (p_t). On the whole the agreement between theory and experiment is good, although there is a clear trend for the coexistence pressures calculated within the LDA to be lower than the corresponding experimental values. The only two

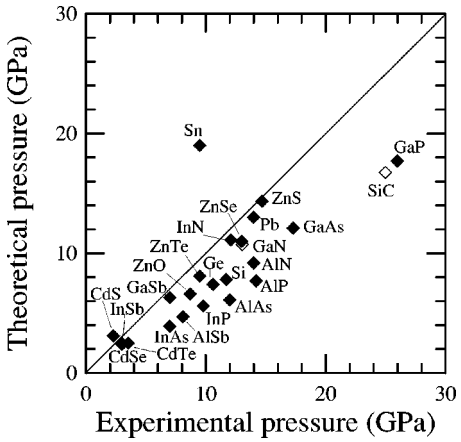

FIG. 11. Theoretical LDA coexistence pressures vs experimental transition pressures for the first phase transition in group-IVA elements and IIIA–VA and IIB–VIA compounds. The data are those in Tables I–III. The values of the pressures for SiC and GaN (◇) have been divided by 4 in order to represent them on the scale shown.

materials not conforming to this rule are Sn [where p_e is subject to a large uncertainty due to the closeness of the $E(V)$ curves for the β-Sn and bct phases, and where the phase boundary has a large T dependence] and CdS (where the discrepancy is very small and is probably within the numerical precision of calculations).

There may be several explanations for this systematic underestimation. At room temperature, a solid phase may remain metastably in a "superpressurized" state well beyond its field of thermodynamic stability. The experimental onset of the transition on increase of pressure must then be regarded as an upper bound on the thermodynamic coexistence pressure, whereas the onset of the reverse transition represents a lower bound. The lowest pressure transition in the materials reviewed here is normally subject to considerable hysteresis at room temperature (see, for example, Figs. 8 and 9 for GaAs and GaSb, respectively), and the true coexistence pressure is therefore difficult to locate from the experiment. In those cases where the reverse transition has been experimentally studied, the calculated coexistence pressure p_e lies between the values of both onsets, that is, within the experimental uncertainty related to hysteresis.

Other factors may add to the uncertainty in the comparison between theoretical and experimental transition pressures. Temperature is certainly an issue here, not only because most LDA calculations are for $T=0$ and neglect the zero-point motion of the ions, but also because heating reduces the hysteresis of the transition observed in experiments (see Fig. 9). The full p-T diagrams of the solid phases of these materials are now beginning to be systematically studied, and a wealth of new information is expected to come from these studies. So far only a few of these compounds have been analyzed in some detail at high temperatures and high pressures. On the theoretical side, Gaál-Nagy *et al.* (1999) have shown that incorporating the effects of lattice vi-

brations at room temperature reduces the calculated cd/β-Sn coexistence pressure in Si and Ge, a result that is likely to carry over to other compounds considered here.

Another potential source of experimental uncertainty arises from the stress conditions within the pressure chamber. It has been observed in experiments that the onset of the cd$\rightarrow\beta$-Sn transition in Si and Ge occurs at lower pressures ($\sim$8 GPa; cf. the values of p_e and p_t given in Table I for hydrostatic conditions) when the conditions in the pressure cell are nonhydrostatic (Baublitz and Ruoff, 1982a; Werner *et al.*, 1982; Qadri *et al.*, 1983; Olijnyk *et al.*, 1984; Hu *et al.*, 1986; Menoni *et al.*, 1986). The same effect is observed in binary compounds (see, for example, the case of GaAs in Besson *et al.*, 1991). Cheng *et al.* (2001) and Hebbache *et al.* (2001) have recently investigated the effects of nonhydrostatic conditions on the phase stability of Si via first-principles calculations. Though the role of shear stress in the kinetics of solid-solid reconstructive phase transitions has not been sufficiently explored, the experimental evidence suggests that it reduces hysteresis, bringing the observed transition pressure closer to the true equilibrium pressure (Besson *et al.*, 1991; Greene, Luo, Ruoff, Trail, and DiSalvo, 1994).

Nevertheless it seems likely that the LDA systematically underestimates the true coexistence pressure for the first transition. Calculations by Moll *et al.* (1995) have shown that using GGA density functionals increases the equilibrium pressure for the cd$\rightarrow\beta$-Sn transition in Si and Ge, bringing the calculated value of p_e closer to the experimental onset of the transition. The effect of the gradient terms is to lower the energy of the diamond phase, which has a significantly less homogeneous valence charge density because of the strong covalent bonds. The LDA is expected to give a better description of the β-Sn phase because it is a metal with relatively smooth valence charge densities. The idea that the LDA places the diamond phase too high in energy has recently received support from highly accurate quantum Monte Carlo calculations (see Foulkes *et al.*, 2001). The dependence of the lowest pressure transition on the density functional indicates that a more sophisticated treatment of the electron correlation is warranted in this case.

It appears likely, however, that the pressures of the higher transitions are less dependent on whether the LDA or GGA functionals are used. The agreement between the best calculated and experimental pressures for higher transitions in Si and Ge is very good. These are transitions between metallic phases with smoother charge densities, so that the LDA and GGA results are expected to be similar, and the experimental hysteresis is generally small. These expectations are given more weight by the recent calculations of Jaffe *et al.* (2000), who reported LDA and GGA calculations on ZnO and MgO, finding that the GGA corrects the tendency of the LDA to underestimate the transition pressures between the lower-pressure phases, but that the LDA and GGA give similar values for the high-pressure transitions.

IX. PHENOMENOLOGICAL SCALES

Many theoretical and experimental data have been accumulated on the high-pressure phases of the group-IVA, IIIA–VA, and IIB–VIA materials. One question that arises is whether we can order these data to reveal underlying trends. A very useful way of doing this is to use phenomenological scales.

The behavior of an A^NB^{8-N} compound is of course entirely determined by the identities of A and B. We could therefore use the atomic numbers, Z_A and Z_B, as coordinates to describe the behavior of A^NB^{8-N} compounds. However, the properties of interest (essentially the relative stability of the structures) are not smooth functions of Z_A and Z_B. For example, Si ($Z_A=14$, $Z_B=14$) and Ge ($Z_A=32$, $Z_B=32$) have very different coordinates on a (Z_A,Z_B) diagram, but their structural behavior is very similar. It is much more useful to use coordinates such as electronegativity differences or ionicity, ionic, metallic, and covalent radii, bond order, and the degree of orbital hybridization, which relate directly to the chemical nature of the compounds. For each compound the different coordinates are assigned values from some quantitative scale. The objective is to construct a systematic way of rationalizing the data, uncovering trends and ultimately making predictions. Such scales have been used in quantitative models for the prediction of physical quantities such as heats of formation of molecules and solids (Miedema, 1973). Ideally the coordinates should be transferable. For example, it is hoped that a scale constructed from free-atom quantities will be applicable to solids.

One well-known coordinate is the *ionicity*, which quantifies the degree of ionic bonding. Scales of ionicity can be set up using experimental data such as heats of formation (Pauling, 1960) or spectroscopic data (Phillips, 1970, 1973), a combination of experimental data and quantum-mechanical results (Coulson *et al.*, 1962), or entirely quantum-mechanical calculations (García and Cohen, 1993a, 1993b). Alternative sets of coordinates based on the sizes of the s and p orbitals have been developed by Simons (1971), St. John and Bloch (1974), Zunger and Cohen (1978), Zunger (1980), and others. St. John and Bloch (1974) introduced the coordinates R_σ and R_π,

$$R_\sigma(A,B)=|(r_p^A+r_s^A)-(r_p^B+r_s^B)|,$$
$$R_\pi(A,B)=|r_p^A-r_s^A|+|r_p^B-r_s^B|, \tag{9}$$

where r_p^A denotes the size of the p orbital of atom A, etc. These coordinates have the simple physical interpretation that R_σ measures the sp contribution to the electronegativity difference between the atoms, while R_π measures the average sp hybridization.

The orbital radii themselves can be obtained as the classical turning points of screened angular-momentum-dependent atomic pseudopotentials (St. John and Bloch, 1974; Zunger and Cohen, 1978), or from the outer radial maxima of the all-electron atomic wave functions (Yeh *et al.*, 1992). Plots for A^NB^{8-N} compounds in the

(R_σ, R_π) plane show that these coordinates give an excellent separation of the different zero-pressure structures (Yeh *et al.*, 1992).

As a word of warning, the two-coordinate picture neglects many effects that may sometimes be significant. For example, the reluctance of diamond to adopt structures with a coordination number greater than four has been associated with the large size of the *d* orbitals, which are inevitably involved in the more highly coordinated structures (Yin and Cohen, 1983). We cannot hope to describe this effect using the orbital radii of Eqs. (9), which involve only the *s* and *p* radii.

X. TRENDS IN BEHAVIOR

In this section we attempt to find relationships between the data for different compounds in terms of a few simple parameters. It is of course impossible to capture the richness of the high-pressure phase diagrams described in Sec. VII in terms of a few parameters. Besides, the experimental and theoretical data are far from complete. We shall therefore be satisfied with the less ambitious aim of identifying a few trends in the theoretical and experimental results.

It is well known that the zero-pressure structures of *sp* bonded materials (Sec. IX) can be separated using a two-coordinate phenomenological model (Van Vechten, 1969; Yeh *et al.*, 1992). This idea can also be applied to high-pressure phases. In this review we have attempted to describe some trends using the orbital radii coordinates of Eqs. (9). We favor this type of coordinate for applications to high-pressure structures because they are derived purely from atomic quantities and not from the properties of a particular structure at zero pressure. We have chosen to use the wave-function radii of Yeh *et al.* (1992), although similar results can be obtained with other orbital radii.

In Fig. 12 we have plotted the (R_σ, R_π) coordinates of 40 $A^N B^{8-N}$ compounds, including some IIA–VIA compounds not covered elsewhere in this review, as their presence helps to identify trends. To use this diagram to discuss high-pressure behavior we must imagine a pressure axis coming out of the page. The values of R_σ and R_π are atomic constants and therefore do not change with pressure, but of course the compounds undergo phase transitions with increasing pressure. The boxes in Fig. 12 delineate regions for various structures adopted after the first transition. Further transitions occur at higher pressures, and therefore the regions enclosed by the boxes vary with pressure, and new boxes are required when new structures appear. These further transitions can, at least to some extent, be rationalized within the framework of Fig. 12. For example, the second transition in many IIIA–VA and IIB–VIA compounds is from NaCl to Cmcm. This correlates very well with Fig. 12, because all of the materials for which the NaCl→Cmcm transition has been observed lie close to the Cmcm region. This indicates that with increasing pressure the Cmcm region gets larger. No pressure-induced phase transitions have been reported for the four compounds with the lowest values of R_π.

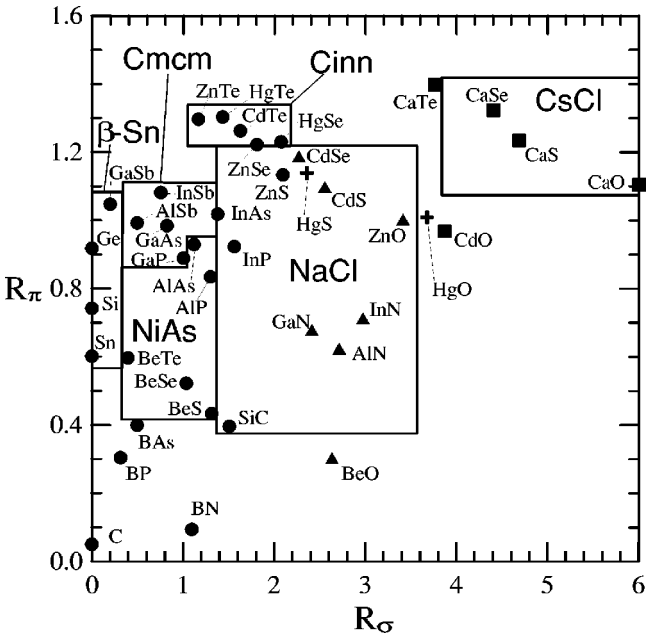

FIG. 12. Structural separation plot for the first high-pressure structure of 40 compounds: ●, compounds whose low-pressure phase is cd/zb; ▲, those whose low-pressure phase is wur; ■, those whose low-pressure phase is NaCl. The two crosses label compounds that adopt other low-pressure phases. The boxes delineate regions for the high-pressure β-Sn, Cmcm, cinn, NaCl, and CsCl structures.

It is clear that Fig. 12 provides a very good separation of both the zero-pressure and the high-pressure structures. This is not immediately obvious because the high-pressure phases involve a significant occupation of the *d* orbitals, which do not enter the definition of the (R_σ, R_π) coordinates. Nevertheless, the structural separation for the high-pressure phases is as good as for the low pressure ones. There are a few special cases that deserve some attention. The zero-pressure phase of HgO has space group *Pnma*, and the high-pressure phase is believed to be a tetragonal distortion of the NaCl structure (see Sec. VII.C.8), and it is therefore quite satisfactory that it lies close to the NaCl region in Fig. 12. HgS forms in the cinnabar structure at zero pressure, which transforms under pressure to NaCl. One could argue that GaSb is an anomalous material, as it has been reported to transform to either a disordered Imma or β-Sn phase (see Sec. VII.B.7). The Imma structure is, however, close to the β-Sn structure. The β-Sn structures occur at $R_\sigma = 0$, so the fact that the binary compound with the smallest value of R_σ transforms to that or a very similar structure is not unexpected.

Figure 12 also reveals other trends. For example, the magnitude of the pressure of the first transition tends to decrease as R_π increases, and indeed no transitions have been reported for any of the materials with $R_\pi < 0.4$. This can be rationalized as R_π measures the average *sp* hybridization, which is stronger in the low-pressure structure.

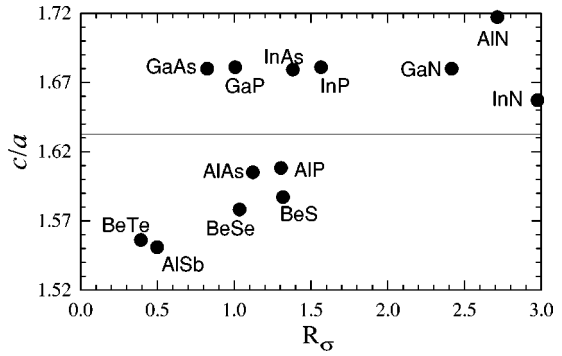

FIG. 13. Calculated c/a ratios vs R_σ for the NiAs phases of several compounds. The ideal value of c/a is indicated by a horizontal line.

In Fig. 13 we plot calculated values of the c/a ratios for NiAs structures against R_σ for a number of IIIA–VA and IIB–VIA compounds. The calculated c/a ratios are in good agreement with experiment for the stable NiAs phases. It turns out that only compounds with ratios lower than the ideal value of $c/a=\sqrt{8/3}$ are stable in the NiAs structure at zero pressure. Such a trend was reported by Lawaetz (1972) for the wurtzite structure. The high-pressure phase of AlSb is actually Cmcm, but calculations (Mujica, Rodríguez-Hernández, *et al.*, 1999) show that the enthalpy of the NiAs structure is very close to that of Cmcm at the zb→Cmcm coexistence pressure. This plot illustrates one of the additional insights that comes from performing calculations. It is only with the ability to calculate the c/a ratios of compounds which are not stable in the NiAs phase that the trend becomes clear.

XI. CONCLUSIONS

We have reviewed the present state of first-principles calculations on the high-pressure phases of group-IVA, IIIA–VA, and IIB–VIA compounds and compared the results with the experimental data. These materials show many phase transitions involving a wide variety of structures. The calculations are required to describe covalent, ionic, and metallic bonded materials with high and low symmetries and coordination numbers ranging from 3 to 12. In some cases energy differences as small as a few meV per atom must be resolved to determine whether a particular structure is stable. On the whole the agreement between theory and experiment is outstanding. There are discrepancies, some of which surely result from inadequacies in the calculations, but overall it is not an exaggeration to say that this field represents a triumph for density-functional theory and the technology of first-principles calculations.

In most of these compounds at least one pressure-induced phase transition has been observed in experiment and studied theoretically, and in some cases several transitions have been reported. In Si, experiments up to 250 GPa have been reported, but in other materials only rather lower pressures have been reached. Of the materials considered here only the IVA elements Si, Ge, and Pb have been observed in close-packed structures. There must therefore be many as yet unobserved pressure-induced phase transitions in the IIIA–VA and IIB–VIA compounds. Also, no pressure-induced phase transitions in diamond have been reported, so that one of the ultimate limitations on the pressure that can be reached in a DAC is currently unknown. Calculations can play an important role here because the experiments get harder at very high pressures, but the calculations do not. The same applies to B compounds, and particularly the technologically important compound BN.

What have the calculations achieved? First, they have provided verification (or otherwise) of experimental results. Second, they have provided predictions of new phases, some of which have been verified by experiment such as the existence of a stable sc16 phase in GaAs. Third, the calculations have provided new understanding, for example, the identification of transition mechanisms in simple cases such as the β-Sn→Imma→sh transitions in Si (Needs and Martin, 1984; Lewis and Cohen, 1993) or the pressure-driven Cmcm distortion of the NaCl structure in several IIIA–VA and IIB–VIA compounds (Mujica and Needs, 1996; Ozoliņš and Zunger, 1999). Fourth, theory has added to experiment by allowing studies of unstable phases, which helps in identifying trends in behavior. Fifth, first-principles calculations of high-pressure phases have been useful in testing and aiding the development of other theoretical methods. For example, first-principles data on the energies of different phases have been used in the fitting of parameters for tight-binding models and empirical potentials.

The study of zero-temperature equilibrium phases in the group-IVA, IIIA–VA, and IIB–VIA compounds using first-principles methods is now a mature field. In the future the scope of these methods will widen to include new and challenging problems in high-pressure physics. An area that is already starting to yield results is the application of density-functional perturbation theory (Baroni *et al.*, 2001) to study the local stability of phases. It is almost certain that the wider application of these methods to high-pressure phases will reveal that some of the currently accepted structures actually undergo small distortions. Another likely area of expansion is the study of finite-temperature effects, including the calculation of equilibrium p-T phase diagrams. The recovery to ambient conditions of new materials formed by application of pressure has long been a goal of high-pressure research. For example, an alloy that might form as an equilibrium phase under pressure might exist as a very long-lived but metastable phase when the pressure is released. First-principles methods already have the capability to calculate the phase diagrams of alloys under pressure and address such questions. Finally, the study of the kinetics of the phase transitions has already been attempted using first-principles molecular-dynamics methods, and such studies could shed light on the mechanisms of phase transitions and ultimately on the formation of microstructures.

ACKNOWLEDGMENTS

A.M., A.R., and A.M. were supported by the Ministerio de Educación y Cultura and the Ministerio de Ciencia y Tecnología of Spain. A. Muñoz was also supported by the Consejería de Educación del Gobierno de Canarias. R.J.N. was supported by the Engineering and Physical Sciences Research Council of Great Britain. We thank W. B. Holzapfel, M. I. McMahon, and R. J. Nelmes for their critical reading and useful comments on Sec. II.

APPENDIX: DESCRIPTION OF THE STRUCTURES

Limited space precludes an in-depth description of the structures adopted by the group-IVA, IIIA–VA, and IIB–VIA materials. Nelmes and McMahon (1998) have recently treated this issue in considerable detail for most of the structures considered here, and Wyckoff (1963) is also a valuable general reference. A list of the structures with a summary of its crystallographic properties is given in Tables IV and V.

Several different nomenclatures for the structures coexist at present, although none of them is entirely satisfactory concerning the amount of information conveyed. The abbreviated designation adopted in this review along with other common names are given in Tables IV and V. It has become normal practice in recent times to name newly discovered structures after their crystallographic space group, using the standard short Hermann-Mauguin symbol. However, this may be the cause of confusion when different structures have the same space group, or when a different setting of the same unit cell is used in the description of the crystal. In this review italics are used when we refer to a space group, while a roman font is used when we refer to a structure named after a space group. In order to help locate the description of each structure within this appendix we use its abbreviation in boldface font where the first reference to a structure appears.

In the representations of structures shown in this appendix by means of their projection onto a certain plane, the elevation with respect to that plane is indicated by different sizes of the circles (or "atoms") representing the atomic positions. Black and white "atoms" are used either to distinguish the sites occupied by each species or, more generally, to distinguish two different types of sites.

The different structures are very varied, having high and low symmetries and coordination numbers ranging from 3 to 12. Many of the structures are related, and we group these together in the discussion below. These relationships between structures are important for understanding the occurrence of structures and the transitions between them, but they also have an importance for the calculations themselves. When two phases have a simple structural relationship they can be represented using the same unit cell. It is then possible to perform extremely accurate comparisons of the energies and relative stability of the phases by varying the structural parameters in such a way as to deform one phase into the other.

1. Diamond, zinc-blende, and related structures

The well-known zinc-blende (**zb**) structure adopted under normal conditions by most of the compounds considered here is represented in Fig. 14. The zb structure has ideal tetrahedral coordination. The hexagonal wurtzite (**wur**) structure observed in AlN, GaN, InN, ZnO, ZnS, CdS, and CdSe under normal conditions also has tetrahedral coordination (ideal when $u=3/8$ and $c/a=\sqrt{8/3}$, values which are almost met in practice but are not determined by symmetry). The (cubic) diamond (**cd**) and hexagonal diamond (or lonsdaleite, **hd**) structures are the analogs of zb and wur in elemental materials.

The wur and zb structures can be seen as two different stackings of hexagonal atomic bilayers, with half the atoms in one bilayer lying on top of the (unlike) atoms in the preceding one (see Fig. 14). The stacking sequence is ABC in zb and AB in wur. (In zb, the direction of stacking coincides with the body diagonal of the cubic cell.) Several other different ***nX*** *polytypic* stackings of n bilayers, resulting in cubic $(X=C)$, hexagonal $(X=H)$, or rhombohedral $(X=R)$ symmetry, have been observed in SiC and ZnS.

A slight distortion of zb leads to the orthorhombic **C222$_1$** structure observed in HgTe and HgSe at moderately high pressures $[b/a=0.981, c/a=1.009, x(\mathrm{Hg})=0.302(1), y(\mathrm{Se})=0.207(2)$ in HgSe at 2.25 GPa (McMahon, Nelmes, Liu, and Belmonte, 1996)]. When $b/a=c/a=1$ and $x=y=0.25$ in C222$_1$ one obtains the zb structure.

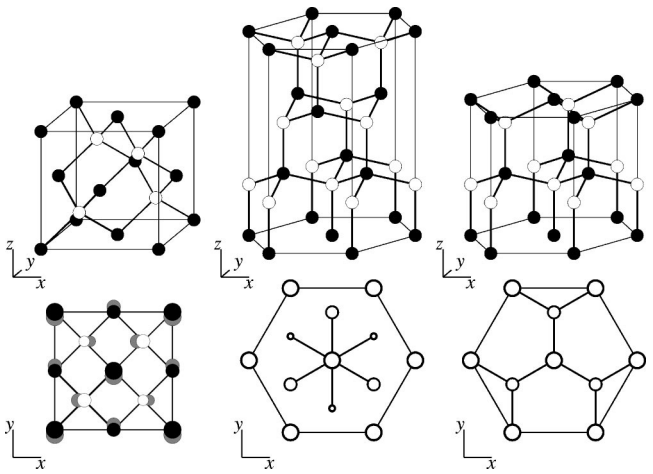

FIG. 14. Structure of zinc-blende and wurtzite: left, the zb structure, represented in the conventional cubic cell; center, zb in a hexagonal cell; right, and the wur structure. When the same species occupy the two atomic positions, zb and wur become cd and hd, respectively. Note the "staggered" and "eclipsed" relative orientations of the bonds in the top views of the hexagonal representations of zb/cd and wur/hd, respectively. The gray "atoms" in the projection of the cubic zb cell (left) indicate the atomic positions in the C222$_1$ distortion of zb observed in HgTe.

TABLE IV. Structures adopted by the group-IVA elements. The so-called *Strukturbericht* designation (Ewald and Hermann, 1931) and the Pearson symbol of the structure are given. The three characters of the Pearson symbol correspond to its crystal system (c, cubic; t, tetragonal; o, orthorhombic; m, monoclinic; a, triclinic; h, hexagonal); centering of lattice [P, primitive; S (formerly O), base- (or one-face-) centered; F, (all)-face-centered; I, body-centered; and R, rhombohedral]; and finally the number of sites in the *conventional* unit cell. (The number of atoms in a *primitive* unit cell is obtained by dividing by 1, 2, 4, 2, and 1 for P, S, F, I, and R types of lattices, respectively.) The space group is given in both short Hermann-Mauguin and (in parenthesis) Schoenflies notation. The sets of equivalent atomic (or Wyckoff) positions, which are sites related by symmetry, are summarily indicated by their multiplicity (number of sites in the conventional unit cell) and Wyckoff letter, as well as by the first member of the set, as it appears in the *International Tables for Crystallography* (Hahn, 1995). The existence of internal parameters, not determined by symmetry, is indicated in the Wyckoff positions. The coordination number (CN) of each site is the number of its nearest neighbors (in most cases at slightly different distances, so the coordination is "irregular"). If the crystal has free structural parameters, the CN depends on the values adopted by them, so this figure must be taken *cum grano salis*. A CN given as, e.g., $4+2$ (β-Sn) means four nearest neighbors and two other neighbors slightly further away. See the text for the actual values of the structural parameters of the observed phases.

Abbreviation	Full and/or common name	*Strukturbericht*/ Pearson	Space group	Wyckoff positions	Coordination number
gra	graphite (bernal)	A9/hP4	$P6_3/mmc$ (D_{6h}^4)	2(b) (0, 0, 1/4)	3
				2(c) (1/3, 2/3, 1/4)	3
r-gra	rhombohedral graphite	-/hR2	$R\bar{3}m$ (D_{3d}^5)	2(c) (x, x, x), $x\sim1/6$	3
cd	diamond	A4/cF8	$Fd\bar{3}m$ (O_h^7)	8(a) (1/8, 1/8, 1/8)	4
hd	hexagonal diamond (lonsdaleite)	-/hP4	$P6_3/mmc$ (D_{6h}^4)	4(f) (1/3, 2/3, z), $z\sim1/16$	4
st12	st12	-/tP12	$P4_32_12$ (D_4^8)	4(a) (u, u, 0)	4
				8(b) (x, y, z)	4
bc8	bc8	-/cI16	$Ia\bar{3}$ (T_h^7)	16(c) (x, x, x), $x\sim0.1$	4
r8	r8	-/hR8	$R\bar{3}$ (C_{3i}^2)	2(c) (u, u, u)	4
				6(f) (x, y, z)	4
β-Sn	β-tin	A5/tI4	$I4_1/amd$ (D_{4h}^{19})	4(a) (0, 3/4, 1/8)	$4+2$
Imma	Imma	-/oI4	$Imma$ (D_{2h}^{28})	4(e) (0, 1/4, v/2)	$4+2-6+2$
sh	simple hexagonal	A_f/hP1	$P6/mmm$ (D_{6h}^1)	1(a) (0, 0, 0)	$6+2$
Ammm	Ammm	-/oS2	$Ammm$ (D_{2h}^{19})	2(a) (0, 0, 0)	$6+2$
bcc	body-centered-cubic	A2/cI2	$Im\bar{3}m$ (O_h^9)	2(a) (0, 0, 0)	8
bct	body-centered-tetragonal	A_a/tI2	$I4/mmm$ (D_{4h}^{17})	2(a) (0, 0, 0)	8
Cmca	Cmca	-/oS16	$Cmca$ (D_{2h}^{18})	8(d) (x, 0, 0)	10
				8(f) (0, y, z)	11
hcp	hexagonal-close-packed	A3/hP2	$P6_3/mmc$ (D_{6h}^4)	2(d) (1/3, 2/3, 3/4)	12
dhcp	double hexagonal-close-packed	A3′/hP4	$P6_3/mmc$ (D_{6h}^4)	2(a) (0, 0, 0)	12
				2(d) (1/3, 2/3, 3/4)	12
fcc	face-centered-cubic	A1/cF4	$Fm\bar{3}m$ (O_h^5)	4(a) (0, 0, 0)	12

2. Graphite and other layered structures

In the common Bernal form of graphite (**gra**), the atoms are arranged in hexagonal honeycomblike (*graphene*) layers with a two-period AB sequence of stacking (see Fig. 15). The less common rhombohedral form (**r-gra**) has ABC stacking. In both cases, each atom has three nearest neighbors in its same graphene plane.

The so-called hexagonal form of BN (**h-BN**) consists of graphitelike planes in which each atomic species is surrounded by three unlike atoms, with a two-period stacking sequence. The rhombohedral form of BN (**r-BN**) can be viewed as r-gra, "decorated" by each atomic species in such a way that three in-plane and one perpendicular near neighbors are unlike atoms. Note the structural relationship between r-BN and zb (or r-gra and cd), and between h-BN and wur, respectively (cf. Figs. 14 and 15).

3. Distorted tetrahedral structures: st12, bc8, r8, and sc16

The **bc8** structure observed in Si and Ge after decompression from the high-pressure phases has a body-centered-cubic unit cell containing eight atoms. For the observed value of the internal parameter of the structure ($x\approx0.1$) each atom has four near neighbors in a distorted tetrahedral environment (see Fig. 16). The bc8 configurations corresponding to values x and $0.25-x$ are identical. A description in terms of $x\approx0.15$ is preferable to make a link with the $Pa\bar{3}$ description of the binary analog of bc8, the so-called **sc16** structure (observed in GaAs), which is simple cubic with 16 atoms in the unit cell (see McMahon *et al.*, 1998). The sc16 structure has also been observed in CuCl and CuBr (Hull and Keen, 1994).

The rhombohedral **r8** structure observed in Si as a precursor to bc8 can be viewed as a distortion of the bc8

TABLE V. Structures adopted by the IIIA–VA and IIB–VIA binary compounds (see caption to Table IV for explanations). Each atomic position is occupied by one atomic species.

Abbreviation	Full and/or common name	*Strukturbericht*/ Pearson	Space group	Wyckoff positions	Coordination number
h-BN	hexagonal boron nitride	B_k/hP4	$P6_3/mmc$ (D^4_{6h})	2(c) (1/3, 2/3, 1/4) 2(d) (1/3, 2/3, 3/4)	3 3
zb	zinc-blende (sphalerite)	B3/cF8	$F\bar{4}3m$ (T^2_d)	4(a) (0, 0, 0) 4(c) (1/4, 1/4, 1/4)	4 4
wur	wurtzite	B4/hP4	$P6_3mc$ (C^4_{6v})	2(b) (1/3, 2/3, $u_1=0$) 2(b) (1/3, 2/3, $u_2=u$), $u\sim3/8$	4 4
$C222_1$	$C222_1$	-/oS8	$C222_1$ (D^5_2)	4(a) (x, 0, 0) 4(b) (0, y, 1/4)	4 4
sc16	sc16	-/cP16	$Pa\bar{3}$ (T^6_h)	8(c) (u, u, u), $u\sim0.15$ 8(c) (v, v, v), $v\sim0.65$	4 4
cinn	cinnabar (α-HgS)	B9/hP6	$P3_121$ (D^4_3)	3(a) (u, 0, 1/3) 3(b) (v, 0, 5/6)	See text See text
NiAs	nickel arsenide	$B8_1$/hP4	$P6_3mc$ (C^4_{6v})	2(a) (0, 0, $u_1=0$) 2(b) (1/3, 2/3, $u_2=u$), $u\sim1/4$	6 6
NaCl	sodium chloride or rocksalt (halite)	B1/cF8	$Fm\bar{3}m$ (O^5_h)	4(a) (0, 0, 0) 4(b) (1/2, 1/2, 1/2)	6 6
Cmcm	Cmcm	-/oS8	$Cmcm$ (D^{17}_{2h})	4(c) (0, y_1, 1/4) 4(c) (0, y_2, 1/4), $\Delta y\sim0.5$	5+3 5+3
s-Cmcm	super-Cmcm	-/oS24	$Cmcm$ (D^{17}_{2h})	4(c) (0, y_1, 1/4), 8(f) (0, y_1', z_1') 4(c) (0, y_2, 1/4), 8(f) (0, y_2', z_2')	See text See text
b-β-Sn	binary β-tin	-/tI4	$I\bar{4}m2$ (D^9_{2d})	2(a) (0, 0, 0) 2(c) (0, 1/2, 1/4)	4+2 4+2
Imm2	Imm2	-/oI4	$Imm2$ (C^{20}_{2v})	2(a) (0, 0, $z_1=0$) 2(b) (0, 1/2, $z_2=v$)	4+2–6+2 4+2–6+2
Immm	Immm	-/oI4	$Immm$ (D^{25}_{2h})	2(a) (0, 0, 0) 2(b) (0, 1/2, 1/2)	6+2 6+2
CsCl	cesium chloride	B2/cP2	$Pm\bar{3}m$ (O^1_h)	1(a) (0, 0, 0) 1(b) (1/2, 1/2, 1/2)	8 8

structure which preserves fourfold coordination. The bc8↔r8 transition entails breaking and reforming bonds along the body diagonal of the cubic cell, but the atomic displacements are otherwise rather small (see Fig. 16). In terms of the structural parameters of r8, the bc8 structure is obtained when $u=2x_{bc8}$, $x=0.5$, $y=0$, $z=0.5-2x_{bc8}$, and the angle α adopts the ideal value of 109.47°. Experimentally, $u=0.2836$, $x=0.4620(5)$, $y=-0.0322(4)$, $z=0.2667$, and $\alpha=110.00(3)°$ in r8-Si at 6.3 GPa (Nelmes and McMahon, 1998). See also Crain, Ackland, *et al.* (1994).

The **st12** structure (Fig. 17) was first described by Bundy and Kasper (1963) after its discovery upon pressure release from β-Sn-Ge. It has 12 atoms in a simple tetragonal unit cell, each with a rather distorted tetrahedral environment. To date, it has not been observed in any other elemental material, though it should be noted that the atomic positions of the Si atoms in the SiO_2 polymorph known as Keatite conform to this structure, with almost the same internal parameters as observed in st12-Ge [$x=0.1730$, $y=0.3784$, $z=0.2486$, $u=0.0912$, $c/a=1.1771$, in st12-Ge at 0 GPa (Kasper and Richards, 1964)]. A feature of st12 that is often remarked upon is the presence of odd-membered rings of atoms, which precludes the formation of a similar binary structure without "wrong" bonds (like atoms in the nearest-neighbor position).

4. β-Sn, simple hexagonal, Imma, and their binary analogs

The body-centered-orthorhombic **Imma** structure, its related forms, and their binary analogs (Fig. 18) play an

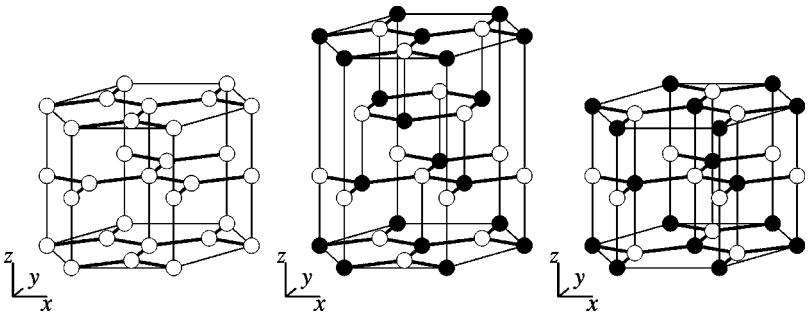

FIG. 15. The structure of graphite (left); the structure of r-BN (or of r-gra when black and white sites are occupied by the same atomic species); and the structure of h-BN.

important role in the polymorphism of the group-IVA elements and some IIIA–VA binary compounds such as InSb and GaSb. The body-centered tetragonal ***β*-Sn** structure observed under normal conditions in Sn and at high pressures in Si and Ge is a special case of Imma (also observed in Si and Ge) corresponding to the structural parameters $b/a=1$ and $v=0.25$. Note also that when $c/a=\sqrt{2}$ in β-Sn one obtains the cd structure. Experimentally, $c/a\approx 0.55$ [see, for example, McMahon *et al.* (1994a) for Si].

The simple (or primitive) hexagonal (**sh**) structure observed in Si and Ge can also be viewed as a special case of Imma corresponding to $b/c=\sqrt{3}$ and $v=0.5$; the c axis is then along the x direction. The experimental value of the axial ratio for the hexagonal cell is ~ 0.93 (McMahon *et al.*, 1994a). The Imma structure can be considered as defining a path of continuous deformation between the approximately sixfold β-Sn structure and the approximately eightfold sh structure.

No ordered binary analog of the sh structure can have true hexagonal symmetry (Nelmes and McMahon, 1998). Placing two different atomic species in an ordered fashion in the sites of sh, subject to the requirement of minimizing the number of unfavorable like neighbors in the hexagonal planes leads, in increasing order of complexity, to the **Immm**, **Cmcm**, and **s-Cmcm** structures, all of which are orthorhombic (see below). Quasi-eightfold-coordinated Immm, Cmcm, and s-Cmcm can therefore be considered as binary analogs of the sh structure (Kelsey and Ackland, 2000).

The simplest ordered binary analogs of β-Sn and Imma are, respectively, the **b-*β*-Sn** and **Imm2** structures (see Fig. 18). In spite of earlier reports of such structures occurring in several IIIA–VA compounds, the most recent experimental studies have ruled them out of the phase diagrams of these compounds (see Sec. VIII.A). When $v=0.5$ the Imm2 structure becomes **Immm**, which has been observed in InSb at high pressures [with $b/a=0.921$, $c/a=0.544$ (Nelmes, McMahon, Hatton, *et al.*, 1993)]. The completely disordered (quasimonatomic) analog of Immm is called **Ammm** after its space group (nonstandard setting) and has been observed in GaSb after heating at high pressures (Vanpeteghem *et al.*, 2002). Ammm can also be viewed as a special case of Imma for $v=0.5$. The disordered analog of the β-Sn structure has also been reported for GaSb and InSb (see Sec. VII).

5. Cmca

The recently discovered base-centered-orthorhombic **Cmca** structure (see Schwarz *et al.*, 1998; Hanfland *et al.*, 1999; Mujica *et al.*, 2001a) appears in Si and Ge at high pressures as an intermediate between eightfold-coordinated forms and 12-fold-coordinated close-packed structures. In Cmca the 8(f) sites are contained in flat (100) planes, while the 8(d) sites form corrugated layers that alternate with the 8(f) planes (see Fig. 19). The 8(f) sites have 11 near neighbors, while the 8(d) sites have 10 near neighbors, although the distances to these neighbors are not all the same. It is interesting to note that in all reported cases of the Cmca structure to date (Cs, Rb, Si, and Ge), the structural parameters are very similar and $b\approx c$ [e.g., in Cmca-Si (Si-VI) at 42.5 GPa: $b/a=0.598$, $c/a=0.597$, $x=0.219(5)$, $y=0.172(5)$, $z=0.328(5)$ (Hanfland *et al.*, 1999)].

Several special configurations lead to an increase in symmetry. This occurs when $y=z=0.25$, which for $b/a=c/a$ corresponds to a tetragonal structure (bct when

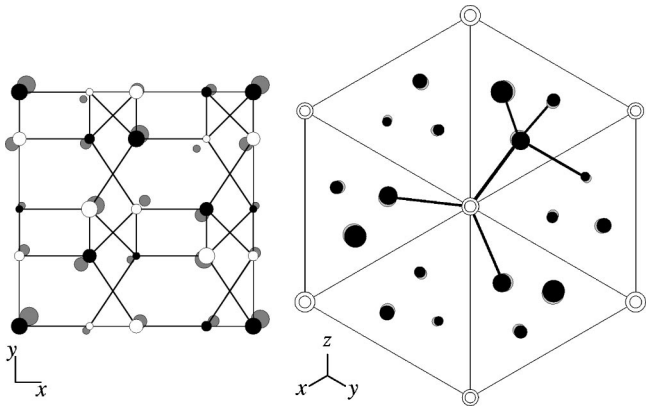

FIG. 16. Distorted tetrahedral structures: left, Projection of the cubic bc8 structure onto the xy plane. The white and black "atoms" indicate the occupation of the 16(c) sites of bc8 by two different atomic species which leads to the binary sc16 structure. For comparison the atomic positions in the r8 structure have also been represented using gray "atoms." Right, the rhombohedral r8 structure viewed along a body diagonal (threefold axis). The 2(c) and 6(f) sites are indicated by white and black "atoms," respectively. Almost completely obliterated by them, the atomic positions of the bc8 structure appear represented by gray "atoms." The bond between two white "atoms" directed along the body diagonal is not visible in this picture.

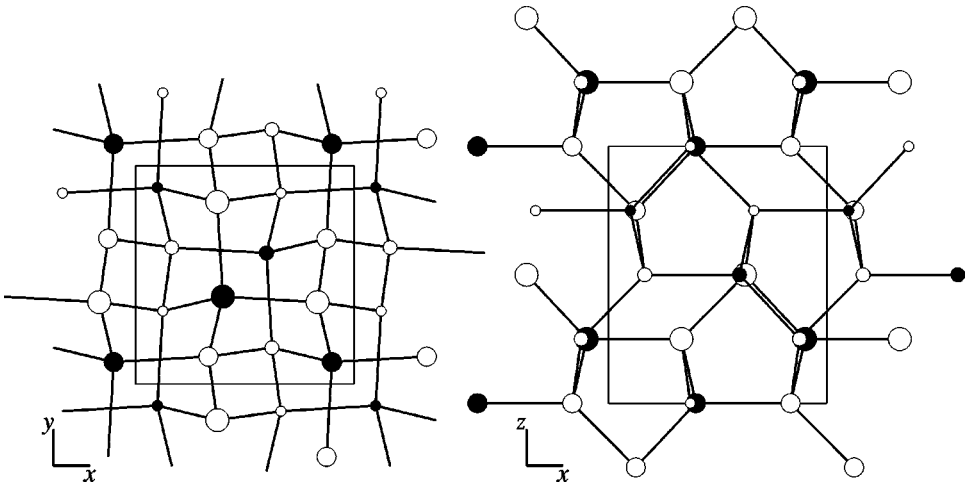

FIG. 17. Projection of the tetragonal st12 structure onto the xy and xz planes. The black and white "atoms" indicate the 4(a) and 8(b) sites, respectively.

$x=0.25$; and fcc when $x=0.25$ and $b/a=c/a=1$). Another special case of Cmca is the sh structure, which can be obtained by taking $x=y=0.25$, $z=0.5$, and $b/a=1/\sqrt{3}$ (c axis in the z direction) or $x=z=0.25$, $y=0.5$, and $c/a=1/\sqrt{3}$ (c axis in the y direction).

6. Hexagonal close packings

In the homonuclear hexagonal-close-packed crystals, the atoms are arranged in hexagonal layers, which are stacked one on top of the other, with atoms in one layer lying above the unoccupied "centers" of the adjacent layers (see Fig. 20). For the ideal interplanar spacing, $d/a=\sqrt{2/3}$, the coordination is exactly 12. The simplest pattern of stacking, AB, corresponds to the (mono) hexagonal-close-packed structure (**hcp**) observed in Si, Ge, and Pb at high pressures. A four-period sequence, ABAC, leads to the double hexagonal-close-packed structure (**dhcp**). The face-centered-cubic structure (**fcc**) can also be viewed as an ideal hcp-type structure with an ABC stacking sequence. It occurs in Pb at normal conditions and in Si at very high pressures.

7. NaCl, Cmcm, and related structures

In the well-known **NaCl** structure each atom has six unlike nearest neighbors (see Fig. 21). A slight uniaxial compression of NaCl results in a tetragonal structure with space group $I4/mmm$ [equivalent atomic sites at 2(a) (0,0,0) and 2(b) (0,0,1/2)], which has been recently proposed for the high-pressure phase of HgO (Zhou *et al.*, 1998). When $c/a=\sqrt{2}=1.414$ in this **I4/mmm** structure one gets the NaCl structure. Experimentally, $c/a\approx 1.380$.

The base-centered-orthorhombic **Cmcm** structure observed in several IIIA–VA and IIB–VIA materials at high pressures can be understood as a distortion of the NaCl structure consisting of (a) a shearing of alternate (001) planes in the [010] direction, (b) a puckering of the [100] atomic rows of NaCl in the [010] direction, and (c) an orthorhombic adjustment of the cell (see Fig. 21). A closely related structure is the *super*-Cmcm (**s-Cmcm**) form observed in InSb at high pressures (see Nelmes and McMahon, 1995). In s-Cmcm the pattern of shearing of NaCl-like planes involves six planes (instead of the two in Cmcm), resulting in a cell that is three times the size of Cmcm in the z direction.

Instead of the standard crystallographic description of Cmcm in terms of the internal parameters y_1 and y_2 (see Table V), it has become normal in theoretical work to employ the parameters $u_1=3-4y_1$ and $u_2=1-4y_2$, which represent the magnitude of the shearing in each atomic sublattice (subindices 1 and 2 refer to cation and anion, respectively). The mean shearing of the NaCl-like planes is then measured by $u=(u_1+u_2)/2$, and the puckering of the atomic rows by $\delta=(u_1-u_2)/2$. Experimentally, Δy is not far from 0.5, so the puckering is

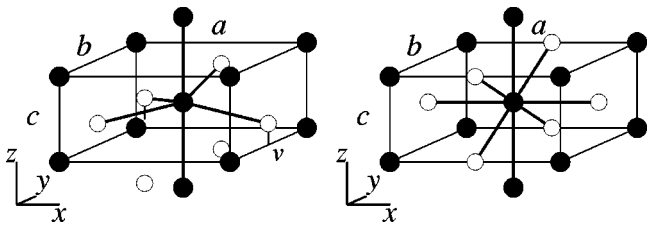

FIG. 18. Body-centered-orthorhombic structures: left, Imm2; right, Immm, a special case of Imm2 corresponding to $v=0.5$. The b-β-Sn structure corresponds to $v=0.25$ and $b/a=1$ in Imm2. When the same species occupy both sites in Imm2 one obtains the Imma structure. The β-Sn ($v=0.25$ and $b/a=1$) and sh ($v=0.5$ and $b/c=\sqrt{3}$) structures are particular cases of Imma. When the same species occupy both sites in Immm one obtains the base-centered-orthorhombic Ammm structure.

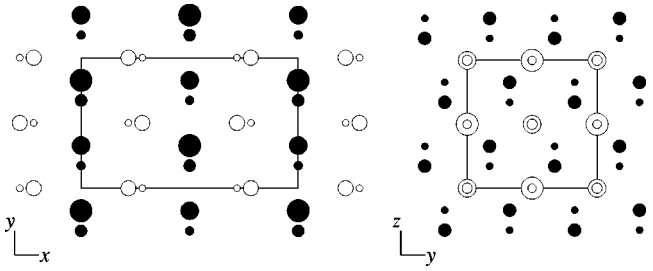

FIG. 19. The Cmca structure of Si-VI drawn in projection: left, onto the xy plane; right, onto the yz plane. Black and white atoms indicate, respectively, the 8(f) and 8(d) sites.

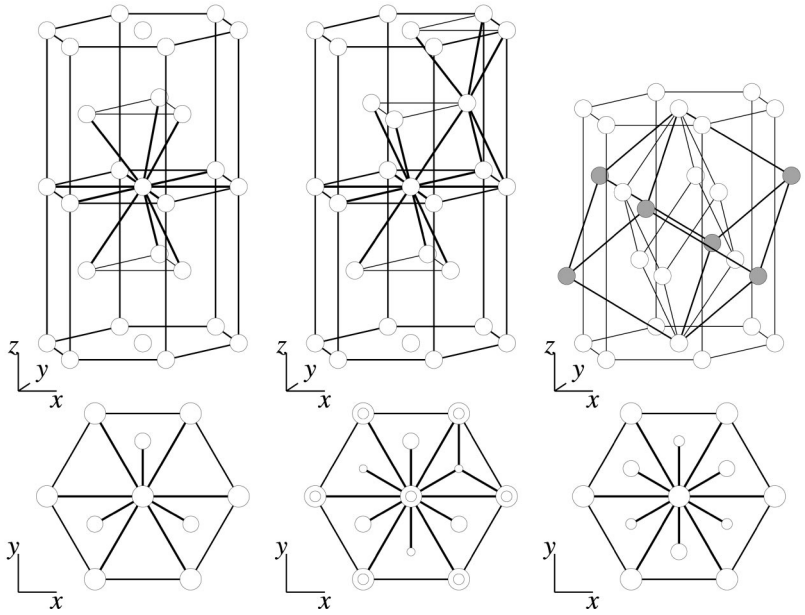

FIG. 20. Close-packed structures: left, the hcp structure; center, the dhcp structure; right, the fcc structure. All are shown in perspective above and in projection onto the xy plane below. The conventional cubic cell and a (less conventional) rhombohedral cell have been drawn, along with the nonprimitive hexagonal cell in the case of fcc. Gray sites lie outside of the hexagonal cell.

rather small. An equivalent $Bmmb$ description is also commonly used, which consists of interchanging the y and z axes of the $Cmcm$ description (Mujica and Needs, 1996, 1997).

The coordination in Cmcm depends critically on the values of the structural parameters. In several cases (e.g., CdTe) the Cmcm phase evolves continuously from a NaCl phase (sixfold-coordinated), which corresponds to taking $u_1=u_2=0$ (or equivalently $y_1=0.75$ and $y_2=0.25$) and $b/a=c/a=1$ in Cmcm. Once the distortion from NaCl has fully developed [$b/a=1.069$, $c/a=0.948$, $y(\mathrm{Cd})=0.650(3)$, $y(\mathrm{Te})=0.180(3)$ in CdTe at 18.6 GPa (Nelmes *et al.*, 1995a)] each atom has five unlike nearest neighbors and three next-nearest neighbors a bit further away (two of which are like-atoms). There are in all six different nearest and next-nearest distances.

As noted before, both the (approximately) eightfold-coordinated Cmcm and s-Cmcm structures can be conceived as originating from different decorations (and accompanying distortions) of the sites of a sh structure by two different species with the maximum number of unlike neighbors (Kelsey and Ackland, 2000). It is also worth noting the relation between Cmcm and the so-called **Pmm2** structure previously proposed for such phases as GaAs-II (Cmcm) and InSb-IV (s-Cmcm; see Secs. VII.B.6 and VII.B.9). The arrangement of sites,

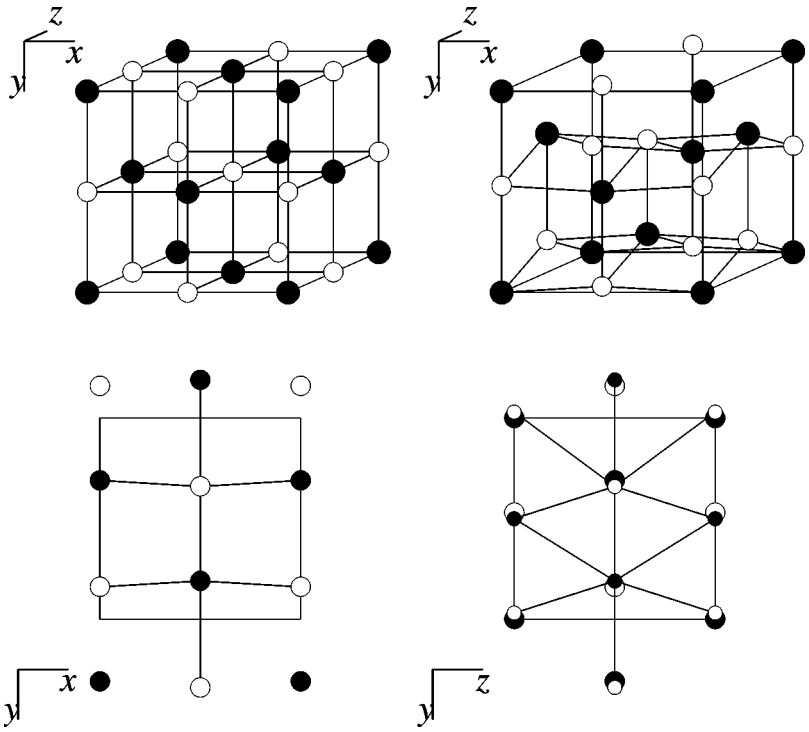

FIG. 21. Comparison of the NaCl and Cmcm structures: upper left, NaCl; upper right, Cmcm. The projections of Cmcm onto the xy and yz planes are represented below.

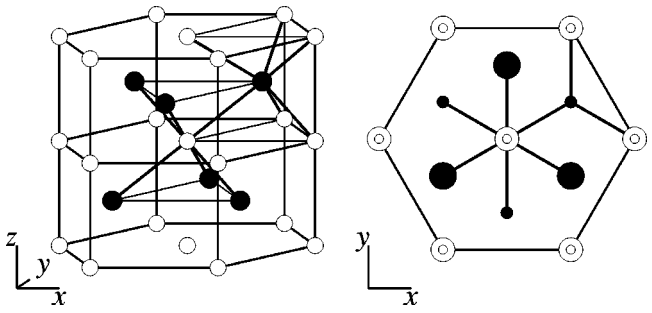

FIG. 22. The NiAs structure: left, in perspective; right, in projection. Black "atoms" represent the 2(a) sites (occupied by the anion) and white "atoms" represent the 2(b) sites (occupied by the cation).

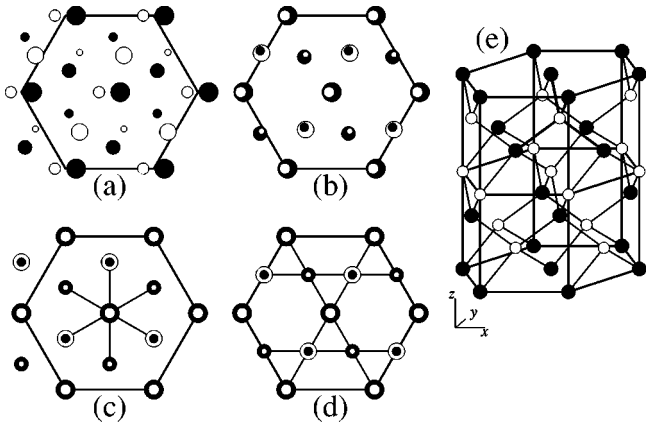

FIG. 23. Varieties of cinnabar: (a) the cinnabar structure of α-HgS [$u(\mathrm{Hg})=0.72$, $v(\mathrm{S})=0.48$]; (b) the structure reported experimentally for *cinn*-GaAs [$u(\mathrm{Ga})=0.539$, $v(\mathrm{As})=0.505$]; (c) the "cinnabar" structure when $u=v=2/3$ [NaCl if $c/a=\sqrt{6}$ and CsCl if $c/a=\sqrt{6}/2$]; and (d) *idem* when $u=v=0.5$. The structure with $u=v=0.5$ (and $c/a\approx 2.2$) is represented in perspective in (e).

regardless of occupation by each atomic species, in Cmcm with u, $\delta=0$ (or equivalently $\Delta y=0.5$) is the same as in Pmm2 with $z=u$ (in the $Pm2m$ setting obtained by interchanging the y and z axes), and similarly for s-Cmcm. That is, if one considers equi-occupation of all the sites of Pmm2, Cmcm, or s-Cmcm by the two atomic species (complete disorder) and further restricts Δy to be 0.5 in Cmcm and s-Cmcm, one finds the same homonuclear structure with $Pmcm$ symmetry (see Nelmes and McMahon, 1998). For $u=0.5$ this structure corresponds to Ammm.

The Cmcm structure has also been observed in CuI at high pressures (Hofmann *et al.*, 1995). Incidentally, Cmcm is isostructural (same space group and type of atomic positions, though rather different values of the structural parameters) to the stable form of CrB named B33 and to the TlI-type structures recently observed in NaBr and NaI at high pressures [see Léger *et al.* (1998) for other occurrences of TlI-type structures]. The value of Δy in these crystals is markedly different from the value ~ 0.5 observed in the Cmcm phases of the IIIA–VA and IIB–VIA materials, which results in a rather different topology.

8. NiAs

In the **NiAs** structure (see Fig. 22) one atomic species (the anion) occupies the sites of an hcp crystal, while the arrangement of the other species (cation) is the same as in the sh structure. Note that the two types of site are not equivalent: the reverse ordering is usually referred to as *anti*-NiAs. Experimentally, in both the NiAs phases of AlAs and AlP $u\approx 0.25$ and the c/a ratio is slightly below the ideal value $\sqrt{8/3}$ (Greene, Luo, Li, and Ruoff, 1994; Greene, Luo, and Ruoff, 1994). [In fact, for $u=0.25$ the structure acquires a center of inversion and the symmetry increases (space group $P6_3/mmc$).] The local environment of anions around each cation is then about the same as in the NaCl structure.

9. Cinnabar and cinnabar-type structures

The range of structures collectively designated as "cinnabar" or "cinnabar-type" (abbreviated as **cinn**) consists of widely different forms, which can all be described in terms of the 3(a) and 3(b) sites of the trigonal $P3_121$ space group (or its enantiomorph, $P3_221$). The actual coordination depends on the values of the structural parameters. In true cinnabar, which is the low-pressure stable form of HgS, values of $u(\mathrm{Hg})=0.72$, $v(\mathrm{S})=0.49$, and $c/a=2.29$ result in a twofold coordination with four next-nearest neighbors at a significantly larger distance (all of them unlike atoms). A similar configuration is observed in the low-pressure metastable cinn form of HgO [$u(\mathrm{Hg})=0.75$, $v(\mathrm{O})=0.46$, $c/a=2.427$ (Aurivillius and Carlsson, 1958)]. However, in CdTe [$u(\mathrm{Cd})=0.622(2)$, $v(\mathrm{Te})=0.565(2)$, $c/a=2.377$ at 3.2 GPa (McMahon *et al.*, 1993a)] and HgTe [$u(\mathrm{Hg})=0.641(1)$, $v(\mathrm{Te})=0.562(1)$, $c/a=2.287$ at 3.6 GPa (Wright *et al.*, 1993)], where the cinn phase is stable at high pressures, the coordination is approximately $4+2$ (instead of $2+4$ in HgS), and in HgSe [$u(\mathrm{Hg})=0.662(1)$, $v(\mathrm{Se})=0.550(1)$, $c/a=2.320$ at 4.0 GPa (Nelmes and McMahon, 1998)] it is best described as $2+2+2$.

In contrast, in ZnTe and GaAs, for which the high-pressure *cinnabar* phase has u and v close to 0.5 [$u(\mathrm{Zn})=0.540$, $v(\mathrm{Te})=0.504$, $c/a=2.289$ at 8.9 GPa (Nelmes *et al.*, 1995b); $u(\mathrm{Ga})=0.539$, $v(\mathrm{As})=0.505$, $c/a=2.229$ at 8.3 GPa (McMahon and Nelmes, 1997)], each atom has four unlike nearest neighbors. For (strictly) $u=v=0.5$ the symmetry increases to that of $P6_222$ (or the $P6_422$ enantiomorph). In this case or for nearby configurations, the structure can be viewed as being formed from twisted tetrahedra (see Fig. 23 and Mujica *et al.*, 1998). In view of the widespread usage of the term *cinnabar* to describe also this special case, which is quite unlike the other cinn-type configurations, we have chosen to signify such tetrahedral structures by using italics, *cinn*.

The cinnabar structure is sometimes described as a distortion of the NaCl structure, which is obtained when $u=v=2/3$ (or 1/3) and $c/a=\sqrt{6}$. The CsCl structure results when $c/a=\sqrt{6}/2$.

10. CsCl and body-centered-cubic structures

The well-known **CsCl** structure has been proposed as a candidate at very high pressures for several IIIA–VA and IIB–VIA compounds, though its existence has yet to be confirmed. Each atom in CsCl has eight unlike nearest neighbors. The completely disordered analog of CsCl is the (quasihomonuclear) body-centered-cubic structure (**bcc**), which has been reported in GaSb, InSb, and HgTe at very high pressures. The truly homonuclear bcc structure occurs in Sn and Pb. Uniaxial deformation of the bcc structure results in the body-centered-tetragonal structure (**bct**) observed in Sn.

REFERENCES

Ackland, G. J., 2001a, Rep. Prog. Phys. **64**, 453.
Ackland, G. J., 2001b, Phys. Rev. Lett. **86**, 5301.
Ahuja, R., O. Eriksson, and B. Johansson, 1999, Phys. Rev. B **60**, 14475.
Ahuja, R., L. Fast, O. Eriksson, J. M. Wills, and B. Johansson, 1998, J. Appl. Phys. **83**, 8065.
Ahuja, R., P. James, O. Eriksson, J. M. Wills, and B. Johansson, 1997, Phys. Status Solidi B **199**, 75.
Albe, K., 1997, Phys. Rev. B **55**, 6203.
Arora, V. K., and T. Sakuntala, 1995, Phys. Rev. B **52**, 11052.
Arora, V. K., E.-K. Suh, U. Debska, and A. K. Ramdas, 1988, Phys. Rev. B **37**, 2927.
Aurivillius, K. L., 1956, Acta Chem. Scand. **4**, 1423.
Aurivillius, K. L. and I.-B. Carlsson, 1958, Acta Chem. Scand. **12**, 1297.
Banus, M. D., and M. C. Lavine, 1967, J. Appl. Phys. **38**, 2042.
Banus, M. D., and M. C. Lavine, 1969, J. Appl. Phys. **40**, 409.
Barnett, J. D., V. E. Dean, and H. T. Hall, 1966, J. Appl. Phys. **37**, 875.
Baroni, S., S. de Gironcoli, A. Dal Corso, and P. Giannozzi, 2001, Rev. Mod. Phys. **73**, 515.
Bates, C., W. White, and R. Roy, 1962, Science **137**, 993.
Baublitz, M., and A. L. Ruoff, 1982a, J. Appl. Phys. **53**, 5669.
Baublitz, M., and A. L. Ruoff, 1982b, J. Appl. Phys. **53**, 6179.
Baublitz, M., and A. L. Ruoff, 1983, J. Appl. Phys. **54**, 2109.
Bellaiche, L., K. Kunc, and J. M. Besson, 1996, Phys. Rev. B **54**, 8945.
Besson, J. M., J. P. Itié, G. Weill, J. L. Mansot, and J. Gonzalez, 1991, Phys. Rev. B **44**, 4214.
Besson, J. M., E. H. Mokhtari, J. Gonzalez, and G. Weill, 1987, Phys. Rev. Lett. **59**, 473.
Biswas, R., R. M. Martin, R. J. Needs, and O. H. Nielsen, 1984, Phys. Rev. B **30**, 3210.
Biswas, R., R. M. Martin, R. J. Needs, and O. H. Nielsen, 1987, Phys. Rev. B **35**, 9559.
Blöchl, P., 1994, Phys. Rev. B **50**, 17 953.
Born, M., and K. Huang, 1956, *Dynamical Theory of Crystal Lattices* (Oxford University Press, Oxford).
Born, M., and J. E. Meyer, 1932, Z. Phys. **75**, 1.
Bouhafs, B., H. Aourag, M. Ferhat, and M. Certier, 1999, J. Phys.: Condens. Matter **11**, 5781.
Boyer, L. L., E. Kaxiras, J. L. Feldman, J. Q. Broughton, and M. J. Mehl, 1991, Phys. Rev. Lett. **67**, 715.
Brazhkin, V. V., A. G. Lyapin, S. V. Popova, and R. N. Voloshin, 1995, Phys. Rev. B **51**, 7549.
Bundy, F. P., W. A. Bassett, M. S. Weathers, R. J. Hemley, H. K. Mao, and A. F. Goncharov, 1996, Carbon **34**, 141.
Bundy, F. P., and J. S. Kasper, 1963, Science **139**, 340.
Bundy, F. P., and J. S. Kasper, 1967, J. Chem. Phys. **46**, 3437.
Callen, H. B., 1985, *Thermodynamics* (Wiley, New York), p. 245.
Camacho, J., I. Loa, A. Cantarero, and K. Syassen, 2002, J. Phys.: Condens. Matter **14**, 739.
Car, R., and M. Parrinello, 1985, Phys. Rev. Lett. **55**, 2471.
Catti, M., 2001, Phys. Rev. Lett. **87**, 035504.
Chang, K. J., and M. L. Cohen, 1984, Phys. Rev. B **30**, 5376.
Chang, K. J., and M. L. Cohen, 1985, Phys. Rev. B **31**, 7819.
Chang, K. J., and M. L. Cohen, 1986, Phys. Rev. B **34**, 8581.
Chang, K. J., and M. L. Cohen, 1987, Phys. Rev. B **35**, 8196.
Cheng, C., W. H. Huang, and H. J. Li, 2001, Phys. Rev. B **63**, 153202.
Cheng, C., R. J. Needs, and V. Heine, 1988, J. Phys. C **21**, 1049.
Cheng, C., R. J. Needs, V. Heine, and N. Churcher, 1987, Europhys. Lett. **3**, 475.
Cheong, B. H., and K. J. Chang, 1991, Phys. Rev. B **44**, 4103.
Christensen, N. E., 1986, Phys. Rev. B **33**, 5096.
Christensen, N. E., and I. Gorczyca, 1993, Phys. Rev. B **47**, 4307.
Christensen, N. E., and I. Gorczyca, 1994, Phys. Rev. B **50**, 4397.
Christensen, N. E., and M. Methfessel, 1993, Phys. Rev. B **48**, 5797.
Christensen, N. E., D. L. Novikov, R. E. Alonso, and C. O. Rodriguez, 1999, Phys. Status Solidi B **211**, 5.
Christensen, N. E., D. L. Novikov, and M. Methfessel, 1999, Solid State Commun. **110**, 615.
Christensen, N. E., S. Satpathy, and Z. Pawlowska, 1986, Phys. Rev. B **34**, 5977.
Clark, S. J., G. J. Ackland, and J. Crain, 1995, Phys. Rev. B **52**, 15 035.
Cline, C. F., and D. R. Stephens, 1965, J. Appl. Phys. **36**, 2869.
Corkill, J. L., A. García, and M. L. Cohen, 1991, Phys. Rev. B **43**, 9251.
Corrigan, F. R., and F. P. Bundy, 1975, J. Chem. Phys. **63**, 3812.
Côté, M., O. Zakharov, A. Rubio, and M. L. Cohen, 1997, Phys. Rev. B **55**, 13 025.
Coulson, C. A., L. B. Redei, and D. Stocker, 1962, Proc. R. Soc. London, Ser. A **270**, 352.
Crain, J., G. J. Ackland, J. R. Maclean, R. O. Piltz, P. D. Hatton, and G. S. Pawley, 1994, Phys. Rev. B **50**, 13 043.
Crain, J., S. J. Clark, G. J. Ackland, M. C. Payne, V. Milman, P. D. Hatton, and B. J. Reid, 1994, Phys. Rev. B **49**, 5329.
Crain, J., P. O. Piltz, G. J. Ackland, S. J. Clark, M. C. Payne, V. Milman, J. S. Lin, P. D. Hatton, and Y. H. Nam, 1994, Phys. Rev. B **50**, 8389; **52**, 16 936(E).
Dal Corso, A., A. Pasquarello, A. Baldereschi, and R. Car, 1996, Phys. Rev. B **53**, 1180.
Darnell, A. J., and W. F. Libby, 1963, Science **139**, 1301.
Decker, D. L., 1971, J. Appl. Phys. **42**, 3239.
Decremps, F., J. Zhang, B. Li, and R. C. Liebermann, 2001, Phys. Rev. B **63**, 224105.
Decremps, F., J. Zhang, and R. C. Liebermann, 2000, Europhys. Lett. **51**, 268.
Desgreniers, S., 1998, Phys. Rev. B **58**, 14 102.
Desgreniers, S., L. Beaulieu, and I. Lepage, 2000, Phys. Rev. B **61**, 8726.
Desgreniers, S., Y. K. Vohra, and A. L. Ruoff, 1989, Phys. Rev. B **39**, 10 359.

Domnich, V., and Y. Gogotsi, 2001, in *Experimental Methods in the Physical Sciences*, edited by R. J. Celotta and T. Lucatorto, Advances in Surface Science No. 38 (Academic, New York), p. 355.
Dreizler, R. M., and E. K. U. Gross, 1990, *Density Functional Theory, an Approach to the Quantum Many Body Problem* (Springer, Berlin).
Dreysse, H., 2000, Ed., *Electronic Structure and Physical Properties of Solids: The Uses of the LMTO Method* (Springer, Berlin).
Duclos, S. J., Y. K. Vohra, and A. L. Ruoff, 1990, Phys. Rev. B **41**, 12 021.
Edwards, A. L., and H. G. Drickamer, 1961, Phys. Rev. **122**, 1149.
Eremets, M. I., 1996, *High-Pressure Experimental Methods* (Oxford University Press, Oxford).
Evarestov, R. A., and V. P. Smirnov, 1993, *Site Symmetry in Crystals: Theory and Applications* (Springer, Berlin/Heidelberg).
Ewald, P. P., and C. Hermann, 1931, Eds., *Strukturbericht, Zeitschrift für Kristallographie* (Akademische Verlagsgesellschaft, Leipzig).
Fahy, S., and S. G. Louie, 1987, Phys. Rev. B **36**, 3373.
Fahy, S., S. G. Louie, and M. L. Cohen, 1986, Phys. Rev. B **34**, 1191.
Ferhat, M., B. Bouhafs, A. Zaoui, and H. Aourag, 1998, J. Phys.: Condens. Matter **10**, 7995.
Fiorentini, V., M. Methfessel, and M. Scheffler, 1993, Phys. Rev. B **47**, 13 353.
Focher, P., G. L. Chiarotti, M. Bernasconi, E. Tosatti, and M. Parrinello, 1994, Europhys. Lett. **26**, 345.
Foulkes, W. M. C., L. Mitas, R. J. Needs, and G. Rajagopal, 2001, Rev. Mod. Phys. **73**, 33.
Froyen, S., and M. L. Cohen, 1983, Phys. Rev. B **28**, 3258.
Furthmüller, J., J. Hafner, and G. Kresse, 1994, Phys. Rev. B **50**, 15 606.
Gaál-Nagy, K., A. Bauer, M. Schmitt, K. Karch, P. Pavone, and D. Strauch, 1999, Phys. Status Solidi B **211**, 275.
García, A., and M. L. Cohen, 1993a, Phys. Rev. B **47**, 4215.
García, A., and M. L. Cohen, 1993b, Phys. Rev. B **47**, 4221.
Gebbie, H. A., P. L. Smith, I. G. Austin, and J. H. King, 1960, Nature (London) **188**, 1096.
Gerward, L., and J. S. Olsen, 1995, J. Synchrotron Radiat. **2**, 233.
Gorczyca, I., N. E. Christensen, and M. Alouani, 1989, Phys. Rev. B **39**, 7705.
Greene, R. G., H. Luo, K. Ghandehari, and A. L. Ruoff, 1995, J. Phys. Chem. Solids **56**, 517.
Greene, R. G., H. Luo, T. Li, and A. L. Ruoff, 1994, Phys. Rev. Lett. **72**, 2045.
Greene, R. G., H. Luo, and A. L. Ruoff, 1994, J. Appl. Phys. **76**, 7296.
Greene, R. G., H. A. Luo, and A. L. Ruoff, 1995, J. Phys. Chem. Solids **56**, 521.
Greene, R. G., H. Luo, A. L. Ruoff, S. S. Trail, and F. J. DiSalvo, 1994, Phys. Rev. Lett. **73**, 2476.
Gross, E. K. U., F. J. Dobson, and M. Petersilka, 1996, *Density Functional Theory* (Springer, New York).
Gross, E. K. U., C. A. Ullright, and U. J. Grossmann, 1994, in *Density Functional Theory*, edited by E. K. U. Gross and R. M. Dreizler, NATO ASI Series (Plenum, New York), p. 194.
Grumbach, M. P., and R. M. Martin, 1996, Phys. Rev. B **54**, 15 730.
Guo, G. Y., J. Crain, P. Blaha, and W. M. Temmerman, 1993, Phys. Rev. B **47**, 4841.
Hafner, J., and V. Heine, 1983, J. Phys. F: Met. Phys. **13**, 2479.
Hahn, Th., 1995, Ed., *International Tables for Crystallography*, Vol. A, *Space Group Symmetry*, fourth revised edition (Kluwer Academic, Dordrecht/Boston/London).
Hanfland, M., U. Schwarz, K. Syassen, and K. Takemura, 1999, Phys. Rev. Lett. **82**, 1197.
Hayes, T. M., and J. B. Boyce, 1982, Solid State Phys. **37**, 173.
Hebbache, M., M. Mattesini, and J. Szeftel, 2001, Phys. Rev. B **63**, 205201.
Heine, V., and D. Weaire, 1970, Solid State Phys. **24**, 249.
Hirano, H., S. Uehara, A. Mori, A. Onodera, K. Takemura, O. Shimomura, Y. Akahama, and H. Kawamura, 2001, J. Phys. Chem. Solids **62**, 941.
Hofmann, M., S. Hull, and D. A. Keen, 1995, Phys. Rev. B **51**, 12 022.
Hohenberg, P., and W. Kohn, 1964, Phys. Rev. **136**, 864B.
Holzapfel, W. B., M. Hartwig, and W. Sievers, 2001, J. Phys. Chem. Ref. Data **30**, 515; private communication.
Holzapfel, W. B., and N. S. Isaacs, 1997, Eds., *High-Pressure Techniques in Chemistry and Physics* (Oxford University Press, Oxford/New York/Tokyo).
Hu, J. Z., 1987, Solid State Commun. **63**, 471.
Hu, J. Z., D. R. Black, and I. L. Spain, 1984, Solid State Commun. **51**, 285.
Hu, J. Z., L. D. Merkle, C. S. Menoni, and I. L. Spain, 1986, Phys. Rev. B **34**, 4679.
Hu, J. Z., and I. L. Spain, 1984, Solid State Commun. **51**, 263.
Huang, T.-L., and A. L. Ruoff, 1985, Phys. Rev. B **31**, 5976.
Hull, S., and D. A. Keen, 1994, Phys. Rev. B **50**, 5868.
Ihm, J., and M. L. Cohen, 1981, Phys. Rev. B **23**, 1576.
Itié, J. P., A. Polian, C. Jauberthie-Carillon, E. Dartyge, A. Fontaine, H. Tolentino, and G. Tourillon, 1989, Phys. Rev. B **40**, 9709.
Jaffe, J. E., and A. C. Hess, 1993, Phys. Rev. B **48**, 7903.
Jaffe, J. E., R. Pandey, and M. J. Seel, 1993, Phys. Rev. B **47**, 6299.
Jaffe, J. E., J. A. Snyder, Z. Lin, and A. C. Hess, 2000, Phys. Rev. B **62**, 1660.
Jamieson, J. C., 1963a, Science **139**, 762.
Jamieson, J. C., 1963b, Science **139**, 845.
Jamieson, J. C., 1970, Phys. Earth Planet. Inter. **3**, 201.
Jamieson, J. C., A. W. Lawson, and N. D. Nachtrieb, 1959, Rev. Sci. Instrum. **30**, 1016.
Jayaraman, A., W. Klement, Jr., and G. C. Kennedy, 1963, Phys. Rev. **130**, 540.
Jayaraman, A., R. C. Newton, and G. C. Kennedy, 1961, Nature (London) **191**, 1288.
Jiang, J. Z., L. Gerward, D. Frost, R. Secco, J. Peyronneau, and J. S. Olsen, 1999, J. Appl. Phys. **86**, 6608.
Jiang, J. Z., J. S. Olsen, L. Gerward, D. Frost, D. Rubie, and J. Peyronneau, 2000, Europhys. Lett. **50**, 48.
Jones, R. O., and O. Gunnarsson, 1989, Rev. Mod. Phys. **61**, 689.
Käckell, P., B. Wenzein, and F. Bechstedt, 1994, Phys. Rev. B **50**, 17 037.
Kafalas, J. A., H. C. Gatos, M. C. Levine, and M. D. Banus, 1962, J. Phys. Chem. Solids **23**, 1541.
Karch, K., F. Bechstedt, P. Pavone, and D. Strauch, 1996, Phys. Rev. B **53**, 13 400.

Karzel, H., W. Potzel, M. Köfferlein, W. Schiessl, M. Steiner, U. Hiller, G. M. Kalvius, D. W. Mitchell, T. P. Das, P. Blaha, K. Schwarz, and M. P. Pasternak, 1996, Phys. Rev. B **53**, 11 425.

Kasper, J. S., and S. M. Richards, 1964, Acta Crystallogr. **17**, 752.

Kelsey, A. A., and G. J. Ackland, 2000, J. Phys.: Condens. Matter **12**, 7161.

Kelsey, A. A., G. J. Ackland, and S. J. Clark, 1998, Phys. Rev. B **57**, R2029.

Kern, G., G. Kresse, and J. Hafner, 1999, Phys. Rev. B **59**, 8551.

Kim, K., V. Ozoliņš, and A. Zunger, 1999, Phys. Rev. B **60**, R8449.

Klotz, S., J. M. Besson, G. Hamel, R. J. Nelmes, J. S. Loveday, and W. G. Marshall, 1996, High Press. Res. **14**, 249.

Knudson, M. D., Y. M. Gupta, and A. B. Kunz, 1999, Phys. Rev. B **59**, 11 704.

Kohn, W., and L. J. Sham, 1965, Phys. Rev. **140**, A1133.

Kusaba, K., Y. Syono, and T. Kikegawa, 1999, Proc. Jpn. Acad., Ser. B: Phys. Biol. Sci. **75**, 1.

Landau, L. D., 1937, Zh. Eksp. Teor. Fiz. **7**, 19; **7**, 627. Translated in *Collected Papers of L. D. Landau*, edited by D. Ter Haar (Pergamon, Oxford, 1965), pp. 193 and 209.

Landau, L. D., and E. M. Lifshitz, 1980, *Statistical Physics*, Part 1, 3rd Ed. (Butterworth-Heineman, Oxford), Chap. XIV.

Langford, J. I., and D. Louër, 1996, Rep. Prog. Phys. **59**, 131.

Lawaetz, P., 1972, Phys. Rev. B **5**, 4039.

Lee, G. D., C. D. Hwang, M. H. Lee, and J. Ihm, 1997, J. Phys.: Condens. Matter **9**, 6619.

Lee, G. D., and J. Ihm, 1996, Phys. Rev. B **53**, R7622.

Lee, I.-H., and R. M. Martin, 1997, Phys. Rev. B **56**, 7197.

Léger, J. M., J. Haines, C. Danneels, and L. S. de Oliveira, 1998, J. Phys.: Condens. Matter **10**, 4201.

Lei, T., M. Fanciulli, R. J. Molnar, T. D. Moustakas, R. J. Graham, and J. Scanlon, 1991, Appl. Phys. Lett. **59**, 944.

Lewis, S. P., and M. L. Cohen, 1993, Phys. Rev. B **48**, 16 144.

Lewis, S. P., and M. L. Cohen, 1994, Solid State Commun. **89**, 483.

Lin, Ch.-M., D.-S. Chuu, T.-J. Yang, W.-Ch. Chou, J.-A. Xu, and E. Huang, 1997, Phys. Rev. B **55**, 13 641.

Liu, L., and W. A. Basset, 1986, *Elements, Oxides and Silicates* (Oxford University, Oxford), p. 96.

Liu, A. Y., A. García, M. L. Cohen, B. K. Godwal, and R. Jeanloz, 1991, Phys. Rev. B **43**, 1795.

Liu, G. C., Z. W. Lu, and M. Klein, 1995, Phys. Rev. B **51**, 5678.

Liu, M., and L. Liu, 1986, High Temp.-High Press. **18**, 79.

López-Solano, J., A. Mujica, P. Rodríguez-Hernández, and A. Muñoz, 2003, Phys. Status Solidi B **235**, 452.

Lu, Z. W., D. Singh, and H. Krakauer, 1989, Phys. Rev. B **39**, 10 154.

Mailhiot, C., and A. K. McMahan, 1991, Phys. Rev. B **44**, 11 578.

Majewski, J. A., and P. Vogl, 1987, Phys. Rev. B **35**, 9666.

Mao, H. K., 1989, in *Simple Molecular Systems at Very High Density*, edited by A. Polian, P. Loubeyre, and N. Boccara (Plenum, New York), p. 221.

Mao, H. K., Y. Wu, J. F. Shu, J. Z. Hu, R. J. Hemley, and D. E. Cox, 1990, Solid State Commun. **74**, 1027.

Mariano, A. N., and E. P. Warekois, 1963, Science **142**, 672.

Martínez-García, D., Y. Le Godec, M. Mezouar, G. Syfosse, J. P. Itié, and J. M. Besson, 1999, Phys. Status Solidi B **211**, 461.

Martínez-García, D., Y. Le Godec, G. Syfosse, and J. P. Itié, 1999, Phys. Status Solidi B **211**, 475.

McMahon, M. I., and R. J. Nelmes, 1993, Phys. Rev. B **47**, 8337.

McMahon, M. I., and R. J. Nelmes, 1996, Phys. Status Solidi B **198**, 389.

McMahon, M. I., and R. J. Nelmes, 1997, Phys. Rev. Lett. **78**, 3697.

McMahon, M. I., R. J. Nelmes, D. R. Allan, S. A. Belmonte, and T. Bovornratanaraks, 1998, Phys. Rev. Lett. **80**, 5564.

McMahon, M. I., R. J. Nelmes, H. Liu, and S. A. Belmonte, 1996, Phys. Rev. Lett. **77**, 1781.

McMahon, M. I., R. J. Nelmes, N. G. Wright, and D. R. Allan, 1993a, Phys. Rev. B **48**, 16 246.

McMahon, M. I., R. J. Nelmes, N. G. Wright, and D. R. Allan, 1993b, in *Proceedings of the Joint Conference of the AIRAPT/APS on High-Pressure Science and Technology*, edited by S. C. Schmidt, J. W. Shaner, G. A. Samara, and M. Ross, p. 629 [as cited by Nelmes and McMahon (1998)].

McMahon, M. I., R. J. Nelmes, N. G. Wright, and D. R. Allan, 1993c, in *Proceedings of the Joint Conference of the AIRAPT/APS on High-Pressure Science and Technology*, edited by S. C. Schmidt, J. W. Shaner, G. A. Samara, and M. Ross, p. 633 [as cited by Nelmes and McMahon (1998)].

McMahon, M. I., R. J. Nelmes, N. G. Wright, and D. R. Allan, 1994a, Phys. Rev. B **50**, 739.

McMahon, M. I., R. J. Nelmes, N. G. Wright, and D. R. Allan, 1994b, Phys. Rev. B **50**, 13 047.

McMahon, M. I., N. G. Wright, D. R. Allan, and R. J. Nelmes, 1996, Phys. Rev. B **53**, 2163.

Menoni, C. S., J. Z. Hu, and I. L. Spain, 1986, Phys. Rev. B **34**, 362.

Menoni, C. S., and I. L. Spain, 1987, Phys. Rev. B **35**, 7520.

Methfessel, M., C. O. Rodriguez, and O. K. Andersen, 1989, Phys. Rev. B **40**, 2009.

Mezouar, M., J. M. Besson, G. Syfosse, J. P. Itié, D. Häusermann, and M. Hanfland, 1996, Phys. Status Solidi B **198**, 403.

Mezouar, M., H. Libotte, S. Députier, T. Le Bihan, and D. Häusermann, 1999, Phys. Status Solidi B **211**, 395.

Miao, M. S., M. Prikhodko, and W. R. L. Lambrecht, 2002, Phys. Rev. B **66**, 064107.

Miedema, A. R., 1973, J. Less-Common Met. **32**, 117.

Minomura, S., and H. G. Drickamer, 1962, J. Phys. Chem. Solids **23**, 451.

Mirkarimi, P. B., K. F. McCarty, and D. L. Medlin, 1997, Mater. Sci. Eng., R. **21**, 47.

Moll, N., M. Bockstedte, M. Fuchs, E. Pehlke, and M. Scheffler, 1995, Phys. Rev. B **52**, 2550.

Mott, N. F., and J. Jones, 1936, *The Theory of the Properties of Metals and Alloys* (Oxford University Press, Oxford).

Mujica, A., A. Muñoz, and R. J. Needs, 1998, Phys. Rev. B **57**, 1344.

Mujica, A., A. Muñoz, S. Radescu, and R. J. Needs, 1999, Phys. Status Solidi B **211**, 345.

Mujica, A., and R. J. Needs, 1993, Phys. Rev. B **48**, 17 010.

Mujica, A., and R. J. Needs, 1996, J. Phys.: Condens. Matter **8**, L237.

Mujica, A., and R. J. Needs, 1997, Phys. Rev. B **55**, 9659; **56**, 12653(E).

Mujica, A., R. J. Needs, and A. Muñoz, 1995, Phys. Rev. B **52**, 8881.

Mujica, A., R. J. Needs, and A. Muñoz, 1996, Phys. Status Solidi B **198**, 461.

Mujica, A., S. Radescu, A. Muñoz, and R. J. Needs, 2001a, J. Phys.: Condens. Matter **13**, 35.
Mujica, A., S. Radescu, A. Muñoz, and R. J. Needs, 2001b, Phys. Status Solidi B **223**, 379.
Mujica, A., P. Rodríguez-Hernández, S. Radescu, R. J. Needs, and A. Muñoz, 1999, Phys. Status Solidi B **211**, 39.
Muñoz, A., and K. Kunc, 1991, Phys. Rev. B **44**, 10 372.
Muñoz, A., and K. Kunc, 1993, J. Phys.: Condens. Matter **5**, 6015.
Murnaghan, F. D., 1944, Proc. Natl. Acad. Sci. U.S.A. **50**, 697.
Nazzal, A., and A. Qteish, 1996, Phys. Rev. B **53**, 8262.
Needs, R. J., and R. M. Martin, 1984, Phys. Rev. B **30**, 5390.
Needs, R. J., and A. Mujica, 1995, Phys. Rev. B **51**, 9652.
Nelmes, R. J., H. Liu, S. A. Belmonte, J. S. Loveday, M. I. McMahon, D. R. Allan, D. Häusermann, and M. Hanfland, 1996, Phys. Rev. B **53**, R2907.
Nelmes, R. J., and M. I. McMahon, 1994, J. Synchrotron Radiat. **1**, 69.
Nelmes, R. J., and M. I. McMahon, 1995, Phys. Rev. Lett. **74**, 106; **74**, 2618(E).
Nelmes, R. J., and M. I. McMahon, 1996, Phys. Rev. Lett. **77**, 663.
Nelmes, R. J., and M. I. McMahon, 1998, Semicond. Semimetals **54**, 145.
Nelmes, R. J., M. I. McMahon, and S. A. Belmonte, 1997, Phys. Rev. Lett. **79**, 3668.
Nelmes, R. J., M. I. McMahon, P. D. Hatton, J. Crain, and R. O. Piltz, 1993, Phys. Rev. B **47**, 35; **48**, 9949(E).
Nelmes, R. J., M. I. McMahon, N. G. Wright, and D. R. Allan, 1993, Phys. Rev. B **48**, 1314.
Nelmes, R. J., M. I. McMahon, N. G. Wright, and D. R. Allan, 1994, Phys. Rev. Lett. **73**, 1805.
Nelmes, R. J., M. I. McMahon, N. G. Wright, and D. R. Allan, 1995a, Phys. Rev. B **51**, 15 723.
Nelmes, R. J., M. I. McMahon, N. G. Wright, and D. R. Allan, 1995b, J. Phys. Chem. Solids **56**, 545; 1996, **57**, 141(E).
Nelmes, R. J., M. I. McMahon, N. G. Wright, D. R. Allan, H. Liu, and J. S. Loveday, 1995, J. Phys. Chem. Solids **56**, 539.
Nelmes, R. J., M. I. McMahon, N. G. Wright, D. R. Allan, and J. S. Loveday, 1993, Phys. Rev. B **48**, 9883.
Ohtani, A., M. Motobayashi, and A. Onodera, 1980, Phys. Lett. **75A**, 435.
Ohtani, A., T. Seike, M. Motobayashi, and A. Onodera, 1982, J. Phys. Chem. Solids **43**, 627.
Olijnyk, H., 1992a, Phys. Rev. Lett. **68**, 2232.
Olijnyk, H., 1992b, Phys. Rev. B **46**, 6589.
Olijnyk, H., and W. B. Holzapfel, 1984, J. Phys. (Paris), Colloq. **45**, Suppl. 11, C8-153.
Olijnyk, H., S. K. Sikka, and W. B. Holzapfel, 1984, Phys. Lett. **103A**, 137.
Onodera, A., N. Kawi, K. Ishizaki, and I. L. Spain, 1974, Solid State Commun. **14**, 803.
Onodera, A., A. Ohtani, M. Motobayashi, T. Seike, O. Shimomura, and O. Fukunaga, 1982, in *Proceedings of the 8th AIRAPT Conference*, Uppsala, edited by C. M. Backman, T. Johannisson, and L. Tengner (World Scientific, Singapore), p. 321.
Owen, N. B., P. L. Smith, J. E. Martin, and A. J. Wright, 1963, J. Phys. Chem. Solids **24**, 1519.
Ozoliņš, V., and A. Zunger, 1999, Phys. Rev. Lett. **82**, 767.
Pascarelli, S., G. Aquilanti, W. Crichton, T. Le Bihan, S. de Panfilis, E. Fabiani, M. Mezouar, J. P. Itié, and A. Polian, 2002, High Press. Res. **22**, 331.
Pascarelli, S., G. Aquilanti, W. A. Crichton, T. Le Bihan, M. Mezovar, S. de Panfilis, J. P. Itié, and A. Polian, 2003, Europhys. Lett. **61**, 544.
Pauling, L., 1960, *The Nature of the Chemical Bond* (Cornell University Press, Ithaca, NY).
Pavone, P., S. Baroni, and S. de Gironcoli, 1998, Phys. Rev. B **57**, 10 421.
Payne, M. C., M. P. Teter, D. C. Allan, T. A. Arias, and J. D. Joannopoulos, 1992, Rev. Mod. Phys. **64**, 1045.
Pellicer-Porres, J., A. Segura, V. Muñoz, J. Zúñiga, J. P. Itié, A. Polian, and P. Munsch, 2002, Phys. Rev. B **65**, 012109.
Perdew, J. P., K. Burke, and M. Ernzerhof, 1996, Phys. Rev. Lett. **77**, 3865.
Perlin, P., I. Gorczyca, S. Porowski, T. Suski, N. E. Christensen, and A. Polian, 1993, Jpn. J. Appl. Phys., Suppl. **32-1**, 334.
Perlin, P., C. Jauberthie-Carillon, J. P. Itié, A. San Miguel, I. Grzegory, and A. Polian, 1992, Phys. Rev. B **45**, 83.
Pfrommer, B. G., M. Côté, S. G. Louie, and M. L. Cohen, 1997a, Phys. Rev. B **56**, 6662.
Pfrommer, B. G., M. Côté, S. G. Louie, and M. L. Cohen, 1997b, J. Comput. Phys. **131**, 233.
Phillips, J. C., 1970, Rev. Mod. Phys. **42**, 317.
Phillips, J. C., 1973, *Bands and Bonds in Semiconductors* (Academic, New York).
Phillips, J. C., and L. Kleinman, 1959, Phys. Rev. **116**, 287.
Pickett, W. E., 1989, Comput. Phys. Rep. **9**, 115.
Piermarini, G. J., S. Block, J. D. Barnett, and R. A. Forman, 1975, J. Appl. Phys. **46**, 2774.
Piltz, R. O., J. R. Maclean, S. J. Clark, G. J. Ackland, P. D. Hatton, and J. Crain, 1995, Phys. Rev. B **52**, 4072.
Qadri, S. B., E. F. Skelton, A. D. Dinsmore, J. Z. Hu, W. J. Kim, C. Nelson, and B. R. Ratna, 2001, J. Appl. Phys. **89**, 115.
Qadri, S. B., E. F. Skelton, and A. W. Webb, 1983, J. Appl. Phys. **54**, 3609.
Qteish, A., 2000, J. Phys.: Condens. Matter **12**, 5639.
Qteish, A., M. Abu-Jafar, and A. Nazzal, 1998, J. Phys.: Condens. Matter **10**, 5069.
Qteish, A., and A. Muñoz, 2000, J. Phys.: Condens. Matter **12**, 1705.
Qteish, A., and M. Parrinello, 2000, Phys. Rev. B **61**, 6521.
Recio, J. M., M. A. Blanco, V. Luaña, R. Pandey, L. Gerward, and J. S. Olsen, 1998, Phys. Rev. B **58**, 8949.
Ribeiro, F. J., and M. L. Cohen, 2000, Phys. Rev. B **62**, 11 388.
Rietveld, H. M., 1969, J. Appl. Crystallogr. **2**, 65.
Rooymans, C. J. M., 1963, Phys. Lett. **4**, 186.
Samara, G. A., and H. G. Drickamer, 1962, J. Phys. Chem. Solids **23**, 457.
San Miguel, A., A. Polian, M. Gauthier, and J. P. Itié, 1993, Phys. Rev. B **48**, 8683.
San Miguel, A., N. G. Wright, M. I. McMahon, and R. J. Nelmes, 1995, Phys. Rev. B **51**, 8731.
Scandolo, S., M. Bernasconi, G. L. Chiarotti, P. Focher, and E. Tosatti, 1995, Phys. Rev. Lett. **74**, 4015.
Scandolo, S., G. L. Chiarotti, and E. Tosatti, 1996, Phys. Rev. B **53**, 5051.
Schwarz, U., O. Jepsen, and K. Syassen, 2000, Solid State Commun. **113**, 643.
Schwarz, U., K. Syassen, A. Grzechnik, and M. Hanfland, 1999, Solid State Commun. **112**, 319.
Schwarz, U., K. Takemura, M. Hanfland, and K. Syassen, 1998, Phys. Rev. Lett. **81**, 2711.

Sekine, T., and T. Kobayashi, 1997, Phys. Rev. B **55**, 8034.
Serrano, J., A. Rubio, E. Hernández, A. Muñoz, and A. Mujica, 2000, Phys. Rev. B **62**, 16 612.
Shimojo, F., I. Ebbsjö, R. K. Kalia, A. Nakano, J. P. Rino, and P. Vashishta, 2000, Phys. Rev. Lett. **84**, 3338.
Shimomura, O., K. Takemura, H. Fujihisa, Y. Fujii, Y. Ohishi, T. Kikegawa, Y. Amemiya, and T. Matsushita, 1992, Rev. Sci. Instrum. **63**, 967.
Shimomura, O., W. Utsumi, T. Urakawa, T. Kikegawa, K. Kusaba, and A. Onodera, 1997, in *The Review of High Pressure Science and Technology*, edited by Masoru Nakahara, Vol. 6, p. 207.
Simons, G., 1971, J. Chem. Phys. **55**, 756.
Singh, D. J., 1994, *Planewaves, Pseudopotentials and the LAPW Method* (Kluwer Academic, Dordrecht/Boston/London).
Smelyansky, V. I., and J. S. Tse, 1995, Phys. Rev. B **52**, 4658.
Smith, P. L., and J. E. Martin, 1965, Phys. Lett. **19**, 541.
Solozhenko, V. L., 1995, J. Hard Mater. **6**, 51.
Solozhenko, V. L., V. Z. Turkevich, and W. B. Holzapfel, 1999, J. Phys. Chem. B **103**, 2903.
Soma, T., 1978, J. Phys. C **11**, 2681.
Stampfl, C., and C. G. Van de Walle, 1999, Phys. Rev. B **59**, 5521.
St. John, J., and A. N. Bloch, 1974, Phys. Rev. Lett. **33**, 1095.
Stokes, H. T., and D. M. Match, 2002, Phys. Rev. B **65**, 144114.
Strössner, K., S. Ves, C. K. Kim, and M. Cardona, 1987, Solid State Commun. **61**, 275.
Sugino, O., and R. Car, 1995, Phys. Rev. Lett. **74**, 1823.
Sundqvist, B., 1999, Adv. Phys. **48**, 1.
Suzuki, T., T. Yagi, S. Akimoto, T. Kawamura, S. Toyoda, and S. Endo, 1983, J. Appl. Phys. **54**, 748.
Takahashi, T., H. K. Mao, and W. A. Basset, 1969, Science **165**, 1352.
Takemura, K., U. Schwarz, K. Syassen, M. Hanfland, N. E. Christensen, D. L. Novikov, and I. Loa, 2000, Phys. Rev. B **62**, R10 603.
Tateyama, Y., T. Ogitsu, K. Kusakabe, and S. Tsuneyuki, 1996, Phys. Rev. B **54**, 14 994.
Uchino, M., T. Mashimo, M. Kodama, T. Kobayashi, E. Takasawa, T. Sekine, Y. Noguchi, H. Hikosaka, K. Fukuoka, Y. Syono, T. Kondo, and T. Yagi, 1999, J. Phys. Chem. Solids **60**, 827.
Uehara, S., T. Masamoto, A. Onodera, M. Ueno, O. Shimomura, and K. Takemura, 1997, J. Phys. Chem. Solids **58**, 2093.
Ueno, M., K. Hasegawa, R. Oshima, A. Onodera, O. Shimomura, K. Takemura, H. Nakae, T. Matsuda, and T. Hirai, 1992, Phys. Rev. B **45**, 10 226.
Ueno, M., A. Onodera, O. Shimomura, and K. Takemura, 1992, Phys. Rev. B **45**, 10 123.
Ueno, M., M. Yoshida, A. Onodera, O. Shimomura, and K. Takemura, 1994, Phys. Rev. B **49**, 14.
Van Camp, P. E., V. E. Van Doren, and J. T. Devreese, 1991, Phys. Rev. B **44**, 9056.
Van Camp, P. E., V. E. Van Doren, and J. T. Devreese, 1992, Solid State Commun. **81**, 23.
Vanderbilt, D., 1990, Phys. Rev. B **41**, 7892.
Vanderborgh, C. A., Y. K. Vohra, and A. L. Ruoff, 1989, Phys. Rev. B **40**, 12 450.
Vanderborgh, C. A., Y. K. Vohra, H. Xia, and A. L. Ruoff, 1990, Phys. Rev. B **41**, 7338.
Vanpeteghem, C. B., R. J. Nelmes, D. R. Allan, and M. I. McMahon, 2002, Phys. Rev. B **65**, 012105.
Van Vechten, J. A., 1969, Phys. Rev. **182**, 891.
Venkateswaran, U. D., L. J. Cui, B. A. Weinstein, and F. A. Chambers, 1992, Phys. Rev. B **45**, 9237.
Ves, S., U. Schwarz, N. E. Christensen, K. Syassen, and M. Cardona, 1990, Phys. Rev. B **42**, 9113.
Vohra, Y. G., K. E. Brister, S. Desgreniers, A. L. Ruoff, K. J. Chang, and M. L. Cohen, 1986, Phys. Rev. Lett. **56**, 1944.
Vohra, Y. G., S. T. Weir, and A. L. Ruoff, 1985, Phys. Rev. B **31**, 7344.
Vollstädt, H., E. Ito, M. Akaishi, S. Akimoto, and O. Fukunaga, 1990, Proc. Jpn. Acad., Ser. B: Phys. Biol. Sci. **B66**, 7.
Wanagel, J., V. Arnold, and A. L. Ruoff, 1976, J. Appl. Phys. **47**, 2821.
Wang, J., S. Yip, S. R. Phillpot, and D. Wolf, 1993, Phys. Rev. Lett. **71**, 4182.
Wang, J., S. Yip, S. R. Phillpot, and D. Wolf, 1995, Phys. Rev. B **52**, 12 627.
Weinstein, B. A., S. K. Hark, R. D. Burnham, and R. M. Martin, 1987, Phys. Rev. Lett. **58**, 781.
Weir, C. E., E. R. Lippincott, A. van Valkenburg, and E. N. Bunting, 1959, J. Res. Natl. Bur. Stand., Sect. A **63**, 55.
Weir, S. T., Y. K. Vohra, and A. L. Ruoff, 1987, Phys. Rev. B **36**, 4543.
Weir, S. T., Y. K. Vohra, C. A. Vanderborgh, and A. L. Ruoff, 1989, Phys. Rev. B **39**, 1280.
Wentorf, R. H., and J. S. Kasper, 1963, Science **139**, 338.
Wentzcovitch, R. M., M. L. Cohen, and P. K. Lam, 1987, Phys. Rev. B **36**, 6058.
Wentzcovitch, R. M., S. Fahy, M. L. Cohen, and S. G. Louie, 1988, Phys. Rev. B **38**, 6191.
Werner, A., H. D. Hochheimer, K. Strössner, and A. Jayaraman, 1983, Phys. Rev. B **28**, 3330.
Werner, A., J. A. Sanjurjo, and M. Cardona, 1982, Solid State Commun. **44**, 155.
Wright, A. F., and J. S. Nelson, 1994, Phys. Rev. B **50**, 2159.
Wright, A. F., and J. S. Nelson, 1995, Phys. Rev. B **51**, 7866.
Wright, N. G., M. I. McMahon, R. J. Nelmes, and A. San Miguel, 1993, Phys. Rev. B **48**, 13 111.
Wright, N. G., R. J. Nelmes, S. A. Belmonte, and M. I. McMahon, 1996, J. Synchrotron Radiat. **3**, 112.
Wyckoff, R. W. G., 1963, *Crystal Structures* (Wiley, New York/London/Sydney).
Xia, H., Q. Xia, and A. L. Ruoff, 1993a, Phys. Rev. B **47**, 12 925.
Xia, H., Q. Xia, and A. L. Ruoff, 1993b, J. Appl. Phys. **74**, 1660.
Xia, Q., H. Xia, and A. L. Ruoff, 1993c, J. Appl. Phys. **73**, 8198.
Xia, Q., H. Xia, and A. L. Ruoff, 1994, Mod. Phys. Lett. B **8**, 345.
Yeh, C.-Y., Z. W. Lu, S. Froyen, and A. Zunger, 1992, Phys. Rev. B **46**, 10 086.
Yin, M. T., 1984, Phys. Rev. B **30**, 1773.
Yin, M. T., and M. L. Cohen, 1980, Phys. Rev. Lett. **45**, 1004.
Yin, M. T., and M. L. Cohen, 1982, Phys. Rev. B **26**, 5668.
Yin, M. T., and M. L. Cohen, 1983, Phys. Rev. Lett. **50**, 2006.
Yoshida, M., A. Onodera, M. Ueno, K. Takemura, and O. Shimomura, 1993, Phys. Rev. B **48**, 10 587.
Yu, S.-C., I. L. Spain, and E. F. Skelton, 1978a, J. Appl. Phys. **49**, 4741.

Yu, S.-C., I. L. Spain, and E. F. Skelton, 1978b, Solid State Commun. **25**, 49.
Zhang, S. B., and M. L. Cohen, 1987, Phys. Rev. B **35**, 7604.
Zhang, S. B., and M. L. Cohen, 1989, Phys. Rev. B **39**, 1450.
Zhao, Y.-X., F. Buehler, J. R. Sites, and I. L. Spain, 1986, Solid State Commun. **59**, 679.
Zhou, T., U. Schwarz, M. Hanfland, Z. X. Liu, K. Syassen, and M. Cardona, 1998, Phys. Rev. B **57**, 153.
Zhou, Y. H., A. J. Campbell, and D. L. Heinz, 1991, J. Phys. Chem. Solids **52**, 821.
Zunger, A., 1980, Phys. Rev. B **22**, 5839.
Zunger, A., and M. L. Cohen, 1978, Phys. Rev. Lett. **41**, 53.